Charles University in Prague, Faculty of Science

Department of Physical and Macromolecular Chemistry

Polymeric nanoparticles with biodegradable core and polymer chelates for medical purposes

Doctoral Thesis

Candidate: Michaela Škodová

Institute of Macromolecular Chemistry, ASCR, v.v.i.

Department of Supramolecular Polymer Systems

Supervisor: RNDr. Petr Štěpánek, DrSc.

2013

Universita Karlova v Praze, Přírodovědecká Fakulta

Katedra Fyzikální a Makromolekulární Chemie

Polymerní nanočástice s biodegradovatelným jádrem a polymerní cheláty pro medicínské účely

Disertační práce

Kandidát: Michaela Škodová

Ústav Makromolekulární Chemie, AV ČR, v.v.i.

Oddělení supramolekulárních polymerních systémů

Školitel: RNDr. Petr Štěpánek, DrSc.

2013

I declare hereby that this presented thesis is, to the best of my knowledge, original and has not been submitted in whole or part for a degree in any university. I have written this doctoral thesis independently, under the supervision of my supervisor RNDr. Petr Štěpánek, DrSc. and co-supervisor Mgr. Martin Hrubý, PhD, and I have cited all the sources I have used.

Prague 13.4.2013 Michaela Škodová

motto:

Nullus est liber tam malus, ut non aliqua parte prosit.

There is no book so bad that it is not beneficial in some respect.

Acknowledgement

I would like to thank all the people that helped me with this doctoral thesis.
First of all, I would like to thank my supervisor, Petr Štěpánek, for his great advices and well-meant criticism to all my work done on this topic.
I would like to express here as well thanks to my co-supervisor Martin Hrubý, who provided me not only professional leading, but also a friendly assistance, when I needed it.
My thanks belong also to Charles University for the opportunity for the doctoral studies within the Institute of Macromolecular Chemistry.

Abstract

Application of radionuclides due to their unique nature is still attracting the interest of professionals from different branches of science.

In this thesis, the unifying topic is the utilization of various radioactive labels on polymeric carriers for biomedicinal purposes.

In the introductory part, the area of use of the investigated substances – in terms of their possible application in nuclear medicine, is presented to the reader.

The experimental work is divided into three main sections dealing with synthesis and studying properties of appropriate selected polymers, their metal chelates and radiolabeling.

First part of the study describes development of new strategies for labeling of polymeric carriers with radiometal cations and radioiodine, whereas in the following sections of the study synthesis and investigation of biocompatible polymer materials is discussed.

New possible approaches in the diagnostics and therapy of cancer by using polymeric chelates as carriers are presented as well as the use of macroporous metal chelating polymer beads as potential therapeutics intended for radioembolization of liver malignancies and for the therapy of Wilson's disease.

Investigated polymers have been shown to be non-toxic, to have good *in vitro* stability and to have the ability to be radiolabeled in high yields by selected radionuclide.

Abstrakt

Použití radionuklidů díky jejich jedinečným vlastnostem stále přitahuje pozornost odborníků z různých odvětví vědy.

V této disertační práci je spojujícím činitelem použití nejrůznějších radioaktivních značek na polymerech pro biomedicínské účely.

V úvodní části je čtenáři přiblížena oblast použití zkoumaných polymerů – ve smyslu jejich možného využití v nukleární medicíně.

Experimentální část práce je rozdělena do tří hlavních sekcí zabývajících se studiem vlastností vhodných vybraných polymerů, jejich kovovými cheláty a radioznačením.

V první části studie je popsán vývoj nových přístupů ke značení polymerních nosičů radioaktivními ionty kovů a radiojódem, zatímco v následujících částech je diskutováno zkoumání biokompatibilních polymerních materiálů.

Jsou zde uvedeny nové možné přístupy v problematice diagnostiky a terapie rakoviny za použití polymerních chelátů jako nosičů, stejně tak jako použití makroporézních kovy chelatujících polymerních kuliček zamýšlených pro radioembolizaci jaterních nádorů i jako možných terapeutik pro léčbu Wilsonovy choroby.

Zkoumáním polymerů bylo prokázáno, že jsou netoxické, mají dobrou *in vitro* stabilitu a schopnost být radioaktivně značeny vybranými radionuklidy s vysokým výtěžkem.

Contents

Abbreviations

AAS - Atomic absorption spectroscopy

AIBN – azobisisobutyronitrile

CPT – cloud point temperature

cryo-TEM -Cryo-transmission electron microscopy

DLS – Dynamic Light Scattering

DNA - deoxyribonucleic acid

DOTA – 1,4,7,10- tetraazacyclododecane-1,4,7,10-tetraacetic acid

DTPA – diethylenetriaminepentaacetic acid

EC – Electron Capture (radionuclide decay mode)

FDG – [^{18}F]-2-fluoro-2-deoxy-D-glucose

Gly – glycine

GPC- Gel Permeation Chromatography

HPMA- *N*-(2-hydroxypropyl)-methacrylamide

IEC – Ion Exchange Chromatography

IMAC - Immobilized Metal Affinity Chromatography

IT – Isomeric Transition (radionuclide decay mode)

keV – kiloelectronvolts

LCST- low critical solubility temperature

LET - Linear Energy Transfer

Leu - leucine

MAA - Maximum Allowed Amount

MAEDA- *N*-[2-(methacryloylamino)ethyl] carbamate

NIPAM - *N*-isopropylacrylamide

PBS - Phosphate Buffered Saline

PEO – poly(ethylene oxide)

PET – Positron Emission Tomography

Phe – phenylalanine

SANS - Small Angle Neutron Scattering

SAXS – Small Angle X-ray Scattering

SPECT – Single Photon Emission Computed Tomography

STM - Scanning Tunneling Microscopy

THF - Tetrahydrofuran

Symbols

A	absorbance
A	activity of radionuclide
A_2	second virial coefficient
α	alpha radiation
α_p	polarizability
β	beta radiation
Bq	Becquerel
Ci	Curie
D	dose
D	diffusion coefficient
ΔG	change in *Gibbs energy*
$G(t)$	correlation function
Eγ	energy of γ radiation
γ	gamma radiation
Iγ	intensity branching = probability of each γ link emitted during radioactive decay
k_B	universal Boltzmann constant
K_n	consecutive (partial) stability constant
λ	wavelength
λ_t	decay constant
M	molecular weight
M_w	weight average molecular weight
M_n	number average molecular weight
n	substance amount
n	refractive index
q	wave vector
R_g	radius of gyration
R_H	hydrodynamic radius
ρ	electron density
S	structure factor
T	absolute temperature
$T_{1/2}$	decay half-time of radionuclide
τ	delay time
Σ_n	total stability constant

List of figures

List of Tables

Aims of Thesis

The main aim of the work described in this thesis is the synthesis and detailed study of properties of chelating polymers for biomedicinal purposes.

The following partial aims are considered:

1) Development of new strategies for labeling of polymers with radiometal cations and their comparison with radioiodination.
2) Synthesis and studying properties of macroporous metal chelating polymer beads as potential therapeutics intended for radioembolization of liver malignancies and for the therapy of Wilson's disease.
3) Synthesis and studying properties of supramolecular metal cation-assembled core-shell nanoparticles as potential radionuclide theranostics for solid tumors.

List of publications

D1. ***Novel Polymer Vectors of ^{64}Cu***

Kozempel J, Hrubý M, Nováková M, Kučka J, Lešetický L, Lebeda O; Bioconjugate chemistry, 97, (2009), 747-752 ; co-author

D2. ***New coupling strategy for radionuclide labeling of synthetic polymers***

Hrubý M, Kučka J, Nováková M, Macková H, Vetrík M; Applied Radiation and Isotopes, 68(2), (2009), 334-339; co-author

D3. ***Polyoxazoline Thermoresponsive Micelles as Radionuclide Delivery Systems***

Hrubý M, Filippov S K, Pánek J, Nováková M, Macková H, Kučka J, Větvička D, Ulbrich K; Macromolecular Bioscience, 10, (2010), 916-924 ; co-author

D4. ***Lutetium-177 and iodine-131 loaded chelating polymer microparticles intended for radioembolization of liver malignancies***

Hrubý M, Škodová M, Macková H, Skopal J, Tomeš M, Kropáček M, Zimova J, Kučka J; Reactive and Functional Polymers, 71 (2011) 1155–1159; co-author

D5. ***Novel polymeric nanoparticles assembled by metal ion addition***

Škodová M, Hrubý M, Filippov S K, Karlsson G, Macková H, Špírková M, Kaňková D, Steinhart M, Štěpánek P, Ulbrich K; Macromolecular Chemistry and Physics, 212, (2011), 2339-2348 - first author

D6. ***Self-Assembled Polymeric Chelate Nanoparticles as Potential Theranostic Agents***

Škodová M, Černoch P, Štěpánek P, Chánová E, Kučka J, Kálalová Z, Kaňková D, Hrubý M; ChemPhysChem, 13 (18), (2012), 4244-4250 - first author

D7. ***Chelating polymeric particles intended for the therapy of Wilson's disease***

Škodová M, Jan Kučka, Miroslav Vetrík, Jan Skopal, Zuzana Walterová, Ondřej Sedláček, Petr Štěpánek, Pavla Poučková, Petr Urbánek, and Martin Hrubý; Reactive and Functional Polymers, *currently under second review* - first author

Introduction

1.1. Current cancer treatment overview

In recent years many new strategies for cancer treatment and therapy have been developed. Currently the scientific approach to diagnostics and therapy of cancer is no longer separated from each other and new platform *theranostics* [1] for the unifying approach has been invented. Theranostics provides real-time diagnostic feedback allowing further customization of therapy to the individual patient making the therapy more efficient and with fewer side effects. Actual cancer treatment can be divided into surgery, external radiotherapy/internal radionuclide therapy and chemotherapy. For internal radionuclide therapy and chemotherapy, newer experimental approaches of cancer treatment opened a wide range for use of polymers, polymeric carriers and nanoparticles.

Chemotherapy is based on the use of several cancerostatics, substances acting against rapid growth of tumor cells, usually combining several drugs together.

In the wide range of these drugs, we can find many different mechanisms of action against the tumor cells division. Examples of most often used mechanisms are:

DNA intercalation

Intercalators are commonly used anticancer drugs inserting themselves into DNA chain and further blocking operations the cell needs to operate with genetic information, especially the topoisomerase II activity. DNA topoisomerase II inhibitors block religation of double strand DNA breaks (i.e., sister chromatid separation or cleaved DNA). The most important common examples are etoposide, tenoposide, acridines, ellipticine derivatives, bleomycin, daunomycin, or doxorubicin (see **Figure 1** and **2**). [2] Intercalators are highly efficient anticancer agents, however with usually severe side effects (e.g., the specific side effect of doxorubicin is its cardiotoxicity) and inherent mutagenicity leading to increased incidence of secondary malignancies.

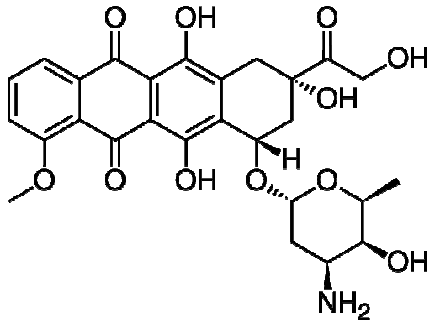

Figure 1 – Structure of doxorubicin

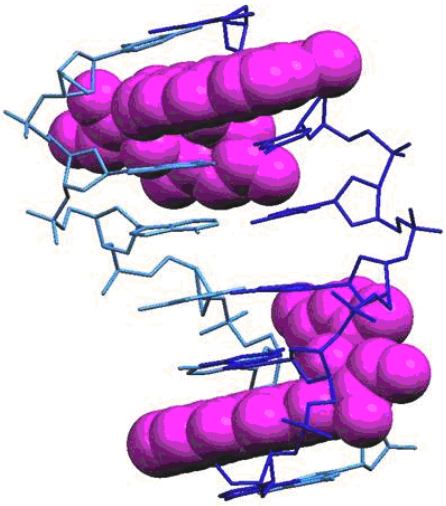

Figure 2 - Structure of a DNA oligonucleotide with two intercalated doxorubicin molecules (shown in pink)

Coordination crosslinking and alkylation of DNA

Another mechanism of action of anticancer agents is irreversible damage of DNA leading to cell death by apoptosis of necrosis.[3] Alkylation agents destroy DNA by alkylation of nitrogen atoms. Bis-alkylating agents are significantly more effective than monoalkylating, because they covalently crosslink DNA. Crosslinking DNA is much more difficult for the cell to repair than alteration of just one base. Alkylating agents are the oldest group of anticancer agents originating from chemical warfare agents of World War I – nitrogen mustard, also called nitrogen yperite. DNA-alkylating agents are very effective, however suffer from severe side effects and are extremely mutagenic and carcinogenic. Cyclophosphamide, melphalan, lomustine and busulfan are known examples of DNA alkylating agents.[4]

Closely related to alkylating agents in the mechanism of action are platinum cancerostatics, cisplatin being the first and still in use example, although newer drugs of this group are available (nedaplatin, oxaliplatin etc.)[5]. Platinum cancerostatics crosslink DNA strands by coordination of platinum to nitrogen atoms of DNA bases. They have some side effects (nausea, nefrotoxicity being the most prominent), but are extremely efficient in some cases, e.g. testicular cancer.

Altering of nucleotide and DNA biosynthesis

The nucleotide antimetabolites are structural analogues of nucleotides that are incorporated into cell components as if they were the essential pyrimidine or purine nucleosides, and as a consequence, disrupt the synthesis of nucleic acids. These compounds are currently more used as anvirotics (e.g., azidothymidine, adefovir or aciclovir)[6, 7, 8] than as cancerostatics. Other antimetabolites disrupt essential enzymatic processes of nucleotide metabolism – such as 5-fluorouracil (inhibiting thymidine biosynthesis) [9] or inhibit folic acid metabolism (metothrexate, raltitrexed). Antimetabolites usually suffer from fewer side effects than most other groups. Involved in the biosynthesis of nucleotides they are usually not mutagenic so they can be used also in non-cancer applications, such as treatment of psoriasis (methotrexate) or warts (5-fluorouracil).

Specific group of nucleotide antimetabolites are hypomethylation drugs such as decitabine[10, 11]. They block DNA methylation, causing epigenetic changes leading to decreased cell division. Hypomethylation drugs have very little side effects, however are effective only in specific cases (myelodysplastic syndrome).

Inhibitors of mitotic spindle

Mitotic spindle inhibitors bind to microtubular proteins and block their ability to polymerize or depolymerize, a process which halts nuclear division or leads to polyploidia[12], which is lethal for mammalian cells. The most known examples of mitotic spindle inhibitors are palcitaxel, docetaxel, vincristine and vinblastine. Colchicine, very potent mitotic spindle inhibitor, has found its use in the treatment of gout. Mitotic spindle inhibitors are very effective; however suffer from severe side effects (myelotoxicity, etc.).

All the above named mechanisms of action can be very effective in destruction of cancer cells. However, cancerostatics often suffer from very significant side effects due to similarity of cancer and healthy cells and therefore it is necessary to lower their dosage to avoid a damage of non-cancer "healthy" cells. In this case, polymers as carriers for several cancerostatics can be a possibility of lowering these unwanted side effects – e.g. the results of clinical testing have shown that for example a polymeric conjugate of doxorubicin has lower non-specific toxicity than a free drug [13, 14]. Its maximum allowed amount (MAA) is 320 mg/m^2 which is 4 to 5 times higher than the clinical amount of free doxorubicin (60-80 mg/m^2)* normally used [15]. Disadvantage of its polymer conjugates is a relatively complex structure requiring inclusion of a peptide sequence from which the drug is released by peptidases, (mostly the GlyPheLeuGly tetrapeptide link), which makes the synthesis more complicated and expensive and also the structure is less defined. [16] One of the convenient solutions, if we want to keep the cancerostatical strategy in cancer therapy, could be a usage of a decreased amount of cancerostatics together with locally functioning radionuclide on the polymeric carrier.

1.2. Biological effects of ionizing radiation

When an organic compound is irradiated by ionizing radiation, consequent ionization of atoms can lead to a number of changes and reactions. Ionized atoms are released from chemical bonds resulting in dissociation of molecules. This process is called *radiolysis*. Atoms and molecules released within radiolysis are ionized with unpaired electrons.

The rate of physico-chemical effects of ionizing radiation on matter (including also a biological material –tissue etc.) is equal to concentration of newly created ions in certain volume of the matter. This concentration of ions is equal to energy of radiation absorbed by this volume. The dosimetrical expression describing physical-chemical and furthermore biological effects of ionizing radiation on matter is called *dose* (**D**).[17]

Dose is general sum, not describing immediate distribution of energy transformed to matter by ionizing radiation. The local distribution of energy significantly influences concrete physical, chemical and biological processes. The energy loss after interaction of radiation with matter is described by Linear Energy Transfer (LET). If the radius of radiation is short (for α radiation), the absorbed energy is distributed along short path, though the ions along the

* both - the weight and height of the patient has to be evaluated, therefore the doses are usually given in mg/m^2

path are distributed with high density. The higher distribution of ions, the lower probability of their recombination before reaction with other molecules around and this leads to more significant chemical effect of radiation, for tissues also higher radiobiological effectiveness.

The main building units of tissues are cells, but the radiobiological effects are manifested through events taking place at the subcellular level. Following what was written about DNA in previous chapter, the most important factor for the fate of irradiated cell is the effect of radiation on DNA structure and its ability of reparation. This is important especially when considering "densely" ionizing radiation (α, β) that induces DNA double strand breaks, which are difficult to repair, resulting in a higher radiobiological effectiveness of ionizing radiation including increased risk of stochastic effects – i.e. tumor origins etc.

1.3. Radionuclides in medicine

Progress in radionuclide application is closely linked not only to development in nuclear medicine and biology but also to chemistry research and development of visualizing and measuring devices.

Applications of radionuclides in medicine have been known more than 45 years and particularly diagnostic preparations and the area of their use is still growing.

Diagnostic radionuclides are nowadays applied for imaging of tissues for various purposes.

It is not only a diagnostics of cancer, but also non-oncological applications – e.g., measurement of pulmonary ventilation, infarction diagnostics, brain imaging, etc.

According to their physical properties radionuclides are used for radiodiagnostics or radiotherapy.

Diagnostic radionuclides are emitters of β^+ and γ radiation. In case of γ radiation, which is emitted by spontaneous emission from, e.g., nuclear isomer ^{99m}Tc (isomeric transition, (IT), $T_{1/2}$ = 6 hours, $E_\gamma = 140$ keV, $I_\gamma = 89\%$) **[18]** by transition to ground state of nucleus ^{99}Tc, a gamma camera or Single Photon Emission Computed Tomography (SPECT) is used. Single-photon emission computed tomography is a nuclear medicine tomographic imaging technique using gamma rays. It is very similar to conventional nuclear medicine planar imaging using a gamma camera. However, it is able to provide true 3D information. **[19]**

A SPECT scan integrates two technologies to view the body: computed tomography (CT) and a radioactive tracer. The technology of single photon emission tomography arises from positioning the camera head at multiple angles around the body accumulating as many as 180° of views at specific angular intervals. A certain number of counts are obtained from each view

and together with the consequent computer analysis create the 3D picture of the investigated tissue.

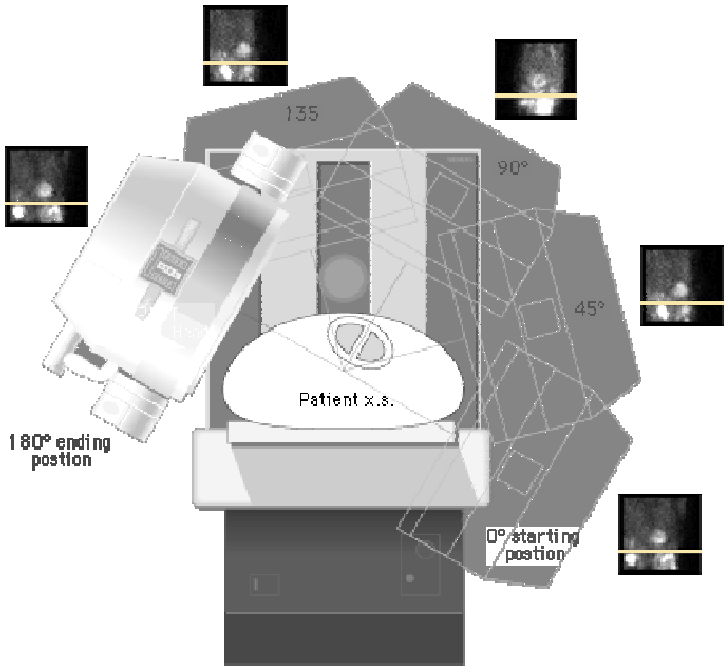

Figure 3 - Collection of scans in SPECT [20]

For positronic emitters eligible for nuclear medicine is important to have β^+ decay as predominant mode of decay for a given radionuclide. For Positron Emission Tomography (PET) imaging (scheme of principle in Figure 4) it is necessary to have the disintegration of nucleus without following γ radiation with energy close to annihilation energy value 511 keV and also with as low positron energy as possible to achieve maximal spatial resolution of the image. The system detects pairs of gamma rays emitted indirectly by a positron-emitting radionuclide (tracer), which is introduced into the body on a carrier molecule. Three-dimensional images of tracer concentration within the body are then constructed by computer analysis.

An often used emitter is for example ^{18}F with short half life ($T_{1/2}$ = 110 minutes) that requires quite rapid preparation and transportation of the radiopharmaceutical substance to clinic and its immediate administration. In order to monitor certain metabolic processes with slower kinetics, considerable effort has been made for finding pharmaceutically suitable positronic emitters with longer half life and their introduction in practice – e.g. ^{64}Cu (T = 12,7 hours) or ^{124}I (T = 4,2 days). **[18]**

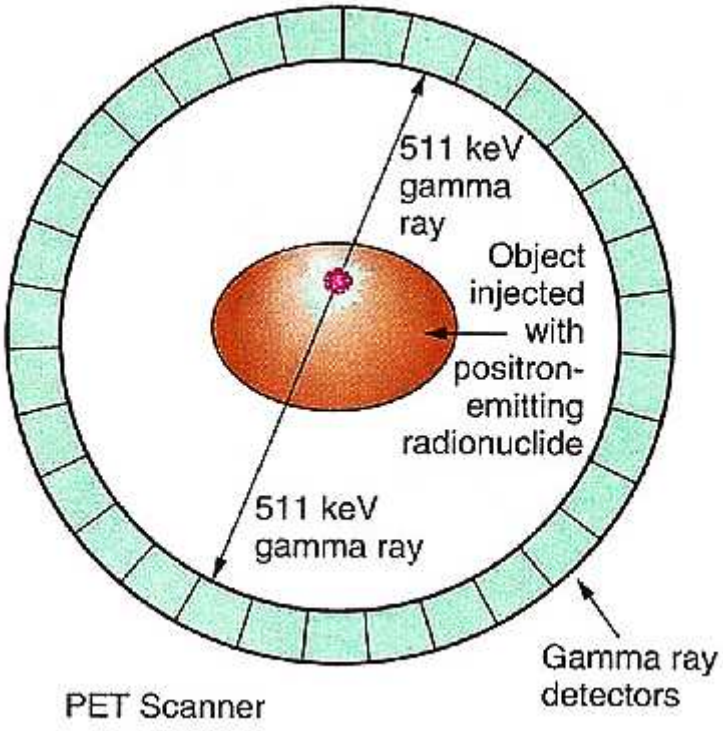

Figure 4 – principle of Positron Emission Tomography PET [21]

However, a number of radionuclides have proved their usability and they have been already used for many years in medicinal practice - in diagnostic applications, the well-known radionuclide ^{99m}Tc can be named [22]. ^{99m}Tc is nowadays a part of more than 30 different radiopharmaceuticals and in the year 2000 its worldwide production was estimated to be 220 TBq weekly. Other similarly widespread radionuclide is ^{18}F which is most used in the form of diagnostic preparative FDG, i.e. 2-fluoro-2-deoxy-D-glucose labeled with ^{18}F. [23]

Representation of individual diagnostic radionuclides significantly outweighs the representation of radionuclides for therapy and includes 90% of overall medicinal radionuclides.

The goal of radiotherapy is to deliver therapeutic doses into target tissue without affecting critical organs. The response of an organ or tissue to ionizing radiation depends on the sensitivity of the individual cells and the rate of the cell proliferation. Total radiation dose and the volume of tissue irradiated are also among the major determinants that regulate the nature of the response. How effective the radiopharmaceutical will be is a function primarily of the absorbed dose rate and the total absorbed dose delivered to a tumor and to surrounding normal tissues. The dose depends on the injected activity, kinetics of its uptake and clearance of radioactivity within the tissues and also on the physical properties of the radionuclide – i.e. type of radiation, range of emitted particles etc.

Radionuclides for therapy in nuclear medicine are β-particles emitting isotopes, Auger electrons emitters and the use of α-emitters for these purposes is being investigated as well. [24, 25] Physical characteristics of radionuclides eligible for cancer therapy are listed in Table 1. Particles from these radioactive emissions produce tracks along with energy transferred to and deposited in biologic matter. The intensity of energy transfer varies and depends on the energy, charge, and mass of the traversing particle. The term linear energy transfer (LET) describes the transfer of energy along the track traversed by the particle. The LET of the β-particle emitters, such as ^{131}I and ^{90}Y, is low (0.2 keV/μm approximately) and the particle traverse several millimeters and they are quite inefficient in damaging DNA of the cancer cells. On the contrary, the LET of α-particles emitted from e.g. ^{211}At or ^{213}Bi and of Auger electrons emitted by e.g. ^{125}I is high.

Table 1 – Physical Characteristics of Therapeutic Radionuclides[22]

Decay mode	Particles	Energy	Range
α	helium nuclei	high (several MeV)	50-100 μm
β	electrons	medium-to-high (0.5-2.3 MeV)	1-12 mm
EC/IT	Auger electrons	very low (eV-keV)	several nm

Consequently, their use as therapeutic agents predicates the presence of high radionuclide concentrations within the targeted tissue.

Therefore, it is quite often complicated to find a suitable radionuclide for each therapeutic use. Aside from well-defined binding to carrier molecule of usually very complicated organic compound, the selected radionuclide must also meet other requirements – such as appropriate half time of disintegration and low radiotoxicity, in order to consider the use of the radionuclide in practice – i.e. application in living organism.

The application of α-particles in medicine requires a broad research because compounds radiolabeled with α-emitters are, due to the characteristics of α radiation, closely monitored for radiotoxicity, whereas all the radionuclides used in this work are β-emitters with very low radiotoxicity.

For the application of radiolabeled ligands *in vivo*, limiting factors are affinity and quantity of receptors for a biotic component of the drug in organism. Moreover, pharmacologically

effective compounds – e.g. peptides (bombesin, lanreotide or octreotide) are tolerated by the organism just in certain low concentrations, because the cell receptors are saturated at a certain level [26]. For therapeutical applications it is appropriate to use radionuclides with high specific activity to reach lower doses of desired drug. Therefore, in case of radionuclides used for both diagnosis and treatment of cancer, it is ideal to have a carrier-free radionuclide or a radionuclide (or its compound) of high specific activity.

Furthermore, the selection of radionuclide and the connecting radiation dose is also dependent on the nature of the illness - in case of cancer on size and specificity of tumor and its location in the body of the patient. [27]

Generally, the type of isotope is selected with regard to the type of disease - e.g. very small tumors and metastases cannot be effectively treated with radionuclides emitting particles of high tissue permeability – such as pure γ-emitters - which are preferably used only for imaging.

In addition, it would be ideal to use such kind of radionuclide for therapy, whose radiation would be also easy to measure so the effectiveness of the therapy can be monitored in real time (theranostical radionuclide). In practice, the radionuclides which have all types of β decay - i.e. EC, β^+ (for diagnostics) a β^- (for therapy), are not that often used, although the possibility of diagnostic and therapy in one time is possible for example with the radionuclide ^{64}Cu ($T_{1/2}$=12.7 h; β^- 39,6%, $E_{\beta^-,max}$= 573 keV; β^+ 17,4%, $E_{\beta^+,max}$= 655 keV)[18]. On the other hand, the use of isotopic pairs is quite spread because two isotopes of one element are metabolized the same way. Examples of some radioisotopic pairs are in the following table:

Table 2 - Examples of isotopic pairs - for therapy and PET diagnostics [28]

Therapeutical nuclide	$T_{1/2}$ [d]	Diagnostic (PET) nuclide	$T_{1/2}$ [d]	β^+[%]
^{89}Sr	50.5	^{83}Sr	1.35	24
^{131}I	8.04	^{124}I	4.18	13
^{67}Cu	2.58	^{64}Cu	0.53	17.4
^{47}Sc	3.35	$^{43,\ 44}$Sc	0.16, 0.16	84.9
^{111}In	2.81	^{110}In	0.05	62

Knowledge about the permeability of different types of radiation can be also applied to the throughput of radiation through tissues which is shown on schematic skin cut **(Fig. 5).**

Copper-64, mentioned in **Table 2** as typical PET nuclide, possessing all 3 types of β decay, can be used also for therapy and therefore we have here a typical example of multifunctional theranostic agent. The well-established coordination chemistry of copper allows its reaction with a wide variety of chelator systems that can potentially be linked to peptides, *bio*polymers and other biologically relevant molecules. The 12.7-hours half-life of ^{64}Cu provides the flexibility to image both smaller molecules (with faster kinetics) and larger, slower clearing proteins and nanoparticles. Due to the versatility of ^{64}Cu, there has been an abundance of novel research in this area over the past 20 years, primarily in the area of PET imaging, but also for the targeted radiotherapy of cancer. **[29]**

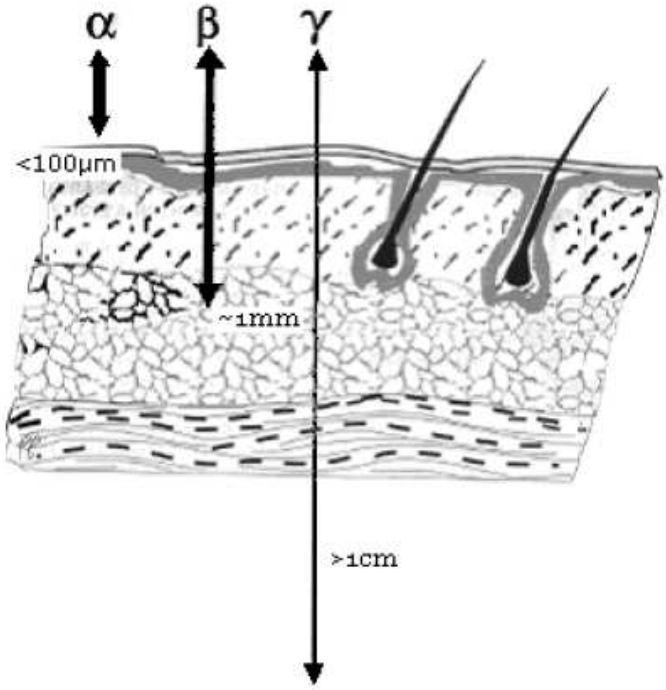

Figure 5 - Penetration of ionizing radiation through skin

Considering non-metal radioactive labels, iodine-125 can be named as another example of theranostic radionuclide that is currently used for several applications in nuclear medicine. ^{125}I ($T_{1/2}$= 59.408 d; EC 100%, E_γ = 35 keV, I_γ = 6.68%; $E_{X\text{-ray}}$ = 27 keV, $I_{X\text{-ray}}$ = 75.7 %)**[18]** is used in biological assays, SPECT imaging and in radiation therapy as brachytherapy for prostate cancer. [30]

As it was discussed in chapter 1.1, it is necessary to lower the dosage of cancerostatical drugs to avoid a damage of non-cancer "healthy" cells.

On the other hand, a combination of radionuclide and cancerostatical drug can lead to more effective intervention against cancer cells. Considering the synergistic effect of therapeutical or theranostic radionuclide together with cancerostatics, the presumed doses of cancerostatics in this case could be much lower.

1.4. Polymer carriers in nuclear medicine

Some of the radiopharmaceuticals are just single ions of the appropriate radionuclide (e.g. I^- for therapy of thyroidea, Tl^+ ion for myocardium diagnostics [31]).

However, most of the radiopharmaceuticals contain (besides the appropriate radionuclide) also a so called *carrier* in various chemical forms. Usually it is a monoclonal antibody and its fragments, or a peptide, polymer, nanoparticle, microsphere or a simple compound of the radionuclide – e.g. the FDG mentioned above. The carrier molecule is responsible for targeting radioactivity where desirable.

For the interconnection between a complex carrier and radionuclide label, a proper connecting functional group – so called *linker* - must exist.

Carriers of all types of therapeutics (i.e. also therapeutical radionuclides) should above all enable prolonged circulation of the therapeutics in blood stream and enable selective targeting to treated tissue - a set of cells (e.g., tumor), individual cell or cell compartments. This way, adverse drug reactions can be reduced, solubility of water-insoluble drugs ensured or the resistance of target tissue to the drug suppressed.

Newly created tumor tissue has many morphological specifics on which the targeting can be based. In most cases there is a higher permeability of vascular system of tumor tissue for larger molecules, which together with missing lymphatic drainage causes accumulation of large molecules in the tissue – so called Enhanced Permeability and Retention effect – EPR effect[32] That is the reason why macromolecules of certain size – molecular weight, micelles, nanoparticles, and liposomes accumulate in tumor tissue, often with up to twenty times higher selectivity rate in comparison with normal tissue[33] According to the interaction, this targeting is called *passive* and it is widely used in designing of the carrier molecule structures for anticancer drugs.[3334, 35, 36, 37, 38, 39]

Particles with sufficient size can also be targeted to tissues in which constriction of capillaries takes place (embolization [40]) , especially if they are applied to arteries nutrient a competent organ – e.g. TheraSphere™[41] particles. EPR effect is quite versatile for many compact tumors, but on the other hand, for radiopharmaceuticals with short half time, the EPR effect is

too slow (accumulation takes hours). Furthermore, the EPR effect targets to interstitial space of the tissue (see Fig. 6), not inside the cells.[42] Therefore it is convenient to combine EPR effect with ligand targeting, pH controlled release (pH of tumor tissue is around 5-6, whereas pH of normal tissue is around 7.4 and pH of endosome around 5) etc.[43]

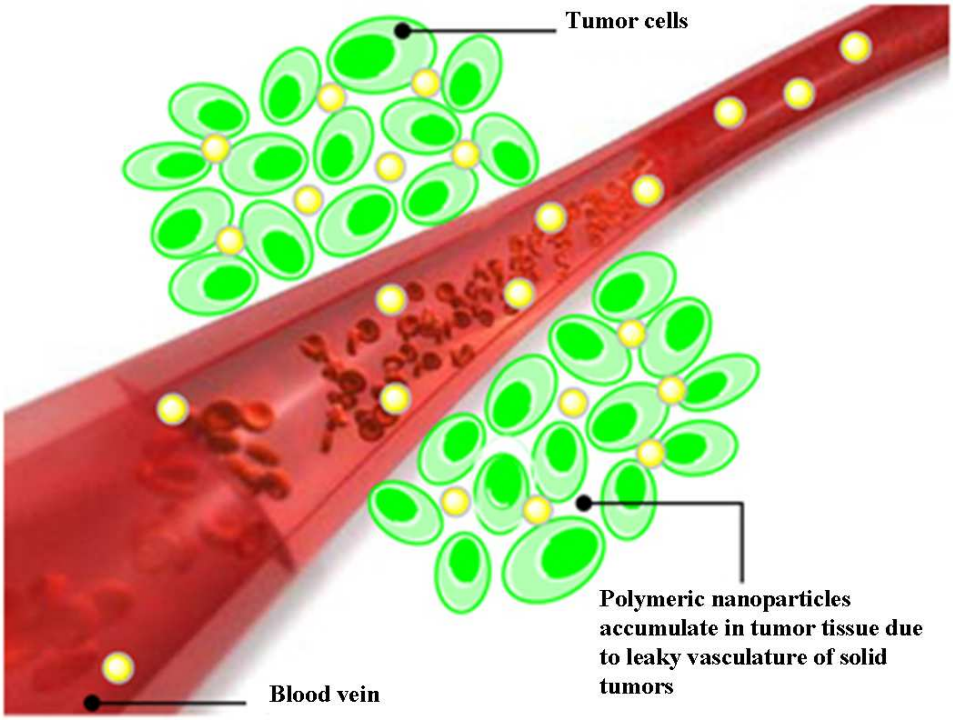

Figure 6 – EPR effect principle[44]

1.5. Radiolabeling of carriers by metal radionuclides

As discussed previously, for radiolabeling of carriers (either polymeric or peptide) with radiometal cations it is necessary to have a suitable interconnection between the carrier and the metal radionuclide. This connection for metal ion radionuclides is realized by chelating agents. The chelating agent is chemically bound to an organic carrier and then through this chelate moiety, the compound is radiolabeled with metal radionuclide.

Generally, bifunctional linkers are used for radiolabeling, containing metal chelating moiety and reactive group enabling covalent attachment to the targeting carrier. Metal chelates are the type of coordination compounds that are created by metal ion reactions with multi-donor base, which is capable to displace water molecules [45] bound via coordination bond to the metal ion. This process can be expressed by the general equation (1.1):

$$\left[\mathrm{ML}_{(n\text{-}1)}\right] + \mathrm{L} \xrightarrow{K_n} \mathrm{ML}_n \qquad (1.1)$$

K_n……consecutive (partial) stability constant

For stability constant K_n we can write the following equation (1.2):

$$K_n = \frac{\left[\mathrm{ML}_n\right]}{\left[\mathrm{ML}_{n-1}\right] \cdot \left[\mathrm{L}\right]} \qquad (1.2)$$

Total stability constant of the process Σ_n is given as product of consecutive constants (1.3):

$$\Sigma_n = K_1 \cdot K_2 ..... \cdot K_n \qquad (1.3)$$

In general, there are the following requirements for both the metal ion and the chelator to form suitable coordinating complex.

Concerning the metal ion, free coordinating spaces given by the free orbitals for its bond to the chelate/ligand must exist. The important feature of the newly created coordination bond between ion and chelate is the stability of the complex.

When the term stability is used in case of coordination compounds there can be two interpretations, thermodynamic or kinetic stability. Thermodynamic stability refers to the change in energy during the process, in which the reactants are transformed to products, i.e., ΔG for the chemical reaction and associated equilibrium constant for the reaction of an aquated metal ion with some other ligand (other than water).

The thermodynamical stability constant describing the coordinating complex forming process is expressed by equation 1.2.

However, the kinetic stability refers to reactivity, generally ligand substitution. Substitution by the ions on the ligand can occur rapidly in some cases and extremely slowly in others depending on the ion radius, chemical structure of the ligand and also sterical hindrance in some cases.

1.6. Polymers with chelating groups and their usage

Also, there is a wide use of polymer matrix with different chelating groups in ion exchange resins in ion exchange chromatography (IEC). For instance, various polymeric sorbents for selective sorption of copper ions in presence of other heavy metal ions were developed for wastewater treatment and hydrometallurgical industry applications. [46, 47, 48, 49, 50, 51, 52, 53, 54] There are also analytical applications for such sorbents, both for pre-concentration of metals before analysis and for the separation of *bio*molecules on chelate-immobilized metal cations (immobilized metal affinity chromatography, IMAC).

1.7. Wilson's disease

Wilson's disease is a genetically conditioned disorder of copper metabolism leading to toxic damage of mainly liver and brain. [55, 56] The cause of the disease is a malfunction of ATPase 7B[57], more than 400 mutations of the respective gene have been described to date. [58]

Average prevalence in population is 1:30 000 [55]. Malfunction of ATPase 7B significantly lowers secretion of copper to bile, which is the main way of elimination of copper from human organism. This leads to accumulation of copper in organism, mainly in liver and central neural system. A Kayser-Fleischer ring (the brown ring on the edge of the iris) is common in Wilson's disease, especially when neurological symptoms are present. Higher concentrations of copper in tissues subsequently lead to a number of symptoms as a result of toxic oxidative stress that damages liver, brain and parenchymal organs.[55, 56, 58, 59] Untreated Wilson's disease is lethal, the most serious complications are liver cirrhosis, portal hypertension and massive bleeding to alimentary tract [55, 60].

The therapy is nowadays based on lowering of copper amounts in organism by administration of low-molecular-weight chelators of copper (II) (penicillamine, triethylenetetramine or tetrathiomolybdate) [55, 58], which leads to lower absorption of copper from food and to its increased elimination from organism. In adjuvant therapy, high doses of zinc(II) salts are administrated because zinc ions competitively block copper uptake from gastrointestinal tract.[55] Unfortunately, suitable forms of zinc are not available worldwide. Current therapy also suffers from serious side effects such as myelosuppression, lupus and penicillamine myasthenia [59, 61] as a consequence of re-formation of complex of essential elements in organism after absorption of chelating agent from gastrointestinal tract. Zinc therapy is typically accompanied with strong gastrointestinal adverse effects, because the typical doses

of zinc are up to 1200 mg / day [62], which is approximately hundred times more than usual daily intake of zinc (ca 8 – 15 mg).[63, 64]

Uptake of copper from food is in average 0.6 – 1.6 mg per day. At the beginning of the therapy of Wilson's disease it is recommended to use diet with low content of copper, *i.e.* avoiding food with high copper content such as liver, nuts or mushrooms [55] (considering the omnipresence of copper in food a copper-less diet is impossible) [65]. Nevertheless, a significant amount of copper is eliminated to alimentary tract and again re-uptaken, this amount represents an even higher amount than that which is present in food (ca 4.4 – 5.3 mg of copper is secreted daily, from which 7 % to saliva, 20 % to gastric juice, 50 % to bile, 18 % to pancreatic juice and 5 % to duodenal secretion). [65]

In this thesis are screened suitable sorbents [containing *N*,*N*-di(2-pyridylmethyl)amine (DPA), triethylenetetraammine (TTA), quinoline-8-ol (8HQ) or 8-hydroxyquinoline-5-sulfonic acid (8HQ5S) chelating groups, respectively] for the entrapment of copper (II) ions. The sorbents are designed for rapidly up-taking copper in gastric milieu and not releasing it under rechelating challenge in intestinal content. Also, the sorbents are not expected to adsorb only copper released from food before it is uptaken, but also to scavenge copper secreted into gastrointestinal tract. After fulfillment of this therapeutic task the sorbents should be eliminated with faeces.

2. Methods of study

2.1. Synthesis of materials

For the described systems (water soluble polymer based macroporous particles and supramolecular polymer particles), the fundamental polymeric backbone or copolymer was prepared by radical polymerization. In case of the polyoxazolines, the preparation of these polymers was done via cationic polymerization route and therefore both polymerization principles are described in following chapters.

2.1.1. Radical polymerization

Radical polymerizations are linear chain reactions by which a polymer is created by the successive addition of free radical.[66] These reactions represent considerable part of the production of polymers worldwide. Active centre in this type of polymerization is a particle

with non-paired electron, called *radical*. Free radicals can be formed via a number of different mechanisms. Monomers of radical polymerizations are usually unsaturated compounds with sterically accessible double-bond carrying substituents withdrawing electrons from this double-bond.

Mechanism of radical polymerization can be divided into four main steps: initiation, propagation, chain transfer reactions and termination. As it was written in the previous paragraph, there are several ways, in which the radical centers are formed during the initiation step – e.g. photoinitiation, thermal initiation, and initiation by initiators. Initiators are compounds whose thermal, stoichiometric or catalytic decomposition creates primary free radical. The most common initiators are miscellaneous peroxo and azo compounds.[66] The initiator route is the most used way of radical polymerizations initiation.

The initiator used within this work was azobisisobutyronitrile (AIBN). The principle of formation of the radical from this compound is shown in Figure 7.

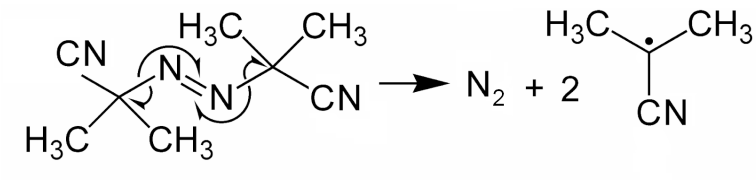

Figure 7 – Scheme of radical formation from AIBN

In propagation macromolecules are created as products of sequential addition of ending radicals on double bond of molecules of monomer. Stereochemical control on radical propagation is practically limited to je sterical effects of substituents and influence of solvate shells of growth sites of monomer molecules. Generally, propagation is not limited by temperature; high temperature is usually needed for initiation, whereas propagation can proceed even under very low temperatures.

Termination is a process when the growth sites of macromolecular chains definitively extinguish. Polymer radical reactions are characterized by spontaneous termination via bilateral reaction of radicals which proceeds like recombination or disproportionation.

2.1.1.1. Radical polymerization in solution

All the radical polymerizations in proposed projects were carried out in solution – i.e. where reaction mixture contains also a solvent. Obviously, the solvent must not react with the

monomer and after the reaction, the polymer stays dissolved inside the reaction mixture, and some increase of viscosity in the reaction mixture can be observed.

The resulting polymer solution is usually poured to intensively stirred precipitating (coagulating) agent – e.g. methanol, ethanol, diethyl ether etc. and the precipitated polymer is isolated by decantation or filtration. Precipitation is also convenient from the polymer purity point of view, because the initiator residua can be removed and the purity of the product can be more increased by repeating the dissolution – precipitation process.

2.1.1.2. Suspension radical polymerization

Suspension radical polymerization belongs upon the heterogenic polymerization group. The reaction initiator is dissolved in the monomer; then is immersed in the water, where surface-stabilized droplets are formed.[66] The micelles are stabilized by a protective colloid, and after the reaction temperature set up, each micelle represents a little reactor in which proceeds the non-solvent reaction. As a result, the re is a suspension of polymeric particles that can be isolated directly or after coagulation by filtration. This method was used in preparation of selective sorbents for the Wilson's disease treatment.

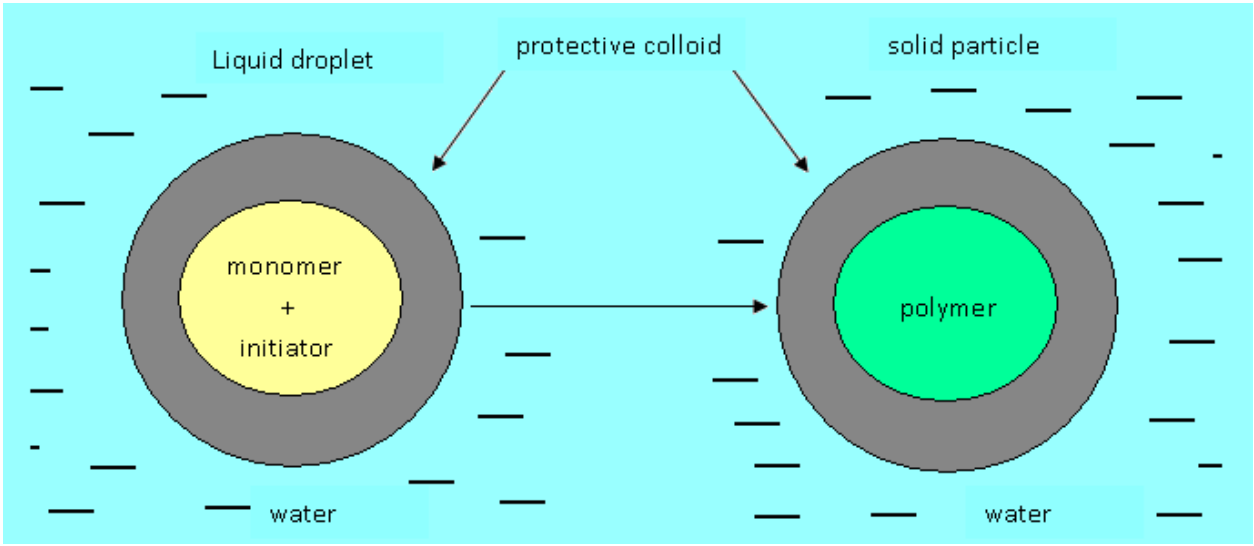

Figure 8 – Scheme of suspension radical polymerization process

2.1.2. Cationic polymerization

The preparation of poly(2-alkyl-2-)oxazolines was performed by living cationic ring opening polymerization. The living cationic polymerization is a group of polymerizations where the reaction mixture contains only cations as active centers of the consequent polymerization with low molecular weight counteranions. [66] This procedure enables obtaining polymers with extremely narrow polydispersity. However, this particular reaction is very sensitive to every impurity, especially water, because water can cause unwanted side reactions – such as transfers and termination of the polymerization. The polymerization of the oxazolines proceeds according to the following scheme (Fig. 9).

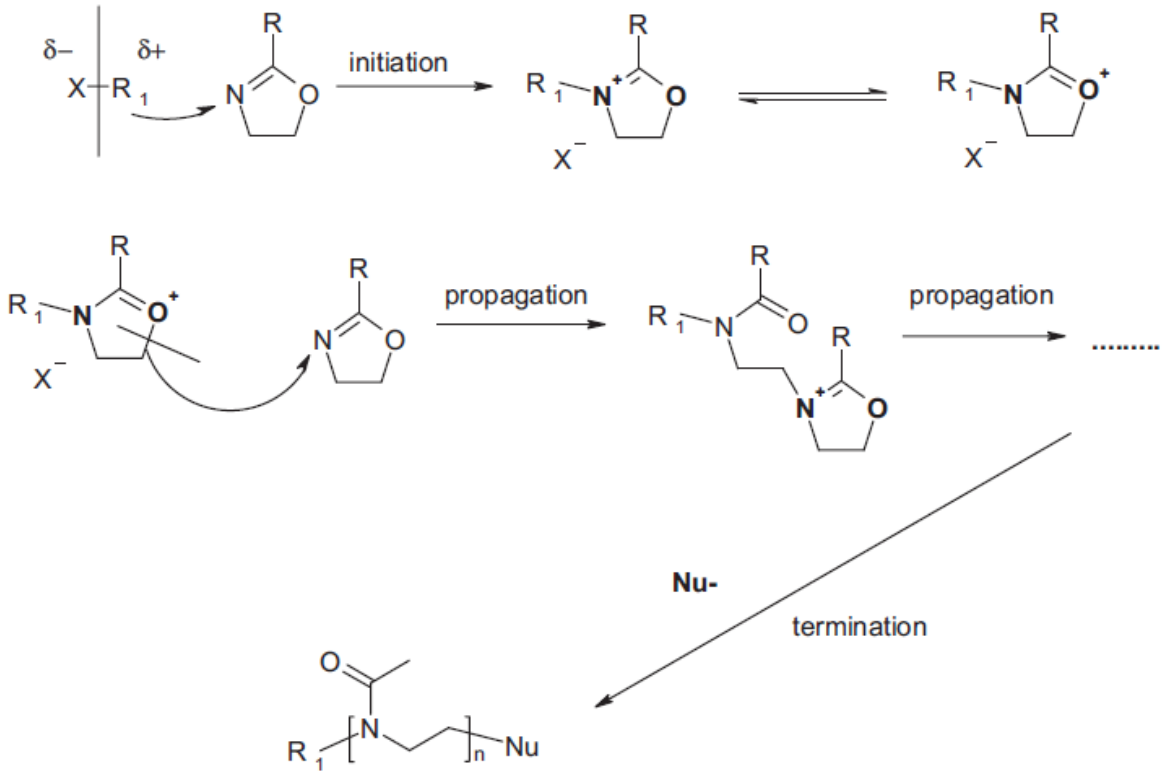

Figure 9 – Ring opening polymerization of oxazolines

2.1.3. Synthetic modifications of polymers

To gather the desired function of our polymer, it is necessary to modify the already synthesized polymer – i.e. chemically bind the functional group to it. First of all it is essential to know which part of the polymer interacts with the introduced reactant and also to control whether the way of binding to the polymer can be realized just in one way. In other words, if there is a possibility that the reactant can attack the polymer and make the bond on a different atom than is desired, it is necessary to work with an intermediate with a protecting group. The deprotection follows after the reactant is bound to the polymer with subsequent deprotection.

2.1.4. Particle formation

As a part of the chemical modification of polymer, the consequential phenomenon such as micellization or formation of highly organized supramolecular structures can be observed. The formation of supramolecular structure is a very complex phenomenon and therefore various methods of investigation were applied for their evaluation.

2.2. Radiolabeling

In general, the use of radioactive nuclides for labeling organic compounds is more versatile than the use of stable nuclides for this purpose.

In case of the radiolabeling of organic compounds, there are several requirements for achieving the desired labeled compound. First of all, the labeling efficiency must be highly specific. This requirement is usually met within radiolabeling by metal labels where the radiometal label is bound via donor-acceptor bond to the ligand. The specificity of the bond between carrier and label can be decreased in case of radioisotopes of iodine, because iodine tends to create also non-covalent bonds with the organic carrier molecule.

Considering the fact that the radioactive label (radioactive metal ion) is in most of the cases in ultra trace concentration (10^{-6} mol.L^{-1} and less), very often instead of concentration expression of amount, the expression of its activity is given. For these purposes, the relation (equation 2.1) between mass and activity of the radiolabel is used.

$$m = 2.4 \cdot 10^{-24} M \cdot A \cdot T_{1/2} \qquad (2.1)$$

A...activity of the nuclide

m...mass of the radionuclide in grams

M...relative atom/molecular weight

The constant $2.4 \cdot 10^{-24}$ derives from fraction $\frac{1}{\ln 2 \cdot N_A}$ in following equations (2.2-2.4):

$$A = \lambda_t N \tag{2.2}$$

$$T_{1/2} = \frac{\ln 2}{\lambda_t} \tag{2.3}$$

$$=> \; A \cdot T_{1/2} = N \cdot \ln 2 \tag{2.4}$$

$$m = \mathbf{n}.\, M = \frac{N}{N_A} \cdot M = M \cdot A \cdot T_{1/2} \cdot \frac{1}{\ln 2 \cdot N_A} = 2.4 \cdot 10^{-24} M \cdot A \cdot T_{1/2}$$

where **n** is amount of substance in mol, N is a number of particles, λ_t is decay constant and N_A is Avogadro's constant.

The validity of equation (2.1) can be easily proved on concrete example of 1 g of ^{226}Ra ($T_{1/2}$ = 1600 years). The activity of this amount of radium is a well-known definition value of 1 Curie (1 Ci) in actual units equal to $3.7 \cdot 10^{10}$ Bq.

2.3. Light Scattering

Almost all objects scatter light that illuminates them into all directions. Light scattering can be considered as the deflection of a ray from a straight path, for example by irregularities in the propagation medium, particles, or at the interface between two media. **Figure 10** shows light scattering off a particle in solution or in vacuum. The intensity of the scattered light depends on the *polarizability* (this term is defined later) and the polarizability depends on the molecular weight. This attribute of light scattering makes it a valuable tool for measuring molecular weight – especially for the macromolecules.

Because the intensity of scattered light depends on concentration and molecular weight of the particle, light scattering will depend on weight average molecular weight. This result contrasts to colligative properties, such as osmotic pressure, which only depend on number of particles and therefore give the number average molecular weight. Besides molecular weight dependence, light scattering also has a direct dependence on particle size. For polymer

solutions, this dependence on size can be used to measure the radius of gyration of the polymer molecule. As with osmotic pressure, we expect all light scattering experiments to be done in non-ideal solutions. Nonideality in general complicates the analysis of data. On the other hand, it allows us to determine second virial coefficient, A_2.

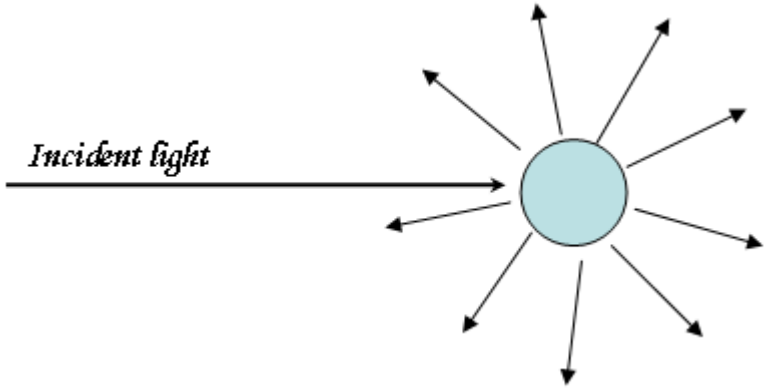

Figure 10 - Scattering of incident light off a particle in solution or in vacuum

In summary, a static light scattering experiment allows to obtain three important characteristics of polymers: weight average molecular weight ($\overline{M_W}$), mean squared radius of gyration ($\left\langle R_g^{\,2} \right\rangle$), and the second virial coefficient (A_2). **[67]**

Considering the fact that the static light scattering theories were for this work used only for determination of molecular weights of polymers (light scattering method is the only way how to determine the absolute value of $\overline{M_W}$), deeper theoretic background will not be discussed. The main instrument for investigation of the particles and their behavior is the application of dynamic light scattering theory and therefore the next chapter comprises a more detailed description of this topic.

2.3.1. Dynamic light scattering

Dynamic light scattering - DLS is a generic term for the light scattering methods comprising all of the scattering methods that provide information on molecular dynamics. **[68]**

On the contrary with static light scattering experiment, in DLS time-dependent fluctuations of the scattering intensity I (q,t) due to Brownian motion of the molecules in solution are detected and the scattering signal is further analyzed via transfer into correlation function. The scattering vector q determines the length over which molecular motions are detected and is defined by equation (2.5):

$$q = \frac{4\pi}{\lambda}\sin\left(\frac{\theta}{2}\right) \tag{2.5}$$

where θ is the scattering angle.

The resulting correlation function (where τ is the delay time) [69]:

$$G(\tau) = \frac{\langle I(t)I(t+\tau)\rangle}{\langle I(t)\rangle^2} \tag{2.6}$$

is accumulated during the experiment where the intensity $I(t)$ is measured and it is expected to show under ideal conditions a single exponential decay:

$$G(\tau) = Ae^{-Dq^2} + B \tag{2.7}$$

where D is the diffusion coefficient of the investigated molecules and A, B are constants – A-amplitude, B - baseline. At short time delays (small τ), the correlation is high because the particles do not have enough time to move to great distance from the initial state that they were in. These two signals are therefore the same when compared after only a very short time interval. As the time delays extends, the correlation decays exponentially, i.e., after a long time period has elapsed, there is no correlation between the scattered intensity of the initial and final state. This exponential decay is related to the motion of the particles, specifically to the diffusion coefficient. The diffusion coefficient is then possible to be counted from Stokes-Einstein relation:

$$D = \frac{k_B T}{6\pi\eta R_H} \tag{2.8}$$

where R_H is hydrodynamic radius, k_B is the universal Boltzmann constant, η the viscosity of the solvent and T absolute temperature. The diffusion coefficient is though convertible into hydrodynamic radius R_H. The hydrodynamic radius represents the size of sphere that has the same diffusion behavior (expressed by D) as the studied particle.

All the scattering methods can provide information about the properties of the system considering the wavelengths of the source used in this technique. For some applications, complementary techniques such as X-ray, neutron and gamma ray scattering, are used. These

methods provide information on shorter wavelength scale and therefore offer additional experimental data that cannot be obtained only by light scattering experiments with "long" wavelengths. The comparison of the most known scattering methods is summarized in Table 3:

Table 3 -Comparison of scattering methods

Method	*Abbreviation*	*λ range*	*information obtained*
Static and Dynamic Light Scattering	DLS	*visible light*	diffusion coefficient (*D*) radius of gyration (R_g) weight average molecular weight (M_w)
Small-angle X-ray Scattering	SAXS	λ ~0.1 nm	shape ,size and structure
Small-angle Neutron Scattering	SANS	λ ~0.1 nm-2 nm	

For the complete understanding of the macromolecular systems, although light scattering methods are very valuable tools, additional complementary techniques – such as various microscopic methods are usually required.

2.4. Small-angle X-ray scattering

Small angle X-ray scattering (SAXS) belongs to the group of methods in which the scattering of electromagnetic waves is used to examine small particles (approximately with diameter around 5-100 nm). This method is mostly applied in investigation of highly organized materials, in size ranges of approximately 1 to 100 nm. SAXS is a technique where the X-rays (typical λ: 0.1- 0.2 nm) by elastic scattering interact with the sample. Suitable X-ray wavelengths are typically generated at synchrotrons or in-house X-ray sources. In case of SAXS the data are recorded at very low angles (typically 0.1 - 10°). This angular range contains information about the shape and size of macromolecules **[70]**, characteristic distances of partially ordered materials, pore sizes, and other data – in the scattering curve. SAXS is capable of delivering structural information of macromolecules between 5 and 25 nm.**[71]**

This method is applicable in solid state as well as in melt and solution [72] to study the organization of membranes and of biopolymers (like DNA and proteins), their interactions, to study the transition and structure organization of different phases in solid materials, gels etc.
With these fundamentals and with the results obtained from calculation of theoretical relations between structure and scattering, we are able to derive probable structure model of our sample.
SAXS results can be interpreted for example using the Porod's law that predicts a decrease of scattered intensity proportional to q^4 (where q is scattering vector defined by equation 2.5 above) at large values of the scattering vector q the intensity is given by:

$$I(q) = I_e 2\pi\rho^2 \frac{S}{q^4} \tag{2.9}$$

where ρ is the electron density difference between particulate domains and the matrix material, S is a structure factor and I_e is a constant. Small angle X-ray scattering method can help to determine the probable shape of investigated particles by fitting a reference curve for certain shape to the actual measured curve. After this, it is possible to conclude whether the shape predicted from the previous applied techniques corresponds with data from SAXS.

2.5. UV-VIS spectroscopy

Absorption of ultraviolet and visible radiation in organic molecules is restricted to certain functional groups (*chromophores*) that contain valence electrons of low excitation energy.
The rate of absorbed light can be quantified by absorbance that can be determined from Beer-Lambert Law that relates the absorption of light to the properties of the material which the light is proceeding through:

$$\mathbf{A} = \varepsilon \cdot l \cdot c \tag{2.10}$$

where **A** is absorbance, ε molar absorptivity, l optical length (usually cuvette diameter) and c molar concentration of the absorber.
The spectrum of a molecule containing these chromophores is quite complex.
In this work, UV-VIS spectroscopy is not only a tool for quantification of the colored species, but also a primal possibility of complex creation observing of kinetics – because the increasing value of absorbance corresponds with the formation of metal polymer complexes.

2.6. Atomic absorption spectroscopy

This technique can be considered as a part of group of light spectroscopic methods such as UV/VIS Spectroscopy and many others. Atomic absorption spectroscopy (AAS) is used for determination of the concentration of an analyte in a sample. Therefore, in this technique, standards with known analyte content is required to establish the relation between the measured absorbance and the analyte concentration and relies therefore on the Beer-Lambert Law.

In the experimental set-up, the electrons of investigated atoms in atomizer (usually flames, acetylene with a temperature of about 2300 °C and nitrous oxide (N_2O)-acetylene flame with a temperature of about 2700 °C)[73] can be promoted to higher orbitals (excited state) for a short period of time (nanoseconds) by absorbing a defined quantity of energy (radiation of a given wavelength). This amount of energy is specific to a particular electron transition for a concrete element - each wavelength corresponds to only one element, and the width of an absorption line is only of the order of a few picometers, which gives the technique its elemental selectivity. The radiation flux in the atomizer is measured using a detector, and the ratio between the two values (the absorbance) is converted to analyte concentration using the Beer-Lambert Law.

2.7. Atomic force microscopy

The Atomic Force Microscopy (AFM) was developed to overcome a basic drawback with Scanning tunneling microscopy (STM) - that it can only image conducting or semiconducting surfaces. The AFM, however, has the advantage of imaging almost any type of surface, including polymers, ceramics, composites, glass, and biological samples.

The diamond tip contacted the surface directly, with the interatomic van der Waals forces providing the interaction mechanism.

Today, most AFM machines use a laser beam deflection system, where a laser is reflected from the back of the reflective AFM lever and onto a position-sensitive detector. AFM tips and cantilevers are microfabricated from Si or Si_3N_4. Typical tip radius is from a few to tens of nm.

Atomic forces microscopy results were obtained in cooperation with Dr. Eliška Chánová and Dr. Milena Špírková from Institute of Macromolecular Chemistry, Prague.

2.8. Transmission electron microscopy

Transmission electron microscopy is in general similar to optical microscopy, except that the photons are replaced by electrons. Since the wavelength of electrons is shorter than that of photons a higher resolution is achieved.

Because of strong interactions of electron with matter, gas particles must be absent in the system. Recent advances have allowed samples to be imaged using lower vacuums and with partially hydrated samples, and the use of an electron transparent membrane between a biological sample and the vacuum has been shown to allow fully hydrated samples to be imaged, although there is a reduction in resolution.

Electron microscopy is very suitable for investigation of conductive or semi-conductive materials. Non-conductive materials can sometimes be imaged by an electron microscope, however the electron beam will be absorbed by the material, which will change the physical properties of the material (for example, the material can burn off). A common preparation technique is to coat the sample with a several-nanometer layer of conductive material (*e.g.*, by spattering of gold, *etc*.); however this process may disturb delicate samples.

Cryo-electron microscopy (cryo-TEM), or electron cryomicroscopy, is a form of transmission electron microscopy (TEM) where the sample is studied at cryogenic temperatures (generally liquid nitrogen temperatures).

The popularity of cryoelectron microscopy arises from the fact that it allows the observation of specimens that have not been stained or fixed in any way, showing them in their native environment. To carry out a cryo-TEM experiment, a drop of the solution under study was placed on a pretreated copper grid which was coated with a perforated polymer film.

The preparation of the sample film is done under controlled environment conditions, i.e., in a chamber at a constant temperature of 25 ° C and with a relative humidity of 98–99% to avoid evaporation of the liquid. Rapid vitrification of the thin film is achieved by plunging the grid into liquid ethane held just above its freezing point. The sample are then transferred to the electron microscope, where the temperature is kept below –165 °C and the specimen is though protected against atmospheric conditions during the entire procedure to prevent sample perturbation and formation of ice crystals.

Cryo-TEM was performed in cooperation with Dr. G. Karlsson, Uppsala University, Sweden.

3. Results and Discussion

This chapter summarizes the approaches and results contained in publications D1-D7. According to the aims of the thesis, these results address three main research topics.

With respect to funding of each project, the work sometimes proceeded in cooperation with other research subjects and institutions. In each part of the project, further investigation (involving *in vivo* biological tests etc.) of the topic was evaluated individually according to the importance of the results obtained.

3.1. Development of new strategies for labeling of polymers with radiometal cations and their comparison with radioiodination (publications D1, D2, D3)

During the past few years, several polymers intended to be used either for therapeutical or diagnostical purposes in nuclear medicine were synthesized in most cases using radical polymerization or living cationic polymerization route (for polyoxazolines).

Firstly, polymers containing *N*-(2-hydroxypropyl-)methacrylamide (HPMA) or *N*-isopropylacrylamide (NIPAM) were functionalized in order to serve as carriers for the radiolabel **[D1]**. Depending on the chemical character of the radiolabel, corresponding moiety was introduced into the structure of polymer. All available investigated radionuclides with their therapeutical and/or diagnostical utilization are summarized in Table 4, the yields and *in vitro* stabilities of the polymers are summarized in Table 5.

In case of radiolabeling with copper-64, five different polymer structures based on *poly*-HPMA and *poly*-NIPAM in backbone polymer chain were synthesized. These polymers contained different chelating groups : 1,4,7,10-tetraazacyclododecane-1,4,7,10-tetraacetic acid (DOTA), diethylenetriaminepentaacetic acid (DTPA), dipocolylamine, thiosemicarbazone or Ag ionophore II, were synthesized and radiolabeled. Functional groups on polymer chain readily react with [^{64}Cu]$CuCl_2$ and the incorporation was high for all types of functional groups tested, exceeding the value of 90%. After the radiolabeling with copper-64, the *in vitro* stability of these polymers was consequently tested in human serum (for 24 hours) – see Table 5 for details. The stability of all the complexes was sufficient for the diagnostical type of utilization of these polymer vectors of ^{64}Cu.

Table 4 - Available radionuclides

radionuclide	$T_{1/2}$	decay type	utilization
^{125}I	59.4 days	EC	Ther/Diag
^{131}I	8.04 hours	β^-	Ther
^{64}Cu	12.7 hours	β^-, β^+, EC	Ther/Diag
^{90}Y	64 hours	β^-	Ther
^{177}Lu	6.73 days	β^-	Ther
^{111}In	2.81 days	EC	Diag

Ther – therapeutical use, Diag – diagnostical use

Table 5 -Yields and *in vitro* stabilities

polymer	labeling yields [%]	24 hours stability [%]
HPMA-*co*-4-allyl-3-thiosemi-carbazide	96	95
HPMA-*co*-glycidyl methacrylate-dipicolylamine	98	96
NIPAM-*co*-MAEDA-NH-DTPA	95	94
NIPAM-*co*-MAEDA-NH-DOTA	99	94
NIPAM-*co*-NH-Ag-ionophore II	99	93

MAEDA=*N*-[2-(methacryloylamino)ethyl] carbamate

Another approach was applied for the use of azo dye which enables both covalent (for radioiodine isotopes **[D2]**) and also chelating (metal ion radionuclides – ^{111}In) labeling modalities.

This was performed on model polymers prepared by radical polymerization of the main monomer [*N*-(2-hydroxypropyl) methacrylamide for polymer 1 and *N*-isopropyl acrylamide for polymer 2] (see Figure 11) with *N*-tyrosinamide and with AIBN as initiator with good yield in both cases (>80%).

Chelating structures were attached to the phenolic moieties on polymer by azo coupling of the diazotized 4-aminophenyl derivatives of the chelators to the phenolic moiety on the *N*-methacryloyl tyrosinamide monomeric unit.

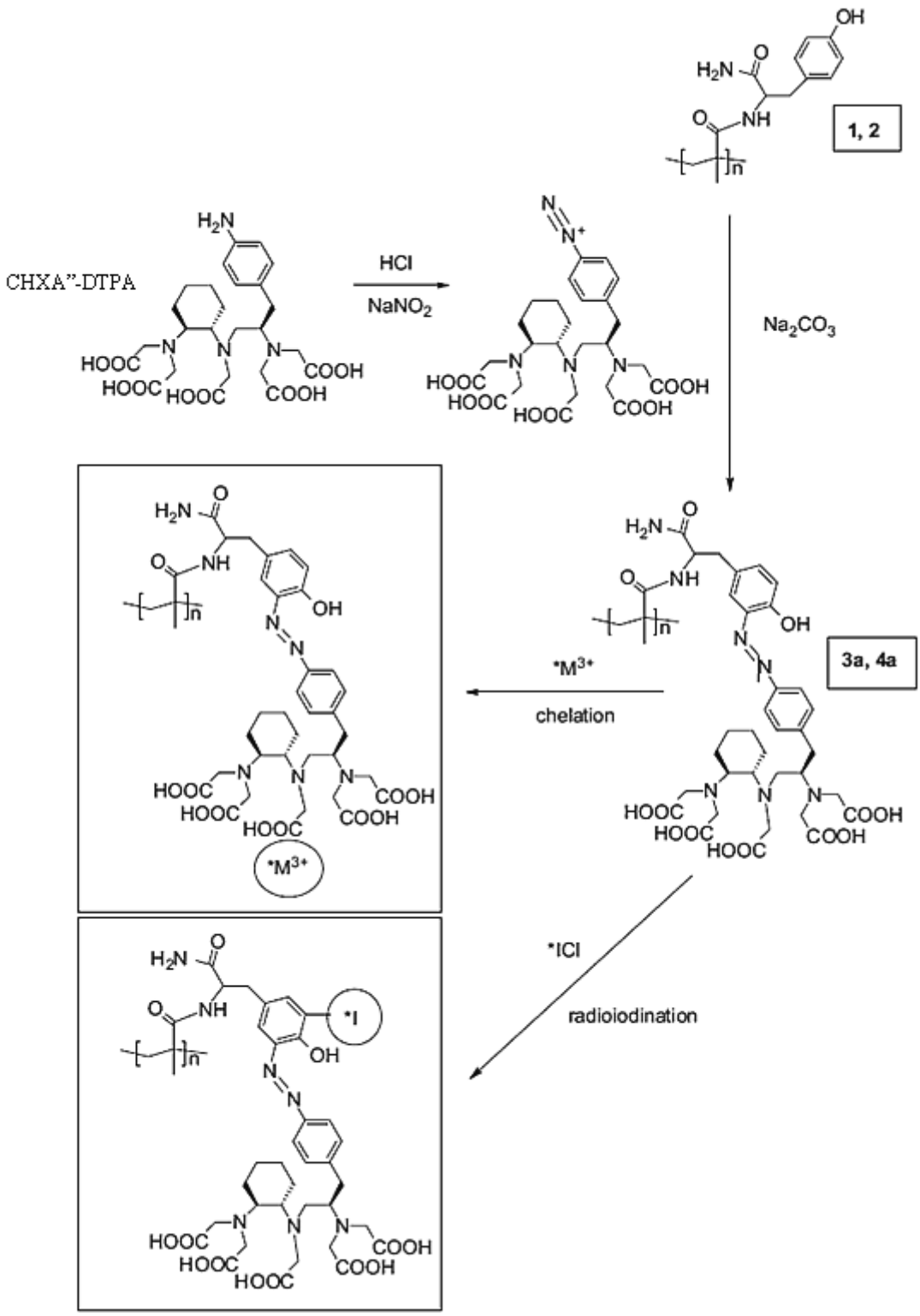

Figure 11 – Introduction of the CHXA"-DTPA chelating group into the copolymers (the *N*-methacryloyl tyrosinamide monomeric unit, which undergoes conjugation is shown only for the polymer in the scheme; the other chelators are used to react in the same way as azo coupling). The polymers 1 and 3 contain *N*-(2-hydroxypropyl)methacrylamide as main monomer and the polymers 2 and 4 contain *N*-isopropyl acrylamide as main monomer

Chelation in the presence of ammonium acetate buffer was used for ^{111}In labeling of the polymers with separation of the labeled polymer from free radionuclide on a PD-10 gel filtration column. ^{111}In labeling proceeds in yields 70–85% for the copolymer 3 and about 60% for the copolymer 4. The lower yield for the copolymer 4 is probably given by the less solvated state and thus higher sterical hindrance of the chelator on the partly hydrophobic thermoresponsive 4a compared to fully hydrophilic 3a. The yields of the ^{111}In labeling are apparently partly worsened by the fact that only the pure polymer containing fractions was taken for the calculation of the yield as polymer peak. Separation of free ^{111}In, in contrast to ^{125}I, needs to be done in solution containing low-molecular-weight ions(ammonium acetate in this case) to avoid ion–ion interactions of the separated species with the column, which however, causes some polymer peak tailing, so some labeled polymer is present in the low-molecular fractions. Stability of the polymer-radionuclide bond under model conditions is an important parameter of characterization of the newly developed labeling strategy. The experimental setup would show not only eventual transchelation or chelate hydrolysis, but also eventual instability due to reversibility of radioiodination or instability of the azo dye bond which is between the polymer and the radionuclide. Stability of the radiolabel was proved by incubation in phosphate buffered saline (PBS) and re-separation on GPC PD10 column. The stability of polymers labeled by ^{111}In, was tested in the presence of environment containing competitive ions in the concentrations typically occurring in blood plasma **[74]**. After 24 hours the stability of the radiolabeled complexes varied from 68% - 88% of the remaining activity based on the measured initial amount of radiolabel, so the stability of most of the polymers in this study was sufficient for *in vivo* experiments.

In following year, systems based on ABA triblock copolymers of poly[2-methyl-2-oxazoline-*block*-(2-isopropyl-2-oxazoline-*co*-2-butyl-2-oxazoline)-*block*-2-methyl-2-oxazoline] (see Figure 12) with two hydrophilic A blocks and one central thermoresponsive B block were synthesized under ring-opening living cationic polymerization **D3**. For detailed chemical composition and properties of ABA triblock copolymers see Table 6.

All of them are soluble in water and molecularly dissolved under the so called cloud point temperature (CPT) of the thermoresponsive B block and form micelles at higher temperature which can be used to enhance the retention of the polymer system in tumor tissue where the temperature is higher than in normal (healthy) tissue.

The temperature-responsive aggregation behavior (see Figure 13 for schematic description) was studied using light scattering methods to characterize temperature-dependent structural behavior of the thermoresponsive polymers with lower critical solubility temperature (LCST).

It was proved that the poly-NIPAM with high molecular weight at low concentrations exists in a coil conformation below the LCST. Approaching the LCST, a homopolymer undergoes a coil-globule transition, wherein the loose macromolecules at first collapse into a compact globule with further aggregation of globules into a mesoglobule. The mesoglobules in this case are uniform and colloidaly stable particles with some amount of water. Once created, with increasing temperature, they tend to shrink.

Our light scattering experiments proved that the synthesized thermosensitive polyoxazolines have similar features to the thermosensitive polymers described above. [D3]

We have completed a basic characterization in water to make the system as principally transparent as possible. In physiological solution (0.9 wt-% NaCl), the temperature-dependent behavior is exactly the same in shape, but everything is shifted 3°C to lower temperatures. All samples visually become turbid when heated above CPT where dynamic light scattering reveals the formation of nanosized objects.

To make the systems labelable with radioiodine, a phenolic moiety was introduced into the structure. Radionuclide labeling was carried out using the chloramine method with good yield (66%). [75] Most of the radioiodine is bound to the polymer by a stable bond and the remaining part was gradually released into low molecular weight fraction during incubation in PBS buffer at 37°C. This means that a part of iodine is bound by a metastable bond; however, if GPC separation on a PD 10 desalting column after 2,5 hours is applied, a more stable product is obtained and the stability should be sufficient for the intended medicinal purposes.

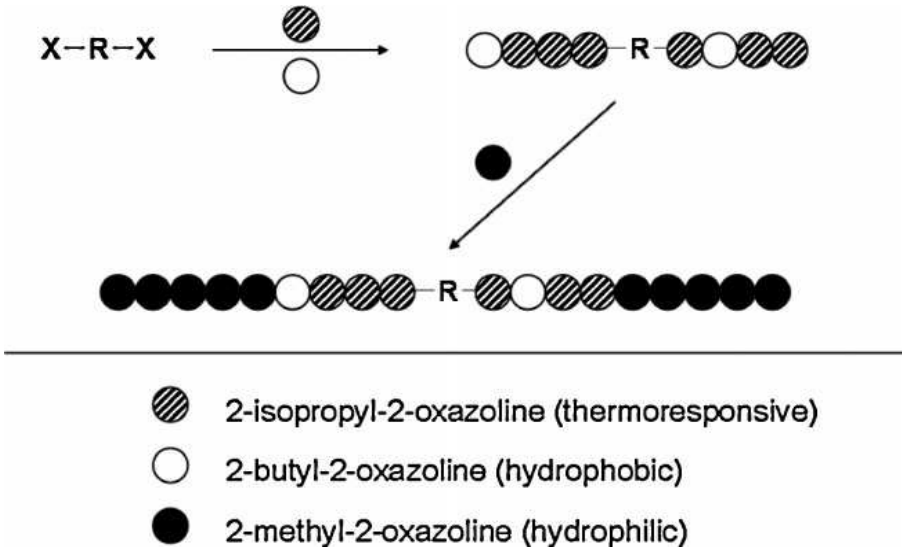

Figure 12 – Schematic illustration of formation of the ABA triblock copolymers

Table 6 -Chemical composition and properties of ABA triblock copolymers poly[2-methyl-2-oxazoline-*block*-(2-isopropyl-2-oxazoline-*co*-2- butyl-2-oxazoline)-*block*-2-methyl-2-oxazoline];

Triblock copolymer	T/H*	BuOX
I	1:2	10
I	1:1	10
I	2:1	10
II	1:2	15
II	1:1	15
II	2:1	15
III	1:2	20
III	1:1	20
III	2:1	20

* T/H – Thermoresponsive to hydrophilic block ratio (w/w); BuOX=2-butyl-2-oxazoline

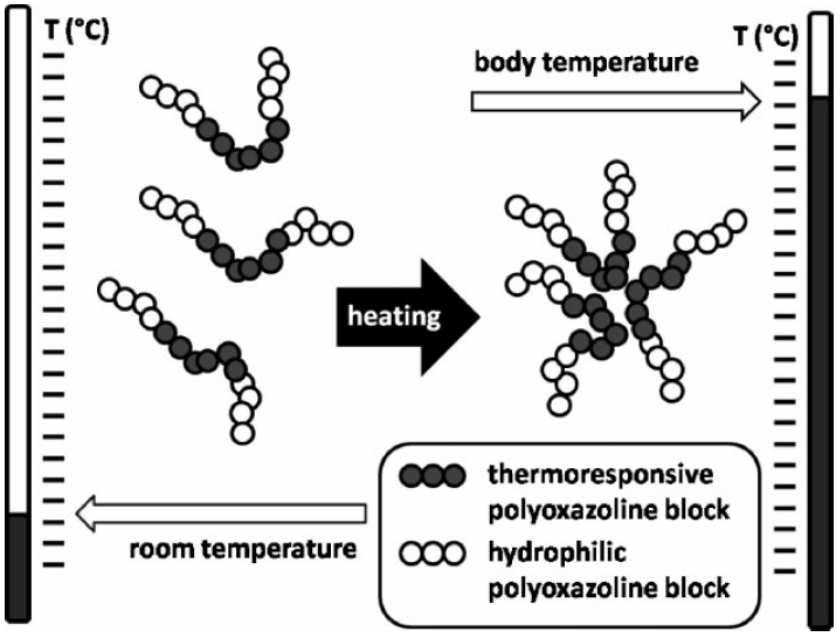

Figure 13 - Temperature-responsive aggregation behavior for ABA triblock copolymers

3.2. Synthesis and studying properties of macroporous metal chelating polymer beads as potential therapeutics intended for radioembolization of liver malignancies and for the therapy of Wilson's disease (publications D4, D7)

The general idea of the polymer beads and their use in medicine is based on their insolubility during their functioning inside the body and their adjustable size.

Radioembolization is a method where microparticles bearing a therapeutical radiolabel or chemotherapeutics are injected into the artery which supplies blood and nutrition to cancer tissue. These microparticles[D4] embolize vessels important for cancer cells growth and the chemotherapeutics or radiation emitted by bound radionuclide (or combination of them) destroys the cancer cells in a way described in chapters 1.1 and 1.2.

For this use, chelating polymer microparticles around 20-40 μm in diameter were prepared. The precursor for the synthesis of chelating microbeads was the epoxide groups containing poly(glycidyl methacrylate-*co*-ethylene dimethacrylate). This polymer allows to introduce both polyacid and quinoline-8-ol-type ligands and assures proper size, mechanical properties and chemical stability.

These beads were reacted with amines to allow attachment of the chelating groups – DOTA, quinoline-8-ol or 8-hydroxyquinoline-5-sulfonic acid group.

For liver malignancies, several radionuclides – such as ^{90}Y, ^{131}I or ^{177}Lu (β-emitters) are used.

The 8-hydroxyquinoline-5-sulfonic acid is in fact same type of ligand as quinoline-8-ol, but contains an additional sulfonic acid group that introduces a negative charge, which is highly advantageous for the binding of Lu^{3+} due to elimination of electrostatic repulsion between lutetium cation bound to the matrix and lutetium cation coming from solution as well as repulsion of the lutetium cation coming from solution with the protonated amines in the polymer matrix. In addition, sulfonic acid group hydrophilizes the whole polymer that further enhances metal ion sorption rate.

All the polymers in our study were quantitatively labeled by ^{177}Lu, the beads containing DOTA however needed heating up to 80° C, whereas polymers with quinoline-8-ol or 8-hydroxyquinoline-5-sulfonic acid moieties were quantitatively radiolabeled within 1 hour of incubation at laboratory temperature. Quinoline-8-ol also allows labeling with ^{131}I, and in this case, the radiolabeling efficiency was 95%. The radiolabeled polymers have undergone stability tests in PBS which showed that after two weeks (approximately two half-lives of

both radionuclides) there was no measurable leak of lutetium-177-labeled beads and 83% of ^{131}I activity remained on beads.

For the therapy of Wilson's disease, we have prepared several selective sorbents based on poly(glycidyl methacrylate-*co*-ethylene dimethacrylate) matrix with particle size 20 – 40 μm. This polymer was synthesized by suspension copolymerization and the chelating group was consequently attached for the copper entrapment. Four sorbents with different Cu^{2+}-chelating moieties [*N*,*N*-di(2-pyridylmethyl)amine, triethylenetetraammine, quinoline-8-ol and 8-hydroxyquinoline-5-sulfonic acid, respectively] were prepared and tested. Under the model conditions their possible use as therapeutics for Wilson's disease treatment was proved. The sorbents effectively and quickly entrap copper in environment modeling gastric content and do not release it significantly in environment modeling intestine content. The sorption is effective even in ultra trace concentration and is not disturbed by zinc salts (see section 1.7.), not even in significant excess, corresponding to therapeutical doses of zinc salts. Also, some primary biological tests were performed to evaluate the potential use of the sorbents. Figure 14 shows the comparison of biodistribution of labeled copper and the polymeric sorbent based on quinoline-8-ol in rats after 8 hours of ingestion. It can be observed that in case of copper without sorbent (a) copper is partially absorbed into the blood and it can be found later in urinary bladder and it is metabolized faster (present in intestine) whereas when sorbent is applied, all copper is present in the alimentary tract (first in stomach and later in intestine) and after 24 hours completely eliminated from body with faeces.

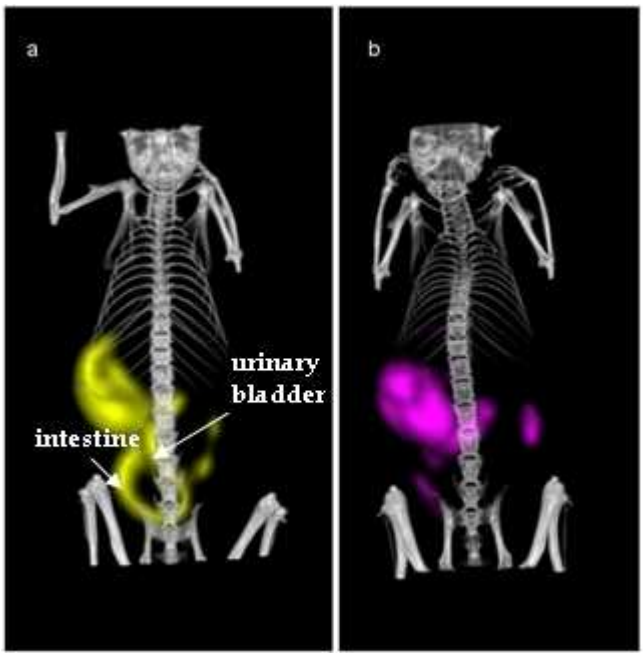

Figure 14 - Biodistribution of copper (a) and sorbent based on quinoline-8-ol (b) both with Cu-64

3.3. Synthesis and studying properties of supramolecular metal cation-assembled core-shell nanoparticles as potential radionuclide theranostics for solid tumors (publications D5, D6)

For this project, the nanoparticles were designed to perform the self-assembly after addition of metal cation to the polymer and also to be biodegradable and have suitable size (to enable targeting via EPR effect). Therefore the polymers consist of hydrophobic backbone bearing chelating group and poly(ethylene oxide) (PEO) grafts as a hydrophilic part.

Systems based on poly(*N*-methyl methacryloyl hydroxamic acid)-*graft*-poly(ethylene oxide) and another on poly{1-[4-(8-hydroxy-quinolin-5-sulfonic acid -7-ylmethyl)-piperazin-1-yl]-propenone-*co*-poly(ethylene oxide) methyl ether methacrylate} were synthesized and completely investigated using methods described in Chapter 2.

The idea of the systems with chelating groups for metal cations derived from the fact that many metal cations are essential for the cell nutrition and these metals (such as iron, copper etc.) are present inside the body. However, the excess of these ions in free form in organism is toxic and therefore they have to be transported in living organisms as chelates. Inside the cells strong biochelation capacity for iron or copper ions is expressed which make these metals available for the organelles. The process of transchelation in which the metal cation is rechelated inside the cell is accompanied with reduction of these metals from Cu^{2+} to Cu^{1+} and from Fe^{3+} to Fe^{2+}.

This mechanism should lead in case of nanoparticles to their biodegradation once they reach their target cell, because the metal ions work as cross-linkers in the whole polymer system and keep the structure together. So, after the entrapment of the cross-linking ion, the polymers would have their molecular weight under the renal threshold and should be released from the organism by kidneys. This phenomenon has not been described by anyone before in literature.

For both of the systems, formation of nanoparticles has been tried with Cu^{2+} and Fe^{3+}ions.

However, the results obtained with copper ions were quite unsatisfactory (were not stable enough), so for the rest of the experiments, iron ions were always added for the preparation of the particles.

In both cases, the complexation capacity of Fe^{3+} for both polymeric systems was studied. The theoretical stoichiometry of polymer with Fe^{3+} was in both cases 3:1. Nevertheless, there are steric considerations that may decrease or increase the real capacity of polymer for complexation of Fe^{3+}. In case of the system with 8-hydroxyquinoline-5-sulfonic acid the real capacity for $Fe^{3+}$is close to 100% of the theoretical capacity (90%). This was different in the

system with hydroxamic acid groups, for which the real capacity was considerably lower than the theoretical capacity (60-70%).

Such a difference in complex capacity was attributed to the kinetics of nanoparticle formation. In system with hydroxamic acid groups, the nanoparticles are formed within milliseconds; thus, there is not enough time for steric rearrangement and exploitation of the chelating capacity of the polymer. On the other hand, the chelate formation of polymer with 8-hydroxyquinoline-5-sulfonic acid proceeds within minutes. This additional time is probably sufficient for steric rearrangement and hence higher chelating capacity of the polymer.

The prepared nanoparticles are in both cases spherical with internal structure and differ in size. For the system with hydroxamic acid groups the Cryo-TEM revealed a core-shell structure and the diameter of the particle was confirmed by AFM and Cryo-TEM around 100-200 nm (Figures 15 and 16).

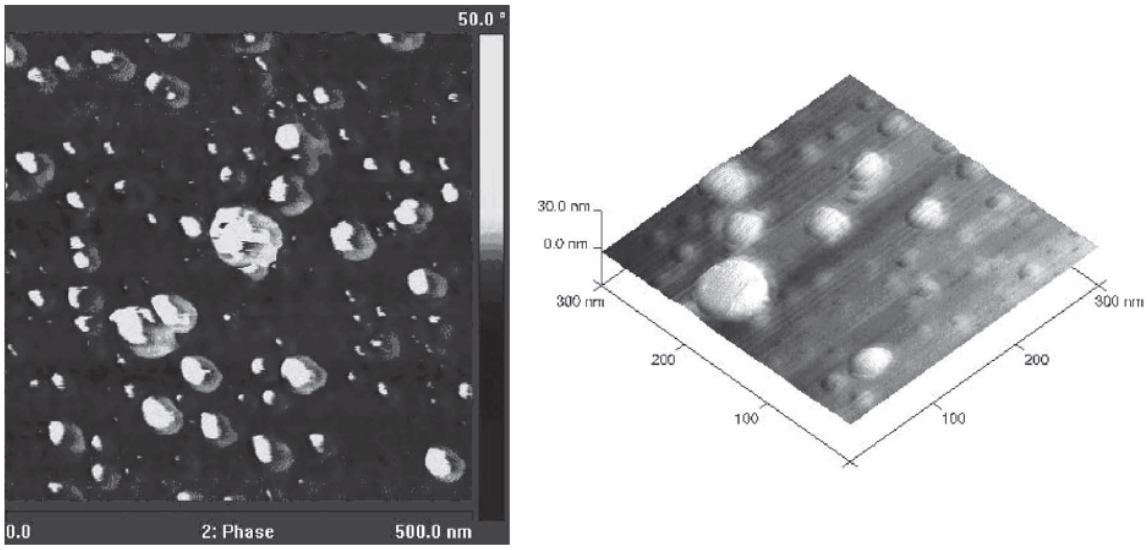

Figure 15 – AFM images of Fe^{3+}-assembled nanoparticles based on polyhydroxamic acid

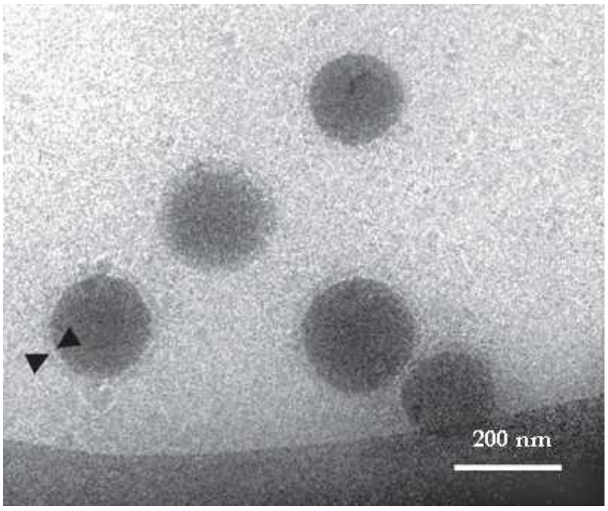

Figure 16 – Cryo-TEM image of the polyhydroxamic acid based nanoparticles with Fe^{3+}; the arrows indicate the shell

The nanoparticles with 8-hydroxyquinoline-5-sulfonic acid were smaller, with diameter around 25 nm (see figure 17). Both types of the nanoparticles are stable in buffered environment modeling physiological conditions for sufficient time period necessary to enable radiolabeling with copper-64. In the radiolabeling test, optimal conditions for the system with 8-hydroxyquinoline-5-sulfonic acid were found. These systems have to be further tested, but the primary biological tests proved that the nanoparticles are completely non toxic. This, together with the high radiolabeling efficiency, enables their utilization as carriers in nuclear medicine.

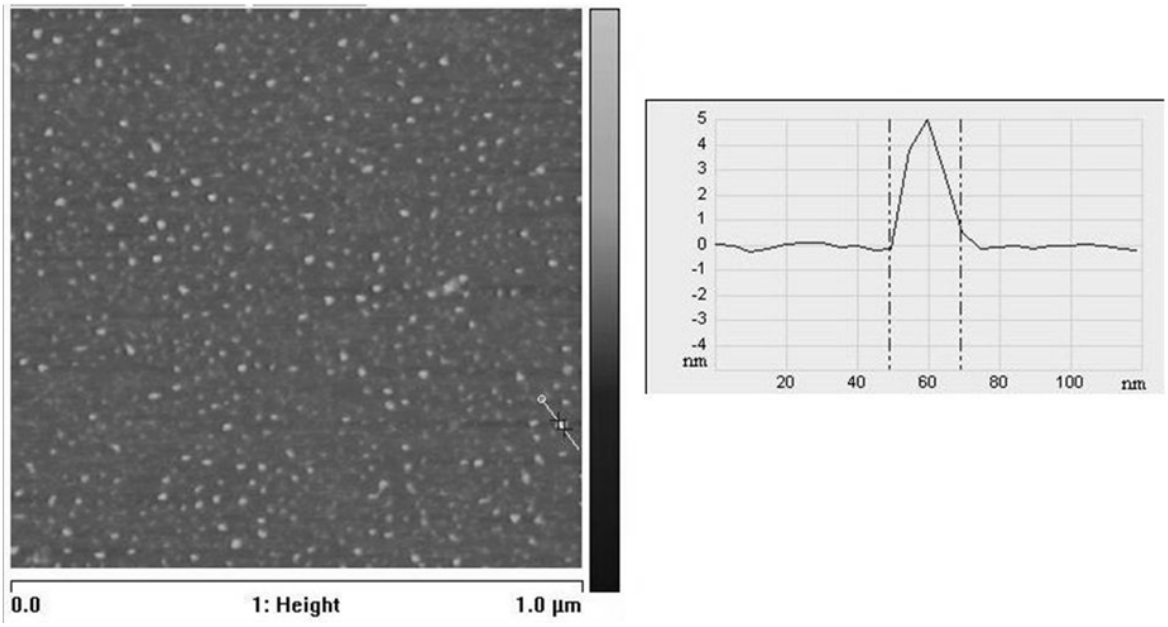

Figure 17 – AFM image of complex nanoparticles deposited from 0,05M HCl after rinsing surface with water

4. Conclusions and outlook

- We have successfully demonstrated the feasibility of the synthesis and developed new strategies of radiolabeling of appropriate carriers based on various polymers. This was performed for metal radionuclides as well as for iodine as a non-metal element and, together with the high radiolabeling efficiency and *in vitro* stability, these polymeric carriers can be possibly used for biomedical purposes.
- Considering supramolecular polymeric chelates based on poly(*N*-methyl methacryloyl hydroxamic acid)-graft-poly(ethylene oxide) and on poly{1-[4-(8-hydroxy-quinolin-5-sulfonic acid-7-yl methyl)-piperazin-1-yl]-propenone-*co*-poly(ethylene oxide) methyl ether methacrylate}assembled by Fe^{3+} ions, their *in vitro* stability and non-toxic nature are eligible for further investigation of the possible incorporation of cancerostatics in the structure to create theranostic pharmaceuticals and for their utilization in medicine. Also, the system bearing 8-hydroxyquinoline-5-sulfonic acid moieties can be involved in the study of Wilson's disease treatment.
- The polymeric beads containing DOTA, quinoline-8-ol or 8-hydroxyquinoline-5-sulfonic acid group were labeled quantitatively by ^{177}Lu. Quinoline-8-ol was labeled with ^{131}I (in this case, the radiolabeling efficiency was 95%). Therefore, both polymeric beads are suitable for radioembolization purposes for the treatment of liver malignancies.
- The sorbents prepared for the Wilson's disease treatment have promising potential for the therapy of Wilson's disease, because the polymeric sorbents are completely non-toxic (macroporous polymer beads are insoluble and thus cannot be uptaken from gastrointestinal tract) and are eliminated from the body with faeces. Preliminary biological results performed with quinoline-8-ol labeled by ^{64}Cu on rats have shown that the beads are insoluble, non-toxic, accumulate in alimentary tract and during 24 hours are completely eliminated from the body.
- Our future research will continue in cooperation with biologists on the *in vivo* tests with sorbents intended for therapy of Wilson's disease and in involvement of the supramolecular system with 8-hydroxyquinoline-5-sulfonic acid moieties in this study.

5. References

[1] Theranostics journal, [online], 2013, Accessible from WWW: http://www.thno.org/

[2] University of Birmingham press release for International science journals and magazines, 2012, Accessible from WWW: http://chemweb.bham.ac.uk/

[3] Krysko D V, Vanden Berghe T, Parthoens E, D'Herde K, Vandenabeele P; *Methods Enzymol*., 442, (2008); 307-341

[4] Bignold L P. ; *Anticancer Res*., 26(2B), (2006), 1327-1336

[5] Yonezawa A, Masuda S, Yokoo S, Katsura T, Inui K.; *J Pharmacol Exp Ther*. 319(2), (2006), 879-886

[6] Amoroso A, Etienne-Mesubi M, Edozien A, et al.; *JAIDS*, 60 (3), (2012), 314-320

[7] Zhao S H, Liu E-Q, Cheng D-X, et al.; *Braz. j. infect. dis*, 16 (4), (2012), 366-372

[8] McDonald E M,; de Kock J, Ram F S F,; *Antiviral Therapy*, 17 (2), (2012), 255-264

[9] Bergeron J J; *Biochem J*., 123(3), (1971), 385-390

[10] Gros C, Fahy J, Halby L, et al.; *Biochimie*, 94 (11), (2012), 2280-2296

[11] Ganetsky A,; *Ann Pharmacother*, 46 (11), (2012), 1511-1517

[12] Ohshima S, Seyama A,; *Hum Cell*., 25(3), (2012), 78-85

[13] Pratesi G, Savi G, Pezzoni G, Bellini O, Penco S, Tinelli S, Zunino F. *Br J Cancer*., 52(6), (1985), 841-8

[14] De Jesus O L P, Ihre H R, Gagne L, Fréchet J M J, Szoka F C Jr.,; *Bioconjugate Chem*., 13, (2002), 453-461

[15] Rahman A, Treat J, Roh J K, Potkul L A, Alvord W G, Forst D, Woolley P V, *JCO*, 8 (6), (1990), 1093-1100

[16] *Ph-sensitive polymeric conjugates of an anthracycline cancerostatic drug for targeted therapy*, US patent; US 2006/0057099 A1

[17] Jaderná fyzika a fyzika ionizujícího záření, RNDr. Vojtěch Ullmann, 2013, Accessible from WWW: http://astronuklfyzika.cz/

[18] Exploring the Table of Isotopes, The Berkeley Laboratory Isotopes Project's, Firestone R B, 2000, Accessible from WWW: http://ie.lbl.gov/education/isotopes.htm

[19] Anderson C J, Ferdani R, *Cancer Biother Radiopharm.*, 24(4), (2009), 379-393

[20] SPECT nuclear imaging cameras, Yale university, school of medicine, Accessible from WWW: http://www.yale.edu/imaging/techniques/spect_camera/index.html

[21] Pattern for the figure [online], 2012, Accessible from WWW: http://www.cellsighttech.com

[22] *Handbook of radiopharmaceuticals*, Ed. Michael J. Welch and Carol S. Redvanly ; (2003), John Wiley & Sons, Ltd. ISBN: 0-471-49560-3

[23] The MICAD Research Team. [18F]Fluoro-2-deoxy-2-D-glucose Molecular Imaging and Contrast Agent Database; Bethesda (MD): (2004-2013), National Center for Biotechnology Information (US); Accessible from WWW: http://www.ncbi.nlm.nih.gov/books/NBK23335/

[24] Cheetham P J, Petrylak D P., Oncology (Williston Park)., 26(4), (2012), 330-7, 341

[25] McDevitt M R, Ma D, Lai L T, Simon J, Borchardt P, Frank R K, Wu K, Pellegrini V, Curcio M J, Miederer M, Bander N H, Scheinberg D A; *Science*. 294(5546), (2001);1537-40

[26] Breeman W A P, de Jong M, Visser T J, Eron J L , Krenning E P,; *Eur. J. Nucl. Med. Mol. Imaging*, 30 (6), (2003), 917-920

[27] Lewington V J,; *Endocrine-Related Cancer*, 10, (2003), 497-501

[28] Lundquist H, Lubberink M, Tomalchev V, Lövquist A, Sundin A, Beshara S, Bruskin A, Carlsson J, Westlin J-E,; *Acta Oncologica*, 38 (3), (1999), 335 -341

[29] Begg A C, Stewart F A, Vens C,; *Nature Reviews Cancer*, 11, (2011), 239-253

[30] Prostate Cancer Therapy, accessible from WWW: http://www.prostatecancercentre.co.uk/treatments/brachy.html

[31] Australian Prescriber, Diagnostic tests Thallium scanning, Accessible from WWW: http://www.australianprescriber.com/magazine/17/3/57/61

[32] Kataoka K, Harada A, Nagasaki Y,; *Adv. Drug Delivery Rev*., 47, (2001), 113-131

[33] Nishiyama N, Okazaki S, Cabral H, Miyamoto M, Kato Y, Sugiyama Y, Nishio K, Matsmura Y, Kataoka K,; *Cancer Res.*, 63, (2003), 8977-8983

[34] Fonseca C, Simoes S, Gaspar R E, *J Controlled Release*, 83, (2002), 273-286

[35] Hoste K, De Winne K, Schlacht E,; *Int. J. Pharm*., 277, (2004) 119-131

[36] Kopeček J, Kopečková P, Minko T, Lu Z R, Peterson C M, *J Controlled Release*, 74, (2001), 147-158

[37] Maeda H, Wua J, Sawaa T, Matsumurab Y, Horic K, *J Controlled Release,* 65 (1–2), (2000), 271–284

[38] Torchilin V P, *Cell Mol Life Sci*, 61, (2004), 2549 -2559

[39] Yokoyama M, Okano T, Sakurai Y, Fukushima S, Okamoto K, Kataoka K, *J Drug Targeting,* 7, (1999),171-186

[40] Kato T, Sato K, Sasaki R, Kakinuma H, Moriyama M, *Cancer Chemother Pharmacol,* 37, (1996), 289-296

[41] *TheraSphere* - Innovative Liver Cancer Treatment; Accessible from WWW:http://www.nordion.com/therasphere/

[42] K Kostarelos, Emfietzoglou D, Papakostas A, Yang W-H, Ballangrud Å, Sgouros G, *Int J Cancer*, 112 (4), (2004), 713-721

[43] Park J W, Hong K, Kirpotin D B, Meyer O, Papahadjopoulos D, Benz C C, *Cancer Lett* 118(2), (1997), 153-160

[44] Pattern for the figure [online], 2012, accessible from WWW: www.nanomedicine.dtu.dk

[45] *Anorganická chemie II (Systematická část),* Lukeš I, Mička Z:,(1998),1.vyd., Karolinum, 139-140, ISBN: 9788071846635

[46] *Method for the removal of copper from a zinc sulphate solution*, US patent, (2010) US 7.682.581

[47] *Process for separating a radionuclide from solution*, US patent, (1995) US 5.409.677

[48] Chouyyok W, Shin Y, Davidson J, Samuels W D, LaFemina N H, Rutledge R D, Fryxell G E,; *Environ. Sci. Technol*., 44, (2010) 6390–6395

[49] *Process for preparing chelating ion exchanger resins and the use thereof for the extraction of metals*, US patent, (1994) US. 5.290.453

[50] *Metal complexing polymers*, US patent, (1982) US 4.317.887

[51] *Microencapsulated chelating agents and their use in removing metal ions from aqueous solutions*, US patent, (1985) US 4.500.494

[52] *Ion adsorbent for metals having a coordination number greater than two*, US patent, (1983) US 4.423.158

[53] Horak D, Benes M J, Gumargalieva K, Zaikov G, *J Appl Polym Sci*, 80, (2001) 913-916

[54] van Berkel P M, Driessen W L, Kodhass G J A A, Reedijk J, Sherington D C, A Novel,; *J. Chem. Soc., Chem. Commun.*, 2, (1995), 147-148

[55] Ala A, Walker A P, Ashkan K, Dooley J S, Schilsky M L, *Lancet*, 369, (2007), 397-408

[56] Butterworth R F,; *Neurotoxicity Research*,18, (2010), 100-105

[57] Bruha R, Mareček Z, Pospíšilová L, Nevšímalová S, Vítek L, Martásek P, Nevoral J, Petrtýl J, Urbánek P, Jiráskova A, Ferenci P; *Liver International*, 31, (2010) 83-91

[58] Merle U, Schaefer M, Ferenci P, Stremmel W, *Gut*, 56, (2007), 115-120

[59] Huster D,; *Best Prac Res Cl Ga*, 24, (2010), 531-539

[60] Uno A, Ishida H, Konno K, Ohnami Y, Naganuma H, Niizawa M, Hamashima Y, Masamune O,; *Abdomin Imaging*, 22, (1997), 72-78

[61] Das S K, Ray K,; *Nat Clin Pract Neurol*., 2, (2006), 482-493

[62] Brewer G J, Yuzbasiyan-Gurkan V, Johnson V, Dick R D, Wang Y, *Am J Med Sci*, 305, (1993), 199-202

[63] Dietary Reference Intakes (DRIs), Estimated Average Requirements, Dietary Reference Intakes for Vitamin A, Vitamin K, Arsenic, Boron, Chromium, Copper, Iodine, Iron, Manganese, Molybdenum, Nickel, Silicon, Vanadium, and Zinc, (2001), Accessible from WWW: http://www.nap.edu

[64] Shimizu N, Fujiwara J, Ohnishi S, Sato M, Kodama H, Kohsaka T, Inui A, Fujisawa T, Tamai H, Ida S, Itoh S, Ito M, Horiike N, Harada M, Yoshino M, Aoki T,; *Translational Research* 156, (2010), 350-357

[65] van den Berghe P V E., Klomp L W J,; *Nutrition Reviews*, 67, (2009), 658-672

[66] *Makromolekulární chemie*, skriptum, Vohlídal Jiří, 1986, 1. vyd, SPN, Praha

[67] *Fyzikální chemie makromolekulárních a koloidních soustav*, skriptum, Pouchlý Julius, 2001, 2 vyd., VŠCHT, Praha

[68] *An Introduction to Dynamic Light Scattering by Molecules*, Schmitz K S,; ed. (1990), academic press, inc., Harcourt Brace Jovanovich, Publishers

[69] Nobbmann U, Connah M, Fish B, Varley P, Gee C, Mulot S, Chen J, Zhou L, Lu Y, Sheng F, Yi J, Harding S E, *Biotechnol*. *Genet*. *Eng*., 24, (2007),117-128

[70] *Základy fyziky pevných polymerů*, Baldrian J. et al., ed. (1987), Edice Macro, Praha

[71] *Small Angle X-ray Scattering*, Glatter O, Kratky O,; ed. (1982), Academic Press. ISBN 0-12-286280-5.

[72] Ligne de lumiere SWING "SAXS/WAXS-ing", (2005), Accessible from WWW:http://www.synchrotron-soleil.fr/francais/viescientifique/experiences/swing/fiche-swing.htm

[73] *Atomic Absorption Spectrometry*, Welz B, Sperling M (1999), Wiley-VCH, Weinheim, Germany

[74] Hrubý M, Šubr V, Kučka J, Kozempel J, Lebeda O, Sikora A, *Appl.Radiat.Isot.* 63 (4) (2005), 423–431

[75] Opresko L, Wiley H S, Wallace R A; *Proc Natl Acad Sci* USA, 1980, 77(3),1556-60

6. Publications

Development of new strategies for labeling of polymers with radiometal cations and their comparison with radioiodination

Publications:

D1. ***Novel Polymer Vectors of ^{64}Cu***

Kozempel J, Hrubý M, Nováková M, Kučka J, Lešetický L, Lebeda O; Bioconjugate chemistry, 97, (2009), 747-752 ; co-author

D2. ***New coupling strategy for radionuclide labeling of synthetic polymers***

Hrubý M, Kučka J, Nováková M, Macková H, Vetrík M; Applied Radiation and Isotopes, 68(2), (2009), 334-339; co-author

D3. ***Polyoxazoline Thermoresponsive Micelles as Radionuclide Delivery Systems***

Hrubý M, Filippov S K, Pánek J, Nováková M, Macková H, Kučka J, Větvička D, Ulbrich K; Macromolecular Bioscience, 10, (2010), 916-924 ; co-author

Radiochim. Acta **97**, 747–752 (2009) / **DOI** 10.1524/ract.2009.1669
© by Oldenbourg Wissenschaftsverlag, München

Novel polymer vectors of ^{64}Cu

By J. Kozempel[1,*], M. Hrubý[2], M. Nováková[2,3], J. Kučka[2,3], L. Lešetický[1] and O. Lebeda[3]

[1] Charles University in Prague, Faculty of Science, Department of Organic & Nuclear Chemistry, Hlavova 8/2030, 12843 Prague 2, Czech Republic
[2] Institute of Macromolecular Chemistry, Academy of Sciences of the Czech Republic, Heyrovsky sq. 2, 16206 Prague 6, Czech Republic
[3] Nuclear Physics Institute, Academy of Sciences of the Czech Republic, 25068 Řež, Czech Republic

(Received March 2, 2009; accepted in revised form June 17, 2009)

Copper / Polymer / ^{64}Cu / Radiotherapy / PET

Summary. We describe a preparation of novel polymer vectors of ^{64}Cu based on co-polymers of *poly*-(*N*-isopropylacrylamide) and *poly*-(*N*-hydroxypropylmethacrylamide). DOTA, DTPA, dipicolylamine, thiosemicarbazone and Ag-ionophore-II ligands were tested to bind ^{64}Cu in a polymer chain. Labeling yields with no-carrier-added ^{64}Cu varied from 95 to 99% in 30 min. at laboratory temperature. Vectors were stable *in vitro* for 24 h in human serum and might be prospective for targeted ^{64}Cu radio or combined radiochemotherapy.

1. Introduction

Tumor specific delivery of a radionuclide with appropriate pharmacokinetics is one of the key issues of current research efforts. Polymer radionuclide drug delivery systems represent an interesting approach to this challenge. They could be targeted into tumors (or other tissues such as joints) either passively *via* the enhanced permeability and retention (EPR) effect [1] or actively by functional groups which are attached to a polymer (*e.g.* antibody fragment, peptides, bisphosphonates, *etc.*) [2–4]. Linear polymer vectors based on *N*-isopropylacrylamide (NIPAM) and 2-hydroxypropylmethacrylamide (HPMA) copolymers have the advantage of good water solubility, their non-immunogenicity in the human organism and therefore biological compatibility. Furthermore, the polymer chain could be easily modified in order to introduce advanced functional properties into the macromolecule (*e.g.* introduction of a chelator group, chemotherapeutics, bond with pH-dependent stability, thermosensitive properties, *etc.*). Such modified polymer carriers are thus versatile and very prospective vectors for targeted radiotherapy or combined radiochemotherapy [5, 6]. Labeled with appropriate radionuclide or radionuclidic cocktail, the therapeutic dose may be adjusted to irradiate the tumor volume and the dose distribution visualized *in vivo* by PET (positron emission tomography) or SPECT (single photon emission tomography) simultaneously. Such a pair of isotopes of recent interest is ^{64}Cu (18% β^+ emitter, $T_{1/2} = 12.7$ h, for PET & therapy) and ^{67}Cu (100% β^- emitter, $T_{1/2} = 2.7$ d, for therapy). To be able to incorporate copper into NIPAM and HPMA copolymers, we have focused on the preparation and labeling of polymer vectors containing two standard reference polycarboxylic acid chelators, DTPA (diethylene triamine pentaacetic acid) **15**, DOTA (1,4,7,10-tetraazacyclododecane-1,4,7,10-tetraacetic acid) **16** and three ligands that are new for ^{64}Cu labeling of polymers (see Scheme 1). Ag-ionophore-II **17**, thiosemicarbazone **13** and dipicolylamine **14** were selected as an alternative to classical polycarboxylic acid ligands, which sometimes cause undesired targeting of the vector to kidneys [7].

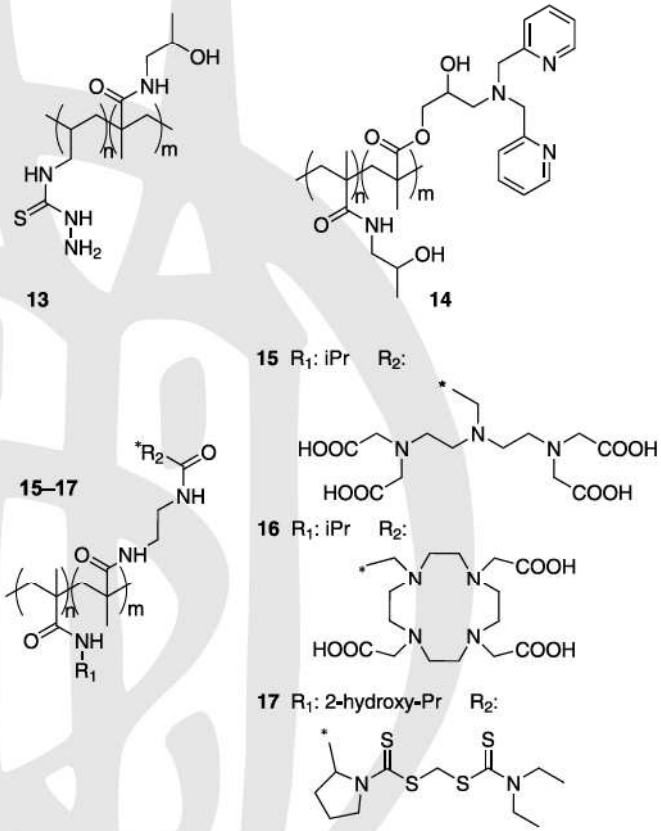

Scheme 1. Polymer vectors of ^{64}Cu; *poly*-(HPMA-co-ATSC) **13**, *poly*-(HPMA-co-GM-dipicolylamine) **14**, *poly*-(NIPAM-co-MA-EDA-NH-DTPA) **15**, *poly*-(NIPAM-co-MA-EDA-NH-DOTA) **16**, *poly*-(HPMA-co-MA-EDA-NH-Ag ionophore II) **17**.

*Author for correspondence (E-mail: kozempel@natur.cuni.cz).

This article is protected by German copyright law. You may copy and distribute this article for your personal use only. Other use is only allowed with written permission by the copyright holder.

2. Experimental

2.1 General

All reagents were purchased from commercial sources and were used without further purification. NMR spectra were measured on a Bruker Avance MSL 200 MHz NMR spectrometer (Bruker Daltonik, Germany). Molecular weights of the polymers were determined by size exclusion chromatography (SEC) in a mixture of acetate buffer (pH 6.5, 0.3 mol L^{-1}) and methanol (20 : 80 v/v) as a mobile phase on a TSK 4000 column or a TSK 3000 column, respectively (Polymer Laboratories Ltd., UK) using a HPLC System ÄKTA Explorer (Amersham Biosciences; Sweden) equipped with RI, UV and multiangle light-scattering DAWN DSP-F (Wyatt, USA) detectors. Radiochemical samples were counted on gamma spectrometric system equipped with HPGe detector (Ortec, USA).

2.2 Synthesis of low molecular weight precursors

Tert-butyl N-[2-(methacryloylamino)ethyl]carbamate (MA-EDA-Boc) (2)

A modified procedure according to Reschel was used [8]. It is a two step synthesis. In the first step one amino group of 1,2-diaminoethane was protected with the *tert*-butoxycarbonyl (Boc) group and in the second step the other amino group was acylated with methacryloyl chloride. 1,2-Diaminoethane (90 mL, 1.34 mol) was dissolved in dioxane (150 mL) and to this solution di-(*tert*-butyl)dicarbonate (32.8 g, 0.149 mol) in dioxane (200 mL) was added dropwise within 2 h. The reaction mixture was then stirred at room temperature for 22 h. Dioxane was evaporated *in vacuo* and water (150 mL) was added to the oily residue. The insoluble by-product [*N*,*N*′-bis-(*tert*-butyloxycarbonyl)-1,2-diaminoethane] was filtered off and the filtrate extracted with dichloromethane (4 × 125 mL). The combined dichloromethane layers were dried with anhydrous sodium sulphate, and dichloromethane was then evaporated *in vacuo*. The residue, which is 2-[(*tert*-butyloxycarbonyl)-amino]ethylamine **1**, was used for the next reaction step (yield 21.9 g, 92%).

The solution of **1** (21.9 g, 0.136 mol) and triethylamine (55 mL, 0.394 mol) in chloroform (220 mL) was cooled in the EtOH + CO_2(s) bath to (−15 to −20 °C). Methacryloyl chloride (14.2 mL, 0.144 mol) in chloroform (110 mL) was added dropwise within 2 h to this solution, so that the temperature of the reaction mixture did not exceed −15 °C. After that the reaction mixture was stirred at room temperature for 15 min. The chloroform layer was washed with water (5 × 250 mL) to remove triethylamine hydrochloride and dried with anhydrous sodium sulfate. Chloroform was then evaporated *in vacuo* and the raw product was recrystallised from the mixture of diethyl ether (60 mL) and hexane (100 mL). After one more crystallization from the mixture of diethyl ether (50 mL) and petrol ether (50 mL) a pure product **2** (19.8 g, 70%) was obtained in the form of white crystals. M.p. 79 °C, elemental analysis: calc. 57.86% C, 8.85% H, 12.27% N; found: 58.12% C, 8.81% H, 12.29% N; ^{1}H NMR ($CDCl_3$): δ 1.42 (9H, s), 1.95 (3H, s), 3.31 (2H, m), 3.40 (2H, m), 5.07 (1H, wide s), 5.31 (1H, s), 5.74 (1H, s), 6.78 (1H, wide s) ppm.

N-(2-hydroxypropyl) methacrylamide (3)

N-(2-hydroxypropyl)methacrylamide **3** was synthesized by the reaction of methacryloyl chloride with 1-aminopropane-2-ol in dichloromethane as described by Ulbrich *et al.* [9].

4-Allyl-thiosemicarbazide (4)

4-Allyl-thiosemicarbazide was prepared by the addition of 4-allyl-isothiocyanate (2.09 g, 20 mmol) in ethanol (25 mL) dropwise to hydrazine hydrate (1.02 g, 20 mmol) solution in ethanol (15 mL). The mixture was allowed to react at laboratory temperature for 1 h. After that, the mixture was partly evaporated and the crystalline product filtered off (yield 1.99 g, 76%). M.p.: 91.5 °C, elemental analysis: calc. 41.35% C, 7.63% H, 28.93% N, 22.08% S; found: 41.96% C, 6.06% H, 24.13% N, 27.60% S. ^{1}H NMR (DMSO): δ 2.50 (2H, t, $J = 1.60$ Hz), 4.10 (2H, s), 5.09 (2H, m), 5.82 (1H, m), 8.08 (1H, s), 9.33 (1H, s) ppm. ^{13}C NMR (DMSO): δ 45.94, 115.35, 134.70, 182.27 ppm.

Ag-ionophore II ligand preparation (7)

For synthetic pathway see Scheme 2.

2-Dithiocarboxy-1-pyrrolidinecarboxylic acid dipotassium salt monohydrate (5)

L-proline (5.00 g, 43.4 mmol) was dissolved in 96% ethanol (50 mL) containing potassium hydroxide (5.73 g 85%, 86.9 mmol) and then carbon disulfide (2.60 mL, 43.4 mmol) was added. After 2 h stirring at room temperature the mixture was cooled down to +5 °C, the white precipitate of the product was filtered off, washed with small amount of ethanol and dried *in vacuo*. Yield of **5** was 11.55 g (40.5 mmol, 93%). Elemental analysis: calc. 25.24% C, 3.18% H, 4.91% N, 22.46% S; found: 25.60% C, 3.12% H, 4.67% N, 22.74% S; ^{13}C NMR (D_2O): δ 27.0 (1C), 33.8 (1C), 58.0 (1C), 71.7 (1C), 182.5 (1C), 208.0 (1C) ppm.

1-{[({[(Diethylamino)carbothioyl]sulfanyl}methyl)-sulfanyl]carbothioyl}-2-pyrrolidine-carboxylic acid (6)

The solution of **5** (3.00 g, 12.8 mmol), sodium *N*,*N*-diethyldithiocarbamate trihydrate (2.87 g, 12.8 mmol) and diiodomethane (1.08 mL, 13.4 mmol) in 96% ethanol (30 mL) and water (15 mL) was refluxed for 4 h. The reaction mixture was poured into water (150 mL) and the mixture was washed with 2 × 150 mL dichloromethane. The dichloromethane layers containing {[(diethylamino)-carbothioyl]-sulfanyl}methyl(diethylamino)methane dithiolate were discarted. The aqueous layer was acidified with aqueous hydrochloric acid (2 mL 35%, 22.4 mmol) and extracted with 3 × 100 mL of dichloromethane. Dichloromethane layer was dried with anhydrous sodium sulfate and evaporated in vacuo. This crude residue (1.3 g) was then separated on silica (150 g) using chloroform/acetic acid (95 : 5 v/v) as a mobile phase giving 618 mg of **6** ($R_F = 0.71$) after evaporation *in vacuo*. ^{1}H NMR ($CDCl_3$): δ 1.28 (6H, t), 2.02 (2H, m), 2.09 (2H, m), 3.99 (4H, q), 4.23 (2H, m), 5.23 (1H, m), 5.31 (2H, s), 6.73 (1H, wide s) ppm. Elemental analysis: calc. 40.88% C, 5.72% H, 7.95% N; 36.38% S; found: 41.02% C, 5.64% H, 7.71% N, 36.05% S.

This article is protected by German copyright law. You may copy and distribute this article for your personal use only. Other use is only allowed with written permission by the copyright holder.

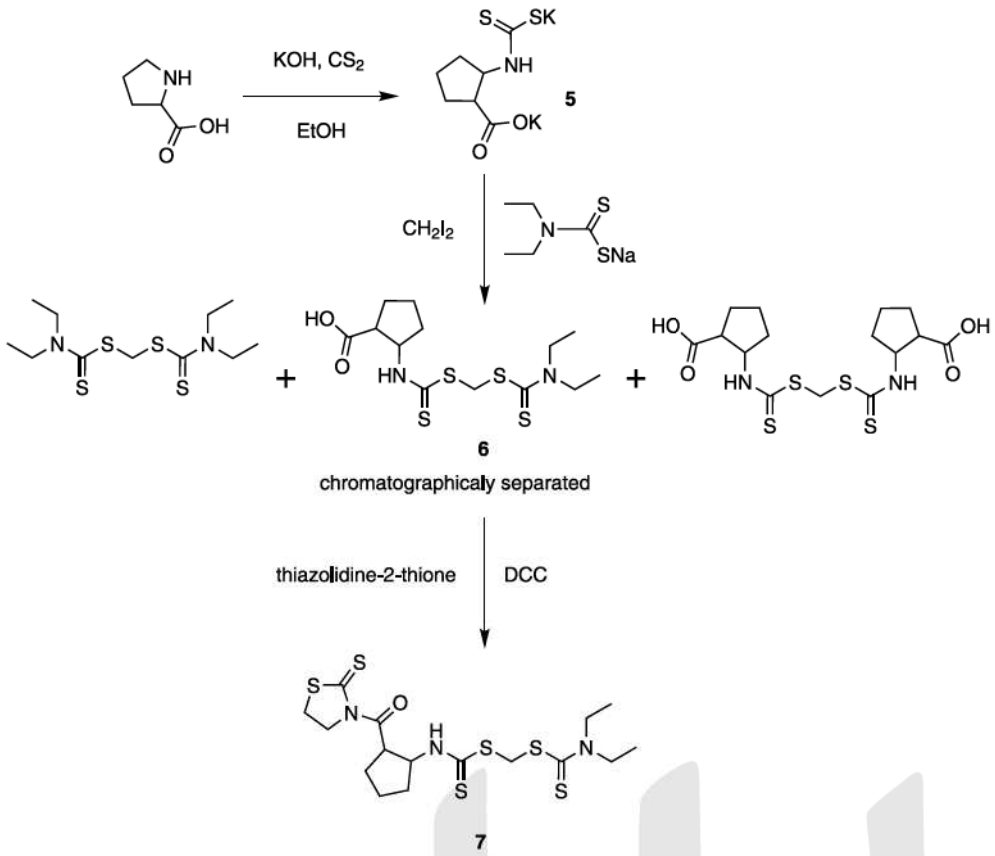

Scheme 2. Preparation of **7**. Reaction of *L*-proline with CS_2 yielded compound **5**. Compound **6** was prepared by the reaction of **5** with *N*,*N*-diethyldithiocarbamate trihydrate and diiodomethane, and chromatographic separation from statistical by-products. In the final step, the acid **6** was reacted with thiazolidine-2-thione to yield the amide **7**.

{[(Diethylamino)carbothioyl]sulfanyl}methyl-2-[(2-thioxo-1,3-thiazolan-3-yl)carbonyl]-1-pyrrolidine-carbodithioate (7)

Compound **6** (618 mg, 1.75 mmol) was reacted with thiazolidine-2-thione (210 mg, 1.75 mmol) and dicyclohexyl carbodiimide (362 mg, 1.75 mmol) in anhydrous dimethylacetamide (6 mL) with 4-dimethyl-aminopyridine as a catalyst (10 mg, 0.09 mmol) at +5 °C for 72 h and then at room temperature for 8 h. The reaction mixture was filtered and the filtrate was evaporated *in vacuo*. The residue was purified by column chromatography on silica (150 g) using toluene/ethyl acetate mixture (1 : 1) as eluent. Yield 516 mg (65%) of the title compound 7 ($R_F = 0.84$). ^{1}H NMR ($CDCl_3$): δ 1.29 (6H, t), 2.03 (2H, m), 2.08 (2H, m), 3.52 (2H, m), 4.01 (6H, m), 4.23 (2H, m), 5.39 (1H, m), 5.31 (2H, s) ppm. Elemental analysis: calc. 39.71% C, 5.11% H, 9.26% N 42.40% S; found: 40.05% C, 5.37% H, 9.10% N, 42.02% S.

2.3 Preparation of polymer precursors

Poly-(NIPAM-co-MA-EDA-Boc) (8)

N-Isopropylacrylamide (1.98 g, 17.5 mmol), MA-EDA-Boc **2** (40.3 mg, 0.177 mmol, 1 mol% of monomeric units) and azobis(isobutyronitrile) (145 mg, 0.88 mmol) were dissolved in THF (10 mL). This mixture was allowed to polymerize at 60 °C under nitrogen atmosphere for 12 h. Afterwards the polymer was precipitated into diethyl ether (150 mL), filtered off, dissolved in THF (15 mL) and reprecipitated into diethyl ether, filtered off and dried. The yield of **8** was 1.64 g (81%). The amount of protected amino groups (v) was determined by ^{1}H NMR, according to Eq. (1).

$$v = 100\% \frac{\left(\frac{S[(CH_3)_{3\,BOC}]}{9}\right)}{\left\{\left(\frac{S[(CH_3)_{3\,BOC}]}{9}\right) + S[CH(CH_3)_{2\,NIPAM}]\right\}} \quad (1)$$

where S – integral intensities of corresponding signals from ^{1}H NMR spectra, $\sigma_{BOC} = 1.48$ Hz, $\sigma_{NIPAM} = 3.90$ Hz.

The amount of Boc-protected primary amino group was 0.76 mol%, $M_w = 23.8$ kDa, $I = M_w/M_n = 2.08$ (SEC see above).

Poly-(NIPAM-co-MA-EDA-NH$_2$) (9)

The deprotection of Boc groups was carried out with trifluoroacetic acid as a reagent. Polymer **7** (1.4 g) was dissolved in the mixture of trifluoroacetic acid/water (80 : 20 v/v) (20 mL) and stirred for 1.5 h at laboratory temperature. The mixture was evaporated to dryness on a vacuum rotatory evaporator, redissolved in water (15 mL) and the polymer fraction was purified on a Sephadex G25 column (120 mL) and freeze-dried. The yield of **9** was 1.32 g (94%). The deprotection of Boc-groups was checked by ^{1}H NMR (the signal of $C(CH_3)_3$ at $\delta = 1.475$ completely diminished). $M_w = 23.6$ kDa, $I = M_w/M_n = 2.28$.

Poly-(HPMA-co-MA-EDA-Boc) (10)

The mixture of monomers (HPMA 6.63 mmol, 950 mg, MA-EDA-BOC 0.35 mmol, 80 mg) was polymerized in

This article is protected by German copyright law. You may copy and distribute this article for your personal use only. Other use is only allowed with written permission by the copyright holder.

methanol (6 mL) using azobis(isobutyronitrile) (2 wt. %; 120 mg) as an initiator. The polymerization was carried out at 60 °C for 24 h under nitrogen atmosphere. The polymer was isolated by precipitation into the acetone/diethyl ether mixture (1 : 2 v/v) and purified by dissolution in methanol and reprecipitation into the acetone/diethyl ether mixture (1 : 2 v/v). The yield was 824 mg (80%). The MA-EDA-Boc content $\omega_{\text{MA-EDA-BOC}}$ in the copolymer in mol % was assayed using ^{1}H NMR in CD_3OD analogically to polymer **8**, using signals from $C(\mathbf{CH_3})_{3\,\text{Boc}}$ and $\mathbf{CH}(OH)_{\text{HPMA}}$ (see Eq. (2)).

$$\omega_{\text{MA-EDA-BOC}} = \frac{\left(\frac{S[C(CH_3)_{3\,\text{BOC}}]}{9}\right)}{\left(\frac{S[C(CH_3)_{3\,\text{BOC}}]}{9}\right) + S[CH(OH)_{\text{HPMA}}]} 100\% \quad (2)$$

where S – integral intensities of corresponding signals from ^{1}H NMR spectra, $\sigma_{\text{BOC}} = 1.45$ Hz, $\sigma_{\text{HPMA}} = 3.88$ Hz.

The amount of Boc-protected primary amino groups: 4.9%, $M_w = 20.9$ kDa; $I = M_w/M_n = 1.70$.

Poly-(HPMA-co-MA-EDA-NH$_2$) (11)

The polymer **10** (700 mg) was dissolved in the mixture of trifluoroacetic acid (5.0 mL; 67 mmol) and water (500 μL) and this solution was stirred at room temperature for 1.5 h. After that, the reaction mixture was poured into the solution of sodium carbonate in water [15.0 g of anhydrous sodium carbonate (142 mmol) in 60 mL water] and this solution was dialyzed against water for 5 days (the water in the outer reservoir was replaced every day; the dialysis tubing with molecular weight cut-off 3.5 kDa was used). Yield of **11** was 560 mg (80%). The ^{1}H NMR (CD_3OD) have shown complete deprotection of the amino groups [no $-C(\mathbf{CH_3})_3$ signal ($\delta = 1.45$)]. $M_w = 20.2$ kDa; $I = M_w/M_n = 1.72$.

Poly-(HPMA-co-GM) (12)

N-(2-Hydroxypropyl methacrylamide) (925 mg, 6.47 mmol) and glycidyl methacrylate (GM) (72 μL, 0.52 mmol) were polymerized in dimethyl sulfoxide (6 mL) using azobis(isobutyronitrile) (57 mg, 0.35 mmol) as an initiator. The polymerization was carried out at 60 °C for 16 h. The polymer was isolated by precipitation onto the acetone/diethyl ether mixture (1 : 2 v/v), filtered off, redissolved in methanol (10 mL) and precipitated again into the acetone/diethyl ether mixture. The filtered-off polymer was then dried *in vacuo*. Yield of **12** was 795 mg. $M_w = 36.2$ kDa, $I = M_w/M_n = 1.96$.

2.4 Preparation of functionalised polymers

Poly-(HPMA-co-ATSC) (13)

HPMA (925 mg, 6.47 mmol) and 4-allyl-3-thiosemi-carbazide **4** (69 mg, 0.52 mmol) were polymerized in dimethyl sulfoxide (6 mL) using azobis(isobutyronitrile) (57 mg, 0.35 mmol) as an initiator. The polymerization was carried out at 60 °C for 16 h. After that, the polymer was isolated by gel permeation chromatography on Sephadex G25 (120 mL bed volume) using water as eluent and subsequent freeze-drying of the polymer fraction. Yield 693 mg (70%). $M_w = 30.1$ kDa, $I = M_w/M_n = 1.96$, $S = 1.02\%$ (0.32 mmol g^{-1}).

Poly-(HPMA-co-GM-dipicolylamine) (14)

The polymer **12** (500 mg) was dissolved in ethanol (8 mL) and di-(2-picolyl)-amine (94 mL, 0.52 mmol) was added. After standing for 1 week at room temperature the polymer was isolated by precipitation onto the acetone/diethyl ether mixture (1 : 2 v/v), filtered off, redissolved in methanol (10 mL) and precipitated again into the acetone/diethyl ether mixture. The filtered-off polymer was then dried *in vacuo*. The dry polymer was then purified on Sephadex G25 column (120 mL) in water and then freeze-dried. Yield 500 mg. Sorption capacity (copper in 5% aqueous ammonia) was 0.31 mmol g^{-1}, $M_w = 38.3$ kDa, $I = M_w/M_n = 2.01$.

Poly-(NIPAM-co-MA-EDA-NH-DTPA) (15)

The polymer **9** (200 mg, 0.0177 mmol $-NH_2$ groups) was dissolved in dimethylacetamide (4 mL), ethyldiisopropylamine (333 μL, 2.01 mmol) and 4-dimethylaminopyridine (33 mg, 0.27 mmol) were added. The mixture was heated to 50 °C and the DTPA anhydride (143 mg, 0.40 mmol) has been added. The mixture was stirred for 3 h at 50 °C. After the dilution with water (15 mL), the mixture was dialysed against water for 24 h through a dialyzation membrane with cut-off molecular weight of 3.5 kDa (Serva GmbH, Germany). The solution of polymer was freeze-dried. The polymer was dissolved in water (15 mL), repurified on a Sephadex G25 (120 mL) column and freeze-dried. The yield of **15** was 183 mg (92%). $M_w = 49.6$ kDa, $I = M_w/M_n = 3.40$.

Poly-(NIPAM-co-MA-EDA-NH-DOTA) (16)

The polymer was prepared in analogy to **15** using 300 mg of polymer precursor **9** (0.0266 mmol of $-NH_2$ groups), and instead of DTPA anhydride, DOTA monosuccinimidyl ester (26 mg, 0.0266 mmol) and 4-dimethylaminopyridine (100 mg, 0.81 mmol) as a base were used. The yield of **16** was 229 mg (76%). $M_w = 27.0$ kDa, $I = M_w/M_n = 2.06$.

Poly-(HPMA-co-MA-EDA-NH-Ag ionophore II) (17)

The polymer **11** (200 mg) was dissolved in the mixture of anhydrous dimethylacetamide (5 mL) and methanol (10 mL). Thereafter the ligand **7** (0.16 mmol, 72 mg) was added and the mixture was stirred at room temperature for 24 h. After that the polymer was precipitated into the acetone/diethyl ether mixture (1 : 2 v/v) and purified by dissolution in methanol and reprecipitation into the acetone-diethyl ether mixture (1 : 2 v/v). The reprecipitated polymer was dissolved in water (5 mL), purified by gel permeation chromatography on Sephadex G25 (120 mL bed volume) and freeze dried. Yield of **17** was 178 mg (75%). Elemental analysis: S 1.73% (0.540 mmol g^{-1} $S \sim 0.135$ mmol g^{-1} ligand). $M_w = 23.1$ kDa; $I = M_w/M_n = 1.80$.

This article is protected by German copyright law. You may copy and distribute this article for your personal use only. Other use is only allowed with written permission by the copyright holder.

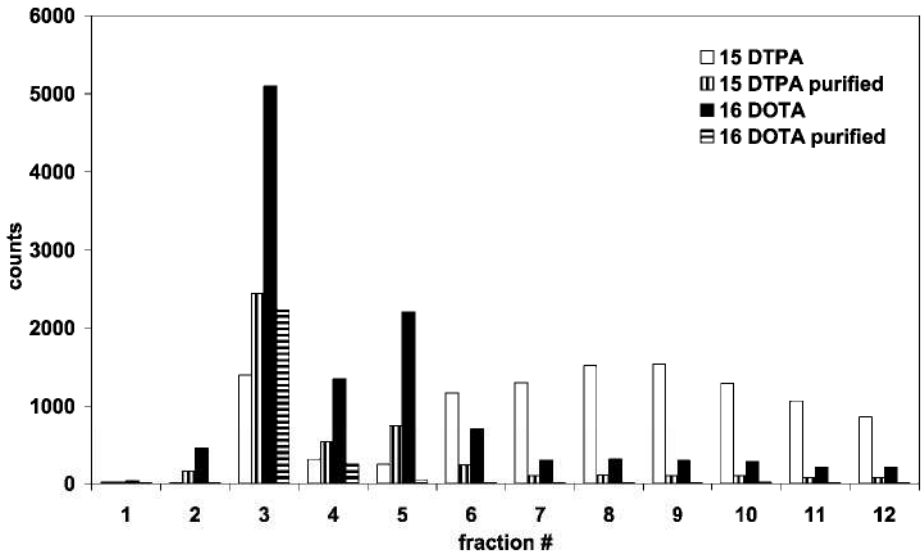

Fig. 1. GPC separation of polymers **15** and **16** labeled with ^{64}Cu, before and after purification from the free chelators (**15**, before purification, empty boxes; purified, vertical lines; **16**, before purification, full boxes; purified, horizontal lines).

2.5 Radiochemistry

^{64}Cu preparation

No-carrier-added ^{64}Cu was prepared by the deuteron irradiation of ^{nat}Zn on cyclotron U-120M at Nuclear Physics Institute of the Academy of Sciences of the Czech Republic (Řež, Czech Republic). Separation of ^{64}Cu was performed as described previously [10]. Briefly, irradiated ^{nat}Zn foil was dissolved in concentrated HCl and ^{64}Cu was separated by subsequent cation and anion exchange chromatography (Dowex® 1 × 8 and Dowex® 50 × 8), yielding ≈ 37 MBq (1 mCi) of ^{64}Cu in 200 μL of 0.1 M HCl solution. This solution was used for labeling.

Labeling

To a 2 mg of each polymer dissolved in 250 μL of distilled water in an Eppendorf® tube, 2.5 μL of [^{64}Cu]$CuCl_2$ solution (≈ 0.46 MBq, 12.5 μCi) was added. The reaction mixtures were incubated at laboratory temperature (25 °C) for 30 min. on a tube shaker. After that, labeled polymers were purified from unreacted [^{64}Cu]$CuCl_2$ by gel permeation chromatography on a PD-10 desalting columns (GE Healthcare, USA) using distilled water as eluent. Radiochemical yields were determined as the ratio of the activity in macromolecular fractions (3 and 4) to the total activity applied on the column. Separated yields are corrected for the losses of activity on tips and tubes.

In vitro tests

Incubation at laboratory temperature for 24 h in human serum was performed as basic *in vitro* stability test. Aliquots of 100 μL of ^{64}Cu-labeled polymer solutions were incubated with 400 μL of human serum on a laboratory shaker. After 24 h, the mixture was analysed by GPC and the stability was determined as a ratio of the activity in macromolecular fractions (3 and 4) to the total activity applied on the column.

3. Results and discussion

The polymers were prepared by copolymerization of HPMA and NIPAM with GM, 4-allylthiosemicarbazide or *t*-Bu-*N*-[2-(methacryloylamino)ethyl]carbamate. These precursors were modificated in next steps to give polymer vectors **13**–**17**. Subsequent labeling with n.c.a. ^{64}Cu was performed at laboratory temperature within 30 min of reaction time. Labeled polymer vectors were purified by low pressure gel permeation chromatography (GPC) on a PD-10 desalting column (Sigma-Aldrich, Czech Republic) using distilled water as eluent. The key parameter for the labelling was the purity of the prepared polymers. DTPA **15** and DOTA **16** polymers had to be purified thoroughly to remove the free chelator, which competed with functionalised polymer as shown on Fig. 1. Final results of labeling, separation by GPC and *in vitro* stability are summarized in Table 1.

Table 1. Yields and *in vitro* stabilities.

Polymer	Labeling yield [%]	Separation yield [%]	24 h stability [%]
13 HPMA-co-ATSC	96	96	95
14 HPMA-co-GM-dipicolylamine	98	97	96
15 NIPAM-co-MA-EDA-NH-DTPA	95	91	94
16 NIPAM-co-MA-EDA-NH-DOTA	99	97	94
17 NIPAM-co-MA-EDA-NH-Ag ionophore II	99	98	93

It can be clearly seen that functional groups bound on polymer chain readily react with [^{64}Cu]$CuCl_2$. The incorporation was high for all types of functional groups tested, exceeding the value of 90%. Unreacted ^{64}Cu was quantitatively separated from the product as shown in Fig. 2. In runs with c.a. ^{64}Cu decreasing of the labeling yield due to the saturation of functional groups bound on polymer was observed (the amount of functional groups was in order of units of molar %). This indicates that n.c.a. ^{64}Cu or high specific activity c.a. ^{64}Cu should be used in order to achieve good labeling yields.

To summarize, we have prepared polymer vectors of ^{64}Cu with five different chelators, with high yields and good *in vitro* stability. Polymers bearing thiosemicarbazone, dipi-

This article is protected by German copyright law. You may copy and distribute this article for your personal use only. Other use is only allowed with written permission by the copyright holder.

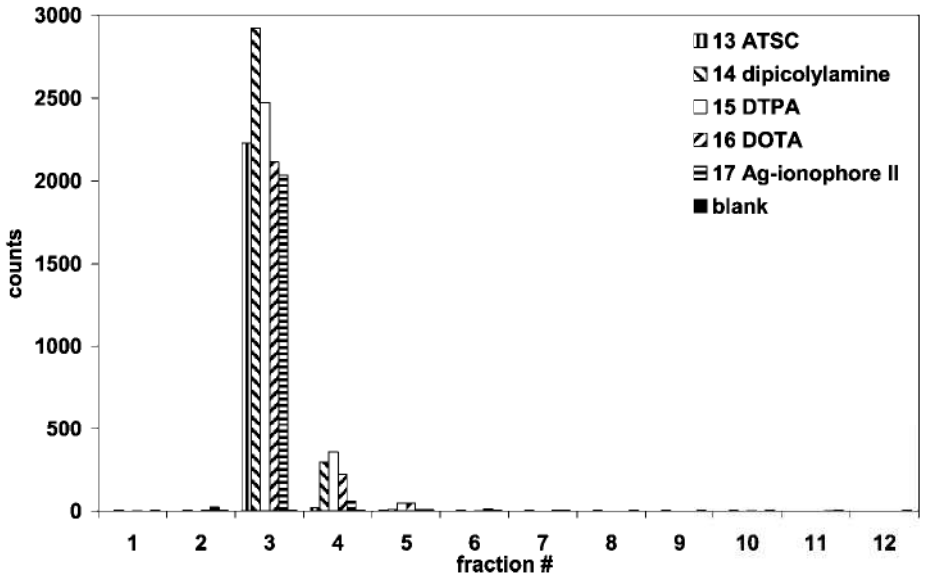

Fig. 2. GPC separation of ^{64}Cu-labeled polymers. Fraction volume was 1.5 mL. Free ^{64}Cu retained in back fractions on column. (Polymer **13**, vertical lines; **14**, descending lines; **15**, empty boxes; **16**, ascending lines; **17**, horizontal lines; blank, full boxes).

colylamine and Ag ionophore II were successfully labeled, besides polymers with standard polyacidic chelators; DOTA and DTPA. Further studies should follow to evaluate the vectors of ^{64}Cu *in vivo*, considering that detailed analysis of biodistribution data is needed [11].

Acknowledgment. Authors gratefully acknowledge the support from the Grant Agency of the Academy of Sciences of the Czech Republic (grants IAA400480616, KJB4050408 and KAN200200651) and Ministry of Education Youth and Sports of the Czech Republic (grants MSM0021620857 and IM4635608802).

References

1. Matsumura, Y., Maeda, H.: A new concept for macromolecular therapeutics in cancer chemotherapy: mechanism of tumoritropic accumulation of proteins and the antitumor agent smancs. Cancer Res. **46**, 6387 (1986).
2. Hruby, M., Etrych, T., Kucka, J., Forsterova, M., Ulbrich, K.: Hydroxybisphosphonate-containing polymer drug-delivery systems designed for targeting into bone tissue. J. Appl. Polym. Sci. **101**(5), 3192 (2006).
3. Pressly, E. D., Rossin, R., Hagooly, A., Fukukawa, K., Benjamin, B. W., Messmore, W., Welch, M. J., Wooley, K. L., Lamm, M. S., Hule, R. A., Pochan, D. J. and Hawker, C. J.: Structural effects on the biodistribution and positron emission tomography (PET) imaging of well-defined ^{64}Cu-labeled nanoparticles comprised of amphiphilic block graft copolymers. Biomacromolecules **8**, 3126 (2007).
4. Rossin, R., Muro, S., Welch, M. J., Muzykantov, V. R., Schuster, D. P.: *In vivo* imaging of ^{64}Cu-labeled polymer nanoparticles targeted to the lung endothelium. J. Nucl. Med. **49**, 103 (2008).
5. Hruby, M., Kucka, J., Mackova, H., Konak, C., Vetrik, M., Kozempel, J., Lebeda, O.: New binary thermoresponsive polymeric system for local chemoradiotherapy. J. Appl. Polym. Sci. **111**, 2220 (2009).
6. Hruby, M., Subr, V., Kucka, J., Kozempel, J., Lebeda, O., Sikora, A.: Thermoresponsive polymers as promising new materials for local radiotherapy. Appl. Radiat. Isot. **63**, 423 (2005).
7. Li, L., Yazaki, P. J., Anderson, A. L., Crow, D., Colcher, D., Wu, A. M., Williams, L. E., Wong, J. Y. C., Raubitschek, A., Shively, J. E.: Improved biodistribution and radioimmunoimaging with poly(ethylene glycol)-DOTA-conjugated anti-CEA diabody. Bioconjug. Chem. **17**(1), 68 (2006).
8. Reschel, T.: Polyelectrolyte complexes of DNA with synthetic polymers as vectors for *in vivo* gene delivery. Dissertation, Faculty of Science, Charles University, Czech Republic, Prague (2002), p. 48.
9. Ulbrich, K., Subr, V., Strohalm, J., Plocova, D., Jelinkova, M., Rihova, B.: Polymeric drugs based on conjugates of synthetic and natural macromolecules I. Synthesis and physico-chemical characterisation. J. Control. Release **64**(1–3), 63 (2000).
10. Kozempel, J., Abbas, K., Simonelli, F., Zampese, M., Holzwarth, U., Gibson, N., Lešetický, L.: A novel method for n.c.a. ^{64}Cu production by the ^{64}Zn(d, $2p$)^{64}Cu reaction and dual ion-exchange column chromatography. Radiochim. Acta **95**(2), 75 (2007).
11. Pirollo, K. F., Chang, E. H.: Does a targeting ligand influence nanoparticle tumor localization or uptake? Trends Biotechnol. **26**(10), 552 (2008).

This article is protected by German copyright law. You may copy and distribute this article for your personal use only. Other use is only allowed with written permission by the copyright holder.

Applied Radiation and Isotopes 68 (2010) 334–339

Contents lists available at ScienceDirect

Applied Radiation and Isotopes

journal homepage: www.elsevier.com/locate/apradiso

New coupling strategy for radionuclide labeling of synthetic polymers

Martin Hruby [a,*], Jan Kucka [a,b], Michaela Novakova [a,b], Hana Mackova [a], Miroslav Vetrik [a,b]

[a] Institute of Macromolecular Chemistry AS CR, v.v.i., Heyrovsky Sq. 2, 162 06 Prague 6, Czech Republic
[b] Nuclear Physics Institute AS CR, v.v.i., 250 68 Rez, Czech Republic

ARTICLE INFO

Article history:
Received 30 August 2009
Received in revised form
4 November 2009
Accepted 13 November 2009

Keywords:
Polymer
Radionuclide
Labeling
Azo dye

ABSTRACT

We have developed a radiolabeling strategy for synthetic polymers based on the formation of azo dye usable for both covalent and chelating labeling modalities under mild conditions. Poly[*N*-(2-hydroxypropyl)methacrylamide] and poly(*N*-isopropyl acrylamide) were used as model polymers. *N*-methacryloyl tyrosinamide was introduced into the polymers and the phenolic moiety was then reacted with diazotized chelator precursors. The conjugates were radiolabeled with both the covalently bound (iodine-125) and chelated (indium-111) radionuclides in high yields and sufficient *in vitro* stability of the labels was proven.

© 2009 Elsevier Ltd. All rights reserved.

1. Introduction

Labeling synthetic polymers with radionuclides is of increasing importance in life sciences research [study of biodistribution, pharmacokinetics (Adams et al., 2004; Herth et al., 2009; Hruby et al., 2005; Kim et al., 2007; Krause et al., 2000), etc.]. Since the molecule of interest may be directly labeled only exceptionally, a suitable coupling strategy is essential. Generally, such linker should meet the following requirements (Quadri and Vriesendorp, 1998): to be readily labelable with the radionuclide of interest under conditions compatible with stability of the labeled molecule, the label should be sufficiently stable under *in vivo* conditions, labeling should not affect the eventual specific binding ability of the biomolecule and non-specific interactions of the radioconjugate in organism should be as low as possible. The coupling strategy design depends on the character of radionuclide binding—whether it is covalent binding (e.g., iodine radioisotopes), or chelation (metal ion radioisotopes).

Chelators for multivalent metal cation radionuclides mostly rank among aminopolycarboxylic acids, e.g., 1,4,7,10-tetraazacyclododecane-1,4,7,10-tetraacetic acid (DOTA) (Fitzsimmons and Atcher, 2007; Liu et al., 2003; Rossin et al., 2008) or diethylenetriaminepentaacetic acid (DTPA) (Fitzsimmons and Atcher, 2007; Hruby et al., 2005; Nichol et al., 1999). Suitable derivatives of these acids reactive towards primary amino groups [containing, e.g., isothiocyanate forming the particular thiourea derivative (Fitzsimmons and Atcher, 2007; Liu et al., 2003), cyclic anhydride (Hruby et al., 2005; Nichol et al., 1999), mixed anhydride (Uzgiris et al., 2004) or succinimidyl ester (Rossin et al., 2008) forming the particular amide derivative] are reacted with the target molecule containing primary amino group and the resulting conjugate is then radioisotopically labeled. Alternatively, more comlex amino-carboxylic acid condensations may be employed for conjugation (Lu et al., 2003).

We have developed a labeling strategy for synthetic polymers based on the formation of azo dye useable for both covalent and chelated binding modalities on the same molecule utilizing L-tyrosine moiety as an anchor for the chelator. In the case of synthetic polymers synthesized by radical polymerization, L-tyrosine may be easily introduced by copolymerization of *N*-methacryloyl tyrosinamide (Kissel et al., 2001). We used the hydrophilic poly[*N*-(2-hydroxypropyl)methacrylamide] (pHPMA) and the thermoresponsive poly(*N*-isopropyl acrylamide) (pNIPAA) as model polymers. Poly[*N*-(2-hydroxypropyl)methacrylamide] is a highly hydrophilic biocompatible polymer frequently used for the construction of water soluble drug delivery systems (Etrych et al., 2008; Herth et al., 2009; Kissel et al., 2001). Poly(*N*-isopropyl acrylamide) is a biocompatible polymer with lower critical solubility temperature, suitable for the construction of thermoresponsive drug delivery systems such as, e.g., micelles, etc. (Hruby et al., 2009, 2008, 2005). The commercially available primary aromatic amine derivatives of the commonly used selective multivalent cation chelators (DTPA, CHX-A″-DTPA and DOTA, see Fig. 1 for structures of the primary amino precursors) were diazotized and azo coupled with the L-tyrosine containing structures under mild conditions (see Figs. 2 and 3 for typical schemes). The resulting azo dye is labelable with metal

* Corresponding author. Tel.: +420 296 809 230; fax: +420 296 809 410.
E-mail addresses: mhruby@centrum.cz (M. Hruby), jkucka@centrum.cz (J. Kucka), misha.novakova@seznam.cz (M. Novakova), mackova@imc.cas.cz (H. Mackova), vetrix@seznam.cz (M. Vetrik).

0969-8043/$ - see front matter © 2009 Elsevier Ltd. All rights reserved.
doi:10.1016/j.apradiso.2009.11.039

cations by chelation and the phenolic moieties in the azo dye structure (as well as unreacted remaining L-tyrosine moieties) remain reactive towards radioiodination. The proposed coupling strategy has also the advantage of facile spectrophotometric determination of conjugation yield due to the presence of azo dye chromophore.

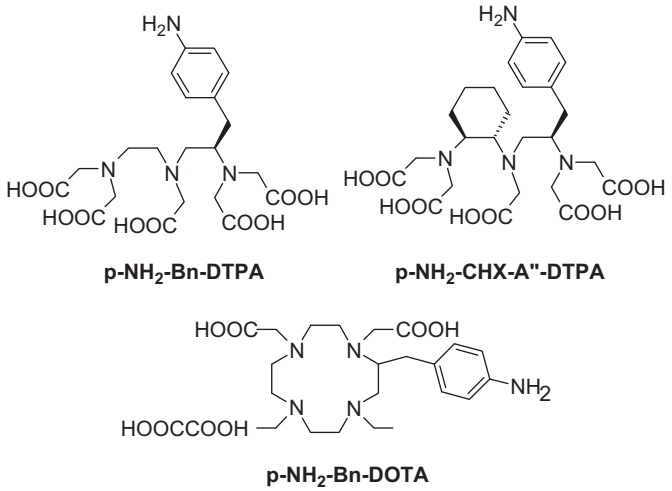

Fig. 1. Structure of the primary amino precursors of the chelators.

2. Experimental procedures

2.1. Materials

N-(2-Hydroxypropyl)methacrylamide was synthesized by methacryloylation of 1-amino-2-propanol according to Ulbrich et al. (2000). *N*-Methacryloyl tyrosinamide was synthesized according to Kissel et al. (2001). The aromatic amino precursors of the chelators (DTPA, CHX-A″-DTPA and DOTA, i.e., *S*-2(4-aminobenzyl)-diethylenetriamine pentaacetic acid, [(*R*)-2-amino-3-(4-aminophenyl) propyl]-trans-(*S*,*S*)-cyclohexane-1,2-diamine-pentaacetic acid and *S*-2-(4-aminobenzyl)-1,4,7,10-tetraazacyclododecane tetraacetic acid, respectively) were purchased from Macrocyclics Ltd. (Dallas, TX, USA). *N*-Isopropyl acrylamide was obtained from Sigma-Aldrich Ltd. (Prague, Czech Republic) and crystallized from hexane before use. Radionuclide stock solutions ($Na^{125}I$ and $^{111}InCl_3$) were obtained from Lacomed Ltd. (Rez, Czech Republic). All other chemicals were obtained from Sigma-Aldrich Ltd. and were used as received. Sephadex G-25 and PD-10 gel filtration columns were obtained from Amersham Biosciences AB (Uppsala, Sweden).

2.2. Synthesis of model polymers ***1*** and ***2***

The poly[*N*-(2-hydroxypropyl)methacrylamide–co–*N*-methacryloyl tyrosinamide] (**1**) was synthesized according to Kissel et al. (2001) using 1 mole% *N*-methacryloyl tyrosinamide in polymerization mixture.

The poly(*N*-isopropyl acrylamide–co–*N*-methacryloyl tyrosinamide) (**2**) was synthesized as follows: *N*-isopropylacrylamide (4.00 g; 35.3 mmol), azobis(isobutyronitrile) (AIBN, 290 mg; 1.77 mmol) and *N*-methacryloyl tyrosinamide (82 mg; 0.36 mmol) were polymerized in tetrahydrofuran (THF; 20 mL) at 60 °C for

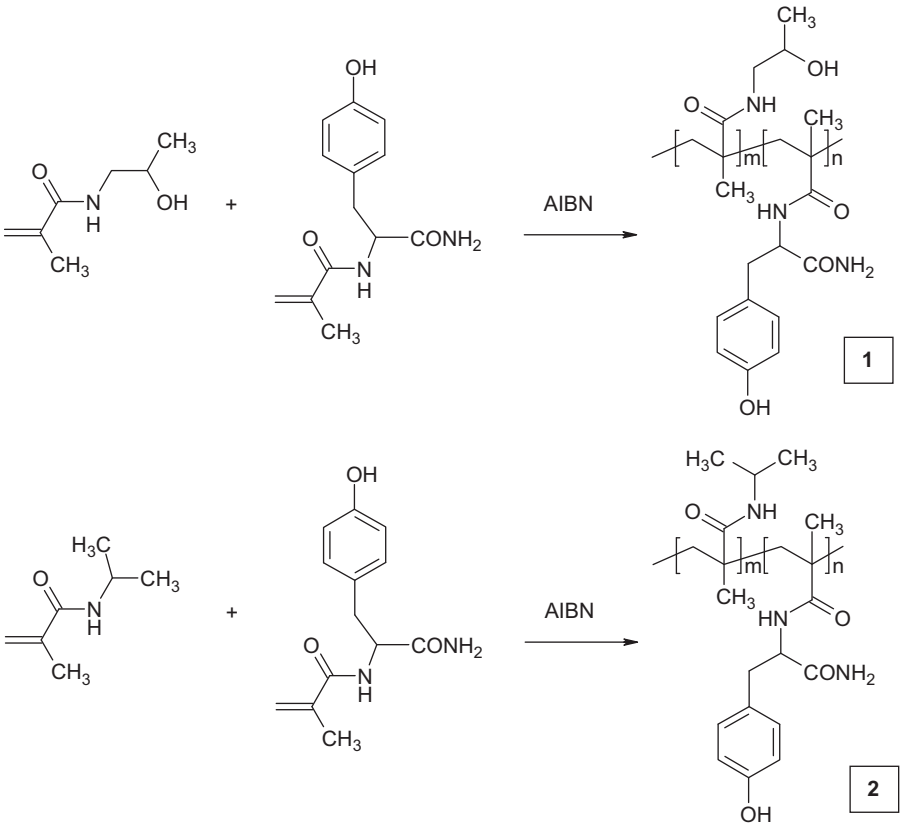

Fig. 2. Synthesis of polymer precursors **1** and **2**.

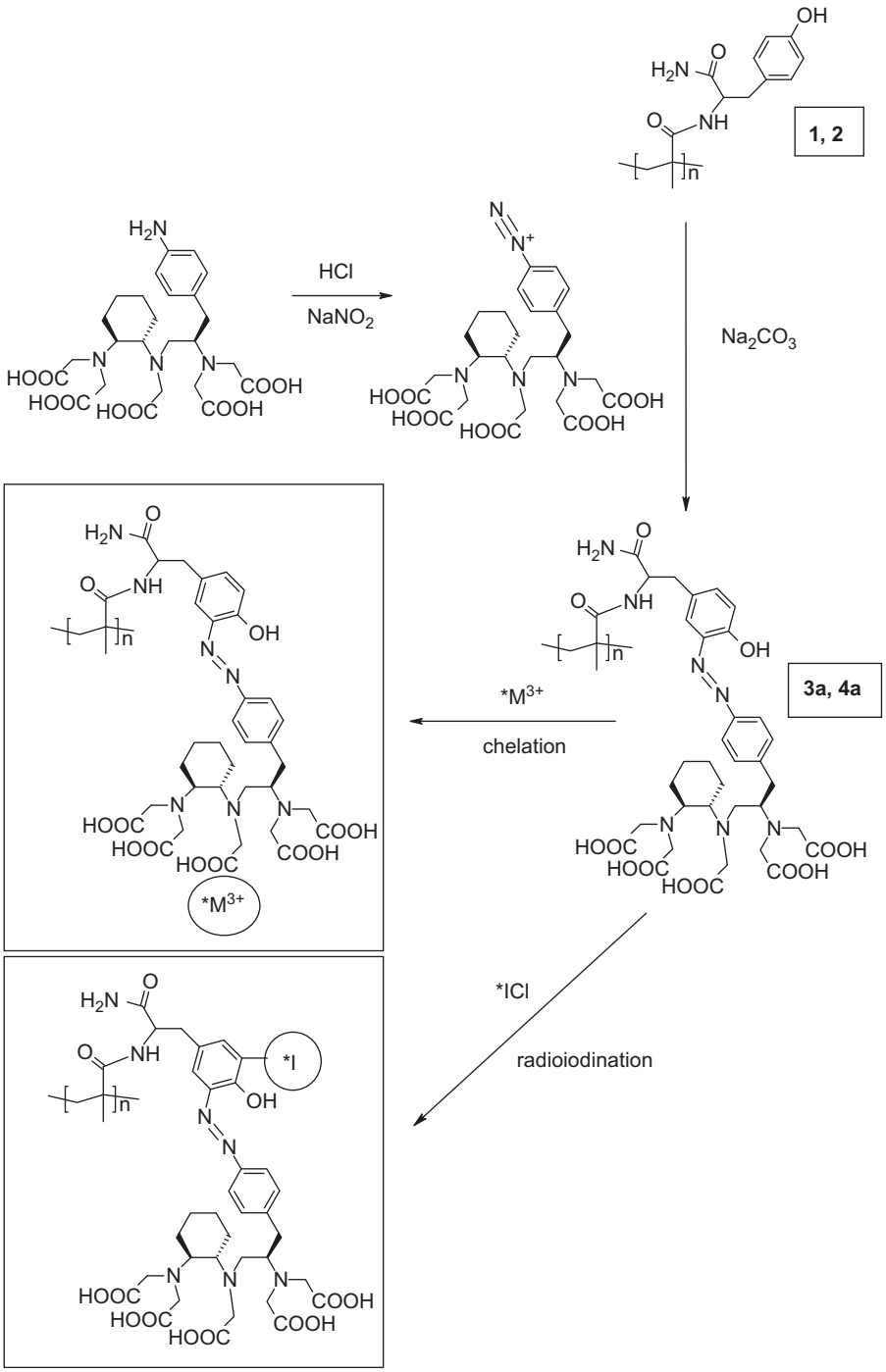

Fig. 3. Introduction of the CHXA″-DTPA chelating groups into the copolymers (the *N*-methacryloyl tyrosinamide monomeric unit, which undergo conjugation, is shown only from the polymer in the scheme; the other chelators are used to react in the same way of azo coupling). The polymers 1 and 3 contain *N*-(2-hydroxypropyl)methacrylamide as main monomer and the polymers 2 and 4 contain *N*-isopropyl acrylamide as main monomer.

16 h. The polymer was precipitated into diethyl ether (300 mL), filtered off, redissolved in THF (20 mL) and precipitated again into diethyl ether (300 mL). Yield 3.60 g (89%). The scheme of the reaction is shown in Fig. 2.

The crude polymer **2** (1.5 g) was dissolved in water (30 mL) and purified by gel permeation chromatography (GPC) on a Sephadex G-25 column (120 mL bed volume) using water as eluent. The polymer-containing fractions were freeze-dried to obtain the purified product.

Molecular weights of the copolymers **1** and **2** (M_w=54.5 and 33.0 kDa, respectively) together with their polydispersities ($I=M_w/M_n$=1.78 for **1** and 1.50 for **2**) were determined by size exclusion chromatography (SEC) in a mixture of acetate buffer (pH 6.5, 0.3 mol/L) and methanol (20:80 v/v) as a mobile phase on a TSK 4000 column (Polymer Laboratories Ltd., UK) using a HPLC system Shimadzu (Shimadzu GmbH, Prague, Czech Republic) equipped with refraction index (RI), UV–VIS and multiangle light-scattering DAWN DSP-F (Wyatt, USA) detectors. The refractive index increment (d*n*/d*c*) of polymers **1** and **2** in this solvent was determined on the Brice–Phoenix visual laboratory type differential refractometer (BP-2000-V, Phoenix Precision Instrument Co., USA) giving the values of $0.173 \pm 0.003\ \mathrm{mL\,g^{-1}}$ for

polymer **1** and $0.153 \pm 0.002\ mL\ g^{-1}$ for polymer **2**, respectively. The L-tyrosinamide content in the polymer was assayed spectrophotometrically [$\lambda_{max}(\varepsilon)$=275 nm ($1738\ L\ mol^{-1}\ cm^{-1}$)] in water.

2.3. Attachment of chelating moiety—synthesis of polymers *3* and *4*

The polymers synthesized from polymer **1** are marked **3** and the polymers synthesized from polymer **2** are marked **4**. Depending on the chelator attached, they are distinguished by letters **a** (CHXA″-DTPA), **b** (DOTA) and **c** (DTPA), respectively; e.g., the polymer **4a** is made by conjugation of CHXA″-DTPA to polymer **2**.

The typical procedure for the conjugation of CHXA″-DTPA to **2** (synthesis of polymer **4a**; 2:1 diazotized chelator to polymeric phenol molar ratio) is stated, the other conjugations were done in analogy with other chelators or polymer. See Fig. 3 for scheme.

The polymer **2** (200 mg, 18 μmol tyrosinamide) was dissolved in water (15 mL) containing sodium carbonate (636 mg, 6.0 mmol). [(*R*)-2-amino-3-(4-aminophenyl)propyl]-*trans*-(S,S)-cyclohexane-1,2-diamine-pentaacetic acid (p-NH_2-CHX-A″-DTPA, 25 mg, 35 μmol) was dissolved in aqueous hydrochloric acid (6 M, 500 μL; 3.0 mmol). Sodium nitrite (2.44 mg, 35 μmol) was dissolved in water (50 μL). The three solutions were cooled to 0 °C. The chelating agent in hydrochloric acid solution was diazotized with the aqueous sodium nitrite at 0 °C for 10 min. This solution was then added to the cool polymer solution. Azo coupling proceeded for 2 h at 0 °C, the polymer was then purified on a Sephadex G-25 column (bed volume 120 mL) using water as an eluent and isolated by freeze-drying. The purification on a Sephadex G-25 column and isolation by freeze-drying was repeated once again. The conjugate yield was 180 mg (90%).

The content of azo dye moieties was determined by UV–VIS spectroscopy in methanol [$2\ mg\ mL^{-1}$ polymer, λ_{max} (ε)=331 nm ($18750\ L\ mol^{-1}\ cm^{-1}$)]. The λ and ε values were measured from the 4-methyl-2-[(4-methylphenyl)azo]phenol model synthesized according to Masoud et al. (1985).

2.4. Radiolabeling of the polymers

Radioactivity measurements were done on an ionizing chamber Bqmetr 4 (Empos Ltd., Prague, Czech Republic).

Labeling with ^{125}I: The particular polymer (1 mg) was dissolved in phosphate buffered saline pH 7.4 (100 μL), $Na^{125}I$ solution (10 μL, 33 MBq) and chloramine T solution ($10\ mg\ mL^{-1}$, 10 μL) were added and the mixture was incubated at ambient temperature for 30 min. After that the mixture was separated on a PD-10 desalting column using water as eluent, 1.5 mL fractions were collected. The polymer containing fractions (#2–4) were merged.

Labeling with ^{111}In: The particular polymer (1 mg) was dissolved in 0.5 M ammonium acetate (200 μL). This solution (100 μL) was mixed with the $^{111}InCl_3$ stock solution (1.5 μL, 18 MBq) and after 15 min the mixture was separated on a PD-10 desalting column (Amersham Biosciences AB, Uppsala, Sweden) using 0.5 M ammonium acetate as an eluent, 1.5 mL fractions were collected. The polymer containing fractions (#2–4) were merged.

Stability studies: The solution of the labeled polymer in water as obtained from the separation after labeling (800 μL) was mixed with the PBS buffer (^{125}I) or stock solution of competing ions (^{111}In; $750\ mmol\ L^{-1}$ NaCl, $50\ mmol\ L^{-1}$ $MgSO_4$, $5.0\ mmol\ L^{-1}$ $CaCl_2$ and $5.0\ mmol\ L^{-1}$ KH_2PO_4) (200 μL) and incubated in an Eppendorf tube at 37 °C. At selected time points (4, 24 and 48 h, respectively) 300 μL aliquots were taken and separated on a PD-10 column as described above. Stability was calculated according to the following equation:

$$S = A_{polymer}/A_{total} * 100\%$$

where S is stability, $A_{polymer}$ is total activity in polymer fractions and A_{total} is total activity before separation.

3. Results and discussion

The model polymers were synthesized by radical copolymerization of the mixture of the main monomer [*N*-(2-hydroxypropyl)methacrylamide for polymer **1** and *N*-isopropyl acrylamide for polymer **2**] with *N*-methacryloyl tyrosinamide with AIBN as an initiator in good yield (>80% in both cases). The obtained tyrosinamide contents (0.74 mole% in polymer **1** and 0.76 mole% in polymer **2**, respectively) are in good correspondence with the methacryloyl tyrosinamide content in the polymerization mixture (1 mole%). This tyrosinamide content provides both sufficient labeling capacity for iodine radioisotopes (theoretical labeling capacity for no-carrier-added ^{125}I 8.6 and 10.6 $GBq\ mg^{-1}$ for **2** and **1**, respectively, for the case of complete iodination of the phenolic moieties in the polymer) and as low effect on the polymer physico-chemical properties as possible. For comparison, the typical doses of radionuclides for human patients are in the range 0.02–20 GBq depending on the radionuclide and particular application (Troncone and Rufini, 1997; Welch and Redvanly, 2003) which enables to introduce the required dose to <1 mg of polymer.

Chelating structures were attached to the phenolic moieties on polymer by azo coupling of the diazotized 4-aminophenyl derivatives of the chelators to the phenolic moiety on the *N*-methacryloyl tyrosinamide monomeric unit (see Fig. 3 for scheme). Conditions for the diazotization of the 4-aminophenyl derivatives of the chelators (sodium nitrite, hydrochloric acid, low temperature) as well as for azo coupling (weakly basic carbonate environment to activate the phenolic moiety on the polymer+low temperature) were adapted from procedures for synthesis of low-molecular-weight azo dyes (Masoud et al., 1985). The content of chelator may be easily followed spectrophotometrically due to the presence of chromophore in the azo dye structure at 331 nm at which the polymer without azo dye-bound chelator is transparent. See Table 1 for results. The wavelength and extinction coefficient were taken from the model low-molecular-weight azo dye containing the same chromophore as the conjugate. The effect of the diazotized chelator–polymeric phenol ratio on the conjugation yield was tested on the reaction of **1** with diazotized 4-aminophenyl CHXA″-DTPA. As expected, by rising of the diazotized chelator–polymeric phenol molar ratio from 1:1 to 2:1 and 3:1, the conjugation yield increases. Since the ratio 2:1 offered sufficient theoretical labeling capacity for ^{111}In ($6.29\ mmol\ g^{-1}$, i.e., $10.8\ GBq\ mg^{-1}$, for the case of the complete use of the chelators present in the polymer conjugate for binding ^{111}In) and acceptable consumption of the relatively expensive 4-aminophenyl chelator derivative, it was used for other conjugations. Conjugation yields of **1** with the diazotized 4-aminophenyl derivative of DTPA was slightly higher with 4-aminophenyl CHXA″-DTPA ($6.70\ \mu mol\ g^{-1}$ for polymer **3c**) and lower with the diazotized 4-aminophenyl derivative of DOTA ($1.49\ \mu mol\ g^{-1}$ for polymer **3b**) compared to 4-aminophenyl CHXA″-DTPA ($6.29\ \mu mol\ g^{-1}$ for polymer **3a**). Conjugation yields of **2** with the diazotized 4-aminophenyl derivatives of both DTPA ($3.00\ \mu mol\ g^{-1}$ for polymer **4c**) and DOTA ($3.09\ \mu mol\ g^{-1}$ for polymer **4b**) were lower than with CHXA″-DTPA ($5.89\ \mu mol\ g^{-1}$ for polymer **4a**). In all cases, sufficiently high chelating group contents above $1.49\ \mu mol\ g^{-1}$ ($2.6\ GBq\ mg^{-1}$ theoretical ^{111}In binding capacity) were achieved (see Table 1). In addition, no significant changes in molecular weights or polydispersity were observed (see Table 1) indicating that no crosslinking or degradation occurred during the conjugation.

Table 1
Conjugation and labeling yields.

Polymer	3a	3b	3c	4a	4b	4c	3a	3a
Chelating group to tyrosine molar ratio	2:1	2:1	2:1	2:1	2:1	2:1	1:1	3:1
Chelating group content (μmol g^{-1})	6.29	1.49	6.70	5.89	3.09	3.00	4.59	10.90
M_w (kDa)	58.0	58.3	59.9	34.3	33.1	52.4	57.4	58.2
I	1.67	1.57	1.55	1.44	1.46	1.79	1.60	1.61
Labeling yield (^{125}I, %)	96	96	95	93	93	n.d.	n.d.	n.d.
Labeling yield (^{111}In, %)	85	83	70	59	62	n.d.	n.d.	n.d.

n.d.=not determined, M_w=weight – average molecular weight, I—polydispersity ($I=M_w/M_n$).

Careful purification of the polymer to be labeled (two gel filtrations on a Sephadex G-25 column) is essential to fully remove free chelator, which would otherwise compete with the polymer during subsequent radionuclide labeling.

Labeling polymers with radionuclide was done by well-established methods for the particular isotopes: chloramine T method (producing the ^{125}ICl intermediate) for ^{125}I (Hruby et al., 2005; Welch and Redvanly, 2003). Iodination proceeds in high yields $>93\%$ in all cases showing that the presence of azo dye does not worsen radioiodination or label stability as we have seen in the case of, e.g., carbohydrate (Hruby et al., 2009) or hydrazide moieties containing polymers (Hruby et al., 2007).

Chelation in the presence of ammonium acetate buffer was used for ^{111}In labeling of the polymers with separation of the labeled polymer from free radionuclide on a PD-10 gel filtration column according to Hruby et al. (2005) and Welch and Redvanly (2003). Chelation labeling with ^{111}In proceeds in yields 70–85% for the copolymer **3** and about 60% for the copolymer **4**. The lower yield for the copolymer **4** is probably given by the less solvated state and thus higher sterical hindrance of the chelator on the partly hydrophobic thermoresponsive **4** compared to fully hydrophilic **3**. The yields of the ^{111}In labeling are apparently partly worsened by the fact that only the pure polymer containing fractions were taken for the calculation of the yield as polymer peak. Separation of free ^{111}In, in contrast to ^{125}I, needs to be done in solution containing low-molecular-weight ions (ammonium acetate in this case) to avoid ion–ion interactions of the separated species with the column, which however, causes some polymer peak tailing, so some labeled polymer is in the low-molecular fractions.

Stability of the polymer-radionuclide bond under model conditions is an important parameter of characterization of the newly developed labeling strategy. The experimental setup would show not only eventual transchelation or chelate hydrolysis, but also eventual unstability due to reversibility of radioiodination or unstability of the azo dye bond which is between the polymer and the radionuclide. Stability of the radioiodination was proven by incubation in phosphate buffered saline and re-separation on a PD-10 column. The stability of the label was in all cases $>96\%$ after 4 h, $>94\%$ after 24 h and $>93\%$ after 48 h incubation. Iodine is thus bound to polymer by a stable bond. Stability of chelation of ^{111}In was checked in the presence of competing ions in the same concentrations as typically present in blood plasma (Hruby et al., 2005). The stability was 82–88% for the pHPMA based polymer **3** and 70–74% for the pNIPAA based polymer **4** after 1 h incubation, 80–87% for the pHPMA based polymer **3** and 71–75% for the pNIPAA based polymer **4** after 4 h incubation and 80–86% for the pHPMA based polymer **3** and 68–73% for the pNIPAA based polymer **4** after 24 h incubation. There are only negligible differences among the three chelators used (DTPA, DOTA and CHXA″-DTPA) and stability of the ^{111}In label is sufficient for *in vivo* experiments. Apparently lower stabilities of the ^{111}In label on the pNIPAA based polymers are probably caused by peak tailing during separation on a PD-10 column (see above).

4. Conclusions

We have developed a radiolabeling strategy for synthetic polymers based on the formation of azo dye usable for both covalent (iodine radionuclides) and chelating (metal ion radionuclides) labeling modalities under mild conditions. Poly[*N*-(2-hydroxypropyl)methacrylamide] and poly(*N*-isopropyl acrylamide) were used as model polymers. *N*-methacryloyl tyrosinamide was introduced into the polymers by radical copolymerization and the phenolic moiety was then reacted with diazotized aromatic amine chelator precursors. The contents of labelable moieties (theoretical labeling capacities) were more than sufficient even for eventual radiotherapeutical use of such polymers. No significant changes in molecular weight of the polymers were observed during the conjugation reactions (no crosslinking). The conjugates were then radiolabeled with both the covalently bound (^{125}I) and chelated (^{111}In) radionuclides in high yields. Sufficient *in vitro* stability of the label was proven in the environment of competing metal ions. The described labeling method is thus a versatile, easy-to-do and sufficient-capacity-offering protocol for labeling polymers with both radioiodine and metal ion radionuclides.

Acknowledgments

Financial support of the Academy of Sciences of the Czech Republic (Grant # KAN 200200651), of the Ministry of Education, Youth and Sports of the Czech Republic (Grants # IM 4635608802 and # 2B06165) and of the Grant Agency of the Czech Republic (Grant # 202/09/2078) is gratefully acknowledged.

References

Adams, G.P., Shaller, C.C., Dadachova, E., Simmons, H.H., Horak, E.M., Tesfaye, A., Klein-Szanto, A.J.P., Marks, J.D., Brechbiel, M.W., Weiner, L.M., 2004. A single treatment of yttrium-90-labeled CHX-A″-C6.5 diabody inhibits the growth of established human tumor xenografts in immunodeficient mice. Cancer Res. 64 (17), 6200–6206.

Etrych, T., Chytil, P., Mrkvan, T., Sirova, M., Rihova, B., Ulbrich, K., 2008. Conjugates of doxorubicin with graft HPMA copolymers for passive tumor targeting. J. Controlled Release 132 (3), 184–192.

Fitzsimmons, J., Atcher, R., 2007. Synthesis and evaluation of a water-soluble polymer to reduce Ac-225 daughter migration. J. Labelled Compd. Radiopharm. 50 (1–2), 147–153.

Herth, M.M., Barz, M., Moderegger, D., Allmeroth, M., Jahn, M., Thews, O., Zentel, R., Rosch, F., 2009. Radioactive labeling of defined HPMA-based polymeric structures using [F-18]FETos for in vivo imaging by positron emission tomography. Biomacromolecules 10 (7), 1697–1703.

Hruby, M., Kucka, J., Lebeda, O., Mackova, H., Babic, M., Konak, C., Studenovsky, M., Sikora, A., Kozempel, J., Ulbrich, K., 2007. New bioerodable thermoresponsive polymers for possible radiotherapeutic applications. J. Controlled Release 119 (1), 25–33.

Hruby, M., Kucka, J., Mackova, H., Konak, C., Vetrik, M., Kozempel, J., Lebeda, O., 2009. New binary thermoresponsive polymeric system for local chemoradiotherapy. J. Appl. Polym. Sci. 111 (5), 2220–2228.

Hruby, M., Kucka, J., Mackova, H., Lebeda, O., Ulbrich, K., 2008. Thermoresponsive polymers—from laboratory curiosity to advanced materials for medicinal applications. Chem. Listy 102 (1), 21–27.

Hruby, M., Subr, V., Kucka, J., Kozempel, J., Lebeda, O., Sikora, A., 2005. Thermoresponsive polymers as promising new materials for local radiotherapy. Appl. Radiat. Isot. 63 (4), 423–431.

Kim, J.H., Park, K., Nam, H.Y., Lee, S., Kim, K., Kwon, I.C., 2007. Polymers for bioimaging. Prog. Polym. Sci. 32, 1031–1053.

Kissel, M., Peschke, P., Subr, V., Ulbrich, K., Schuhmacher, J., Debus, J., Friedrich, E., 2001. Synthetic macromolecular drug carriers: Biodistribution of poly[(N-2-hydroxypropyl)methacrylamide] copolymers and their accumulation in solid rat tumors. PDA J. Pharm. Sci. Technol. 55 (3), 191–201.

Krause, W., Hackmann-Schlichter, N., Maier, F.K., Muller, R., 2000. Dendrimers in diagnostics. Dendrimers II 210, 261–308.

Liu, C.B., Liu, G.Z., Liu, N., Zhang, Y.M., He, J., Rusckowski, M., Hnatowich, D.J., 2003. Radiolabeling morpholinos with Y-90, In-111, Re-188 and Tc-99m. Nucl. Med. Biol. 30 (2), 207–214.

Lu, Z.R., Wang, X.H., Parker, D.L., Goodrich, K.C., Buswell, H.R., 2003. Poly(ʟ-glutamic acid) Gd(III)-DOTA conjugate with a degradable spacer for magnetic resonance imaging. Bioconjugate Chem. 14 (4), 715–719.

Masoud, M.S., Elnahas, H.M., Khalil, E.A., 1985. Substituent effects on stability of complexes of iron (III), cobalt (II), nickel (II) and copper (II) with azocresols. Indian J. Chem. Sect. A Inorg. Bio-inorg. Phys. Theor. Anal. Chem. 24 (4), 347–348.

Nichol, C.A., Yang, D., Humphrey, W., Ilgan, S., Tansey, W., Higuchi, T., Zareneyrizi, F., Wallace, S., Podoloff, D.A., 1999. Biodistribution and imaging of polyethyleneimine—a gene delivery agent. Drug Delivery 6 (3), 187–194.

Quadri, S.M., Vriesendorp, H.M., 1998. Effects of linker chemistry on the pharmacokinetics of radioimmunoconjugates. Q. J. Nucl. Med. 42 (4), 250–261.

Rossin, R., Muro, S., Welch, M.J., Muzykantov, V.R., Schuster, D.P., 2008. In vivo imaging of Cu-64-labeled polymer nanoparticles targeted to the lung endothelium. J. Nucl. Med. 49 (1), 103–111.

Troncone, L., Rufini, V., 1997. I-131-MIBG therapy of neural crest tumours (Review). Anticancer Res. 17 (3B), 1823–1831.

Ulbrich, K., Subr, V., Strohalm, J., Plocova, D., Jelinkova, M., Rihova, B., 2000. polymeric drugs based on conjugates of synthetic and natural macromolecules I. Synthesis and physico-chemical characterisation. J. Controlled Release 64 (1–3), 63–79.

Uzgiris, E.E., Cline, H., Moasser, B., Grimmond, B., Amaratunga, M., Smith, J.F., Goddard, G., 2004. Conformation and structure of polymeric contrast agents for medical imaging. Biomacromolecules 5 (1), 54–61.

Welch, M.J., Redvanly, C.S., 2003. Handbook of Radiopharmaceuticals: Radiochemistry and Applications. Wiley, Chichester.

Polyoxazoline Thermoresponsive Micelles as Radionuclide Delivery Systems[a]

Martin Hruby,* Sergey K. Filippov, Jiri Panek, Michaela Novakova, Hana Mackova, Jan Kucka, David Vetvicka, Karel Ulbrich

Thermoresponsive polymer micelles are promising drug and radionuclide carriers with a strong passive targeting effect into solid tumors. We have synthesized ABA triblock copolymers poly[2-methyl-2-oxazoline-*block*-(2-isopropyl-2-oxazoline-*co*-2-butyl-2-oxazoline)-*block*-2-methyl-2-oxazoline]. These polymers are molecularly dissolved in aqueous millieu below the cloud point temperature (CPT) of the thermoresponsive central block and above CPT form polymer micelles at CMC 5–10 $\times 10^{-5}$ g $\cdot$ mL^{-1} with diameter $\approx$200 nm. The phenolic moiety introduced into the copolymer allowed radionuclide labeling with iodine-125 ongoing in good yield with sufficient in vitro stability under model conditions.

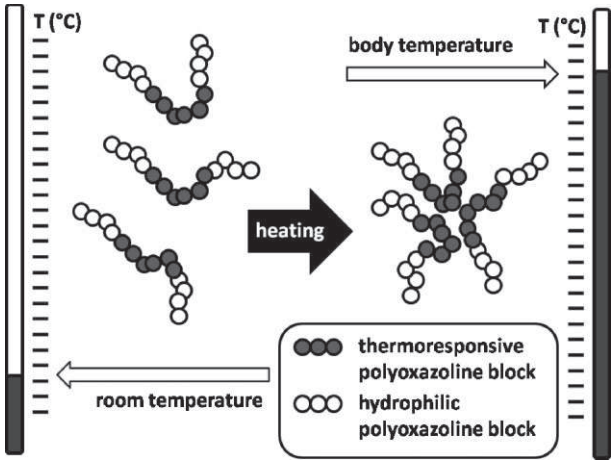

Introduction

Poly(2-alkyl-2-oxazolines) are attracting increasing attention in biomedicinal research due to their peptide-related structure and wide range and adjustable physicochemical and biological properties depending on the alkyl substituent.[1–3] Their properties range from high hydrophilicity enabling synthesis of hydrophilic water soluble biocompatible polymers with excellent antibiofouling properties (alkyl = methyl or ethyl)[4] through thermal sensitivity of thermoresponsive polymers (alkyl = isopropyl)[2,5] to hydrophobicity typical for hydrophobic aromatic or aliphatic polymers (substituent = phenyl, butyl, nonyl etc.).[1,6] Moreover, polyoxazolines may be synthesized by controlled living cationic ring-opening polymerization with polydispersities typically below 1.3 and this method enables synthesis of block copolymers by subsequent addition of different monomers.[7,8] The choice of initiator and terminating agent also enables synthesis of polymers with defined chain ends (see scheme in Scheme 1).[9]

Polymer micelles rank highly among prospective anticancer drug and radionuclide delivery systems, enabling efficient tumor targeting due to their high apparent molecular weight (EPR effect).[10,11] Unimers may be eliminated rapidly from organisms by glomerular filtration after disassembly of the micellar system that fulfilled its task as a drug carrier.[10,11] Many micelles with a thermoresponsive core (made of a polymer block with a lower critical solubility temperature (LCST)) and a hydrophilic corona have the additional advantage of simple preparation by heating of an aqueous solution of the thermoresponsive

M. Hruby, S. K. Filippov, J. Panek, M. Novakova, H. Mackova, J. Kucka, K. Ulbrich
Institute of Macromolecular Chemistry, v.v.i., Academy of Sciences of the Czech Republic, Heyrovsky Sq. 2, 162 06 Prague 6, Czech Republic
Fax: + 420 296 809 410.; E-mail: mhruby@centrum.cz
D. Vetvicka
Institute of Microbiology, v.v.i., Academy of Sciences of the Czech Republic, Videnska 1083, 142 20 Prague 4, Czech Republic

[a] Supporting information for this article is available at the bottom of the article's abstract page, which can be accessed from the journal's homepage at http://www.mbs-journal.de, or from the author.

Macromol. Biosci. **2010**, *10*, 916–924
© 2010 WILEY-VCH Verlag GmbH & Co. KGaA, Weinheim
WILEY InterScience® DISCOVER SOMETHING GREAT
DOI: 10.1002/mabi.201000034

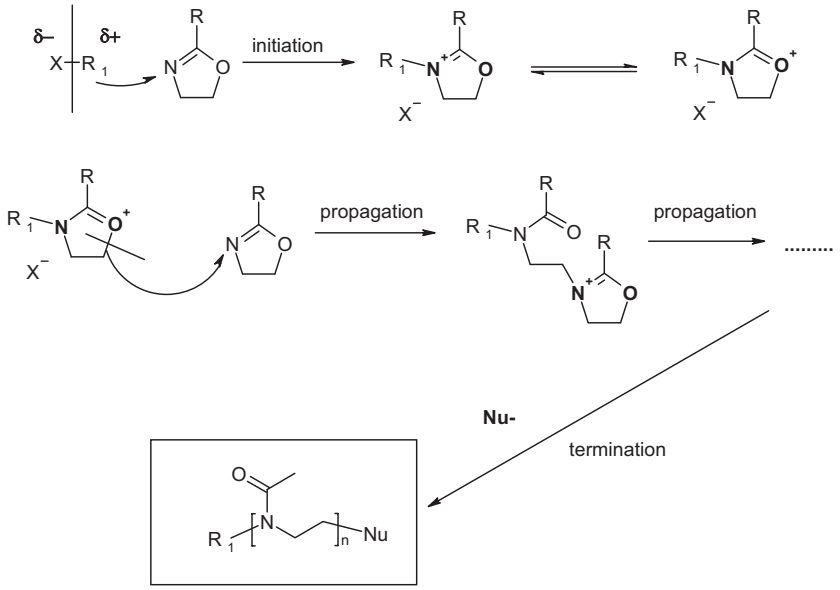

Scheme 1. Mechanism of living cationic polymerization of 2-alkyl-2-oxazolines.

polymer.[12] Since there are thermoresponsive poly(2-alkyl-2-oxazolines) with suitable properties described in the literature,[13–17] we decided to use this class of polymers for the construction of our thermoresponsive micellar radionuclide delivery systems.

In this paper we describe the synthesis and study of the properties of ABA triblock copolymer poly[2-methyl-2-oxazoline-*block*-(2-isopropyl-2-oxazoline-*co*-2-butyl-2-oxazoline)-*block*-2-methyl-2-oxazoline] with two hydrophilic A blocks (poly(2-methyl-2-oxazoline)) and one central thermoresponsive B block copolymer (poly(2-isopropyl-2-oxazoline-*co*-2-butyl-2-oxazoline)) with different monomer unit ratios. These polymers are molecularly soluble in aqueous milieu below the cloud point temperature (CPT) of the thermoresponsive block and self-assemble into micelles at higher temperature. Micelles are formed within a narrow temperature range. The CPT of the thermoresponsive block may be adjusted with the 2-butyl-2-oxazoline (hydrophobic monomer lowering the CPT) to 2-isopropyl-2-oxazoline (main monomer giving thermoresponsive properties to its copolymers) ratio and the size of the micelles can be controlled by the A to B block weight ratio. A phenolic moiety was introduced into the above stated polymer to allow radionuclide labeling with iodine radioisotopes for both diagnostics (^{123}I, ^{124}I) and therapy (^{131}I) of solid tumors. The polymers were isotopically labeled and the in vitro stability of the radiolabel was checked.

Experimental Part

Low Molecular Weight Precursors

2-Isopropyl-2-oxazoline (IprOX), 2-butyl-2-oxazoline (BuOX) and 2-butenyl-2-oxazoline (EnOX) were synthesized according to ref.[5,18] by condensation of ethanolamine with the particular carboxylic acid (isobutyric or valeric for IprOX and BuOX, respectively), or by a multistep method according to ref. [18] (EnOX). *N*-(2-sulfanylethyl)-2-(4-hydroxyphenyl) acetamide was synthesized by condensation of 4-hydroxyphenylacetic acid and cystamine with (EEDQ) as a condensation reagent according to the following procedure (see Scheme 2). Cysteamine (2.00 g, 25.9 mmol) was dissolved by gentle heating in tetrahydrofuran (THF, 200 mL), 2-ethoxy-1-ethoxycarbonyl-1,2-dihydroquinoline (6.41 g, 25.9 mmol) was dissolved in THF (50 mL) and 4-hydroxyphenylacetic acid (3.44 g, 22.6 mmol) was also dissolved in THF (20 mL). The solution of EEDQ was mixed with the solution of 4-hydroxyphenylacetic acid and then the solution of cysteamine was added. The mixture was stirred overnight at ambient temperature, heated at 60 °C for 1 h and then evaporated in vacuo. The solid residue was vigorously shaken with water and diethyl ether (aa 100 mL). The suspension was filtered and the collected precipitated product was recrystallized from methanol. The yield was 3.34 g (70%).

^{1}H NMR (CD_3OD): $\delta = 2.75$ (t, $-CH_2-S-$), 3.33 (s, Aryl$-CH_2-CO-$), 3.43 (t, $N-CH_2-$), 6.72 (d, Aryl$-$H on positions 2 and 6), 7.08 (d, Aryl$-$H on positions 3 and 5). ^{13}C NMR (CD_3OD): $\delta = 38.4$ ($-CH_2-S-$), 39.7 ($N-CH_2-$), 43.1 (Aryl$-CH_2-$), 116.4 (aromatic carbons in positions 3 and 5), 127.5 (aromatic carbon in position 1), 131.2 (aromatic carbons in positions 2 and 6), 157.5 (aromatic carbon in position 4), 175.0 ($-CO-$). $C_{10}H_{13}NO_2S$ (211.3): Calcd. C 56.85, H 6.20, N 6.63, S 15.18; Found C 56.90, H 6.03, N 6.50, S 15.10.

All other chemicals were purchased from Sigma-Aldrich Ltd. (Prague, Czech Republic). 2-Methyl-2-oxazoline (MeOX) was distilled with calcium hydride before use, and all other chemicals were used as obtained.

Synthesis of Polymers

Living cationic ring opening polymerization was performed in acetonitril using tosylates as initiators. Thermoresponsive polymers poly(IprOX-*co*-BuOX) as models of the thermoresponsive central block were synthesized as follows. The mixture of monomers (IprOX with 0, 10 and 20 mol-% BuOX, respectively, total weight 1.00 g in all cases) was polymerized in anhydrous acetonitrile (1.00 mL) using methyl *p*-toluenesulfonate (37 mg, 0.2 mmol) as an initiator. The polymerization was carried out at 42 °C for 8 d in a 15 mL Ace pressure tube (Sigma-Aldrich Ltd., Prague, Czech Republic) under a dry nitrogen atmosphere. The polymerization mixture was mixed with ethanol (30 mL), left overnight at room temperature and evaporated in vacuo. The raw polymer was purified by gel permeation chromatography on Sephadex LH-20 using methanol as the eluent and evaporation of the polymer-containing fractions in vacuo. The polymer was redissolved in ethanol and evaporated in vacuo to obtain solid foam, which was easier to manipulate. A typical yield was ca. 0.90 g (90%).

© 2010 WILEY-VCH Verlag GmbH & Co. KGaA, Weinheim

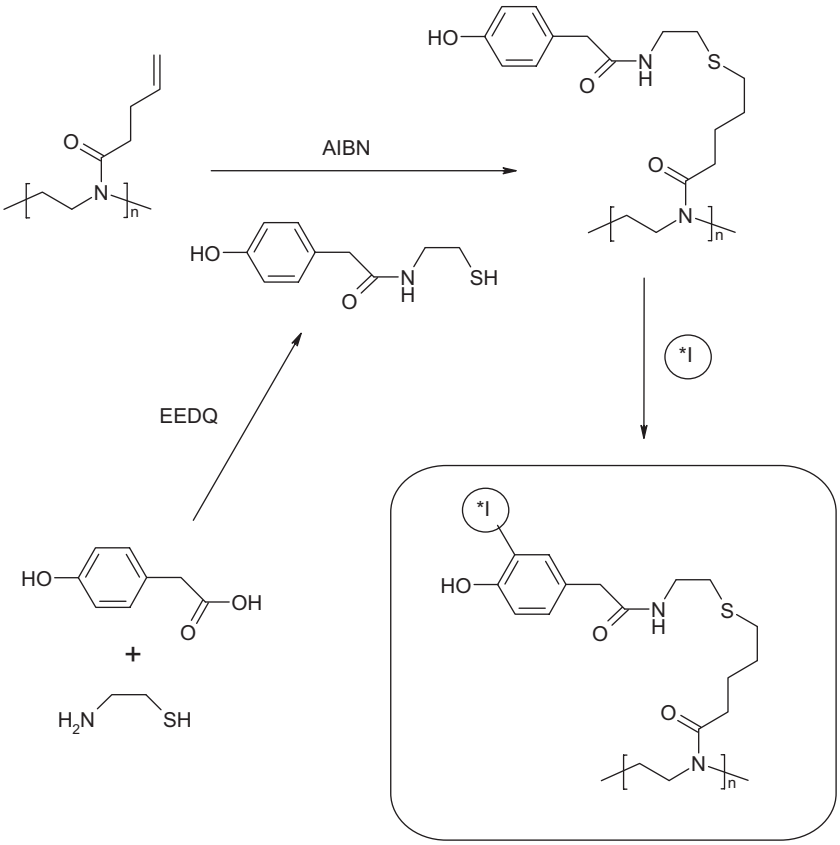

Scheme 2. Scheme of synthesis of sulfanylethyl-2-(4-hydroxyphenyl)acetamide and introduction of isotopically labelable phenolic moiety into the block copolymers.

The triblock ABA copolymers poly[MeOX-*b*-(IprOX-*co*-BuOX)-*b*-2-MeOX] were synthesized as follows in nine alternatives with three different central block compositions (10, 15 and 20 mol-% BuOX, respectively) and thermoresponsive to hydrophilic block ratios (1:2, 1:1 and 2:1 w/w, respectively) in all possible combinations (see Scheme 3). The mixture of 2-isopropyl-2-oxazoline with 10, 15 and 20 mol-% BuOX, respectively, and total weights 0.66, 1.00 and 1.33 g, respectively, was polymerized using diethylene glycol di(*p*-toluenesulfonate) (83 mg, 0.20) as the initiator in anhydrous acetonitrile (1.00 mL). The polymerization was carried out at 42 °C for 7 d in a 15 mL Ace pressure tube (Sigma-Aldrich Ltd., Prague, Czech republic) under a dry nitrogen atmosphere. After this, 2-methyl-2-oxazoline (to the total weight of the sum of oxazoline monomers 2.00 g, i.e., 1.33, 1.00 and 0.66 g, respectively) and anhydrous acetonitrile (1.00 mL) were added and the polymerization continued for 7 d. The polymerization mixture was mixed with ethanol (30 mL) and the mixture was worked up as described above for the polymerization of model poly(IprOX-*co*-BuOX) copolymers. A typical yield was ca. 1.85 g (93%).

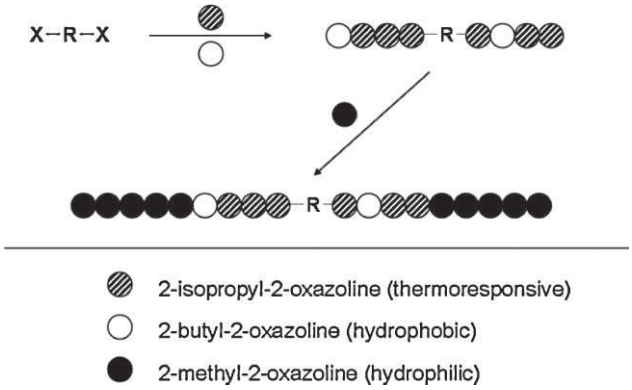

Scheme 3. Schematic imaging of formation of triblock copolymers.

In the case of the polymers to be isotopically labeled, EnOX (25 mg, 0.20 mmol) was used instead of the equimolar part of BuOX thus forming poly[MeOX-*b*-(IprOX-*co*-BuOX-*co*-EnOX)-*b*-MeOX].

Molecular weights of the polymers were determined by size exclusion chromatography (SEC) in a mixture of acetate buffer (pH 6.5; 0.3 mol · L^{-1}) and methanol (20:80 v/v) as a mobile phase on a TSK 3000 column (Polymer Laboratories Ltd., UK) using HPLC System ÄKTA Explorer (Amersham Biosciences; Sweden) equipped with RI, UV and multi-angle light-scattering DAWN DSP-F (Wyatt, USA) detectors. The refractive index increments of polyMeOX ($dn/dc = 0.181 \pm 0.001$ mL · g^{-1}) and polyIprOX ($dn/dc = 0.177 \pm 0.002$ mL · g^{-1}) in the mobile phase used for molecular weight determination were measured on a Brice-Phoenix visual laboratory type differential refractometer BP-2000-V (Phoenix Precision Instrument Co., USA), and the dn/dc of the copolymers was calculated as a weighted average reflecting monomeric composition.

The content of BuOX monomeric moiety in the thermoresponsive block poly[IprOX-*co*-BuOX] was calculated according to Equation (1) from the ^{1}H NMR spectra measured in $CDCl_3$.

$$w_1 = S_{0.91}/(S_{0.91} + (S_{1.09}/2)) \quad (1)$$

where $S_{0.91}$ is the integral signal of the terminal $-CH_3$ hydrogen nuclei in the BuOX monomeric unit at $\delta = 0.91$, $S_{1.09}$ is the integral signal of the $-CH_3$ hydrogen nuclei in the IprOX monomeric units at $\delta = 1.09$ ppm and w_1 is the mole fraction of the BuOX monomeric unit in the thermoresponsive block.

The content of the MeOX monomeric moiety in the copolymer was calculated according to Equation (2) from the ^{1}H NMR spectra measured in $CDCl_3$.

$$w_2 = (S_{2.09}/3)/((S_{3.46}/4) - (S_{1.09}/6)) \quad (2)$$

where $S_{2.09}$ is the integral signal of the $-CO-CH_3$ hydrogen nuclei in the MeOX monomeric unit at $\delta = 2.09$, $S_{3.46}$ is the integral signal of the oxazoline backbone $N-CH_2-CH_2-N$ hydrogen nuclei at

© 2010 WILEY-VCH Verlag GmbH & Co. KGaA, Weinheim
Macromolecular Journals
DOI: 10.1002/mabi.201000034

$\delta = 3.46$ ppm, $S_{1.09}$ is the integral signal of the $-CH_3$ hydrogen nuclei in the IprOX monomeric units at $\delta = 1.09$ ppm and w_2 is the mole fraction of the MeOX monomeric unit in the copolymer.

Addition of *N*-(2-Sulfanylethyl)-2-(4-hydroxyphenyl)acetamide to Double Bonds of Poly[MeOX-*b*-(IprOX-*co*-BuOX-*co*-EnOX)-*b*-MeOX]

Poly[MeOX-*b*-(IprOX-*co*-BuOX-*co*-EnOX)-*b*-MeOX] (100 mg) and *N*-(2-sulfanylethyl)-2-(4-hydroxyphenyl)acetamide (100 mg) were dissolved in *N*,*N*-dimethylacetamide (DMAc, 1.2 mL). Azobis(isobutyronitril) (AIBN, 50 mg) was dissolved in DMAc (800 μL). The solution of polymer and thiol was heated at 100 °C for 24 h while the solution of AIBN was added in four 200 μL aliquots every 2 h (i.e., at $t = 0$, 2, 4 and 6 h). The solution was cooled to ambient temperature, methanol (3.0 mL) was added and the polymer was isolated by gel permeation chromatography on Sephadex LH-20 column using methanol as the eluent and evaporation of the polymer containing fraction. The yield was 82 mg (82%).

The content of the phenolic moiety was determined by ^{1}H NMR in $CDCl_3$ according to Equation (3):

$$c_{\text{phenol}} = 2 \times 10^6 \times S_{7.12}/(M \times S_{3.46}) \quad (3)$$

where $S_{7.12}$ is the integral signal of the Aryl-H hydrogen nuclei in the *ortho*- position relative to the hydroxy group on the aromatic ring at $\delta = 7.12$ ppm, $S_{3.46}$ is the integral signal of the oxazoline backbone $N-CH_2-CH_2-N$ hydrogen nuclei at $\delta = 3.46$ ppm, M is the average molecular weight of monomeric units weighted in respect to their content in the copolymer and c_{phenol} is the phenolic unit content in micromol per gram of polymer.

Cloud Point Temperature Determination

Cloud point temperatures (CPT) of the polymers were determined in aqueous solutions of the particular polymer (25 mg · mL^{-1}) at a heating rate of 1 °C · min^{-1} with laser scattering detection.

Static (SLS) and Dynamic (DLS) Light Scattering

The temperature-induced micelle formation in aqueous solutions, temperature dependences of the apparent hydrodynamic radius of the particle, R_h, and scattering intensity, I_s, were automatically measured at a scattering angle $\theta = 173°$ on a Zetasizer Nano-ZS, Model ZEN3600 (Malvern Instruments, UK). For evaluation of data, the DTS (Nano) program was used. It provides a R_h intensity, volume and number-weighted distribution function $G(R_h)$. A volume-weighted value of apparent R_h was chosen for the monitoring of temperature changes in the system because it gives a more realistic view of the characteristic particle size in a solution. Such information is more valuable for assessing possible biomedical impact. The temperature dependences of micelle formation and disintegration (a hysteresis measurement) were measured by heating from 10 to 70 °C and back in variable steps: 0.5 or 1.2 °C (slow temperature variations). After every temperature change, heating or cooling, five measurements were performed after reaching steady state conditions.

The accurate determination of the shape factor of the particle R_g/R_h was carried out by static and dynamic light scattering measurements at a temperature just above a threshold, to avoid multiple scattering influence, in the angular range 30–150° using an ALV instrument equipped with a 30 mW He-Ne laser (vertically polarized light at $\lambda = 632.8$ nm). The light scattering data were taken after a fixed waiting time of 20 min to achieve equilibration of the sample. The Zimm plot procedure was used for the R_g evaluation. Dynamic light scattering measurements were carried out multiple times at a 90° angle. The obtained correlation functions were analyzed by REPES analytical software providing a hydrodynamic radius distribution function, $G(R_h)$. To account for the logarithmic scale on the R_h axis, all DLS distribution diagrams are shown in the equal area representation, $R_hG(R_h)$. The values of R_h for each system were averaged over three runs.

If not otherwise stated, all measurements were done with a polymer concentration of 0.5 g · L^{-1} in water and all solutions were filtered through a 0.22 μm PVDF syringe filter before a measurement.

Determination of Critical Micelle Concentration (CMC) by Static Light Scattering Measurements

For polymers that have a cloud point temperature below body temperature, CMC values were determined by static light scattering experiments as the intersection points of straight lines drawn through the data at small and large concentrations (see Supporting Information for a typical example). Static light scattering measurements were carried out multiple times at a 90° angle using an ALV instrument equipped with a 30 mW He-Ne laser (vertically polarized light at $\lambda = 632.8$ nm). Heating was achieved by immersion of the polymer solution (ca 1 mL) in a measuring cell placed into a pre-heated thermostated bath (37 °C).

Radioisotope Labeling Studies

Radioisotope labeling with ^{125}I and stability studies were performed as described in the literature.[19]

Haemolytic Assay

Human blood from a healthy volunteer was collected in 5 mL Heparin coated vacutainers (Greiner Bio-One, Austria) and centrifuged for 5 min at 3 000 rpm. The blood sediment was twice washed in fresh PBS (pH 7.4) and 4% human red blood cell (RBC) suspension was prepared. The micellar delivery system was added to RBC suspensions to achieve final concentrations in the range 1–1 000 μg · mL^{-1}. All samples were incubated at 37 °C in a humidified 5% CO_2 – 95% air atmosphere for either 30 min or 24 h and then centrifuged for 5 min at 3 000 rpm. The supernatants were spectrophotometricaly analyzed at 550 nm (Spectra Rainbow, Tecan, Austria). Distilled water was used as a positive control of haemolysis and PBS as a negative control. The value of haemolytic activity was calculated by considering absorbance of positive

© 2010 WILEY-VCH Verlag GmbH & Co. KGaA, Weinheim

control as 100% haemolysis. The results are the means of two independent experiments, and the standard deviation was lower than 5%.

Results and Discussion

Polymer Synthesis

The thermoresponsive polymeric micellar drug delivery system was made of a ABA triblock copolymers poly[MeOX-*b*-(IprOX-*co*-BuOX)-*b*-MeOX] with two hydrophilic A blocks (polyMeOX) and one central thermoresponsive B block [poly(IprOX-*co*-BuOX)] with different monomer unit ratios. The triblock copolymers were synthesized by living cationic ring-opening polymerization using diethylene glycol ditosylate as the initiator. This highly reactive commercially available bifunctional initiator allows synthesis of triblock copolymer by a one pot method in two steps starting with the middle copolymer block. In the first step, the mixture of monomers forming the thermoresponsive block (IprOX + BuOX) is polymerized with diethylene glycol ditosylate forming a thermoresponsive polymer block with two living cationic ends. In the second step, the monomer forming the hydrophilic terminal blocks (MeOX) was added and the polymerization continued on both chain ends forming two terminal hydrophilic polymer chains. The polymerization was done under conditions (anhydrous acetonitrile, 42 °C) described in the literature[2] to keep the polymerization living without significant chain transfer or termination. Copolymerization was set by the initiator-monomer ratio to synthesize copolymers of a theoretical molar weight of 10 kDa. This molar weight is sufficiently low to allow elimination of unimers by kidneys (the renal threshold is ca. 45 kDa for hydrophilic polymers) after disassembly of the system, but still sufficiently high to suppress intermolecular heterogeneity (given by the statistical nature of the IprOX-BuOX copolymerization) among the polymer chains.

Before using central thermoresponsive IprOX-BuOX copolymer for the synthesis of the triblock copolymers, we optimized its composition with respect to the cloud point temperature. IprOX homopolymer itself has relatively high cloud point temperature only slightly below body temperature (33 °C at $c_{\mathrm{polymer}} = 25\ \mathrm{mg \cdot mL^{-1}}$). This is why it should be decreased to assure formation of micelles at body temperature if also more hydrophilic corona-forming blocks are present in the macromolecule. The hydrophilic blocks significantly increase the micelle-forming temperature compared to the cloud point temperature of the thermoresponsive block alone (see below). The presence of hydrophobic groups (monomer units) in the polymer makes solvation interactions weaker, which results in a decrease in CPT of such copolymers (LCST is an entropy-driven transition, i.e., the release of water in the solvation shell into the bulk water resulting in an entropy gain is the driving force).

We have chosen BuOX as a more hydrophobic monomer for this study. Synthesis of the model thermoresponsive copolymers was carried out under the same conditions as synthesis of the block copolymers (anhydrous acetonitrile, 42 °C). The molar weight was set to be the average value as in the triblock copolymers (5.0 kDa). Methyl tosylate was used as an initiator in this case. The copolymers were obtained in high yields (> 90% after purification), had molar weights in good correspondence with theory (weight-average molecular weights $\overline{M}_{\mathrm{w}} = 4.72$ kDa in the range ± 0.19 kDa) and narrow molecular weight distributions (polydispersities $I = \overline{M}_{\mathrm{w}}/\overline{M}_{\mathrm{n}} = 1.15$ in the range ± 0.02, where $\overline{M}_{\mathrm{n}}$ is the number-average molecular weight); see Supporting Information for a typical size-exclusion chromatogram. The content of the BuOX monomeric unit in the copolymers is within the experimental error identical (correlation coefficient 0.997, i.e., within 15 relative % of the theoretical value in all cases) with the composition of the polymerization mixture, consistent with the nearly quantitative polymer yield and thus nearly complete monomer consumption. The monomer unit composition in the copolymer was followed by ^{1}H NMR (see Experimental Part for details and Supporting Information for typical NMR). An increase in the content of BuOX in the copolymers within a range 0–20 mol-% of BuOX causes a nearly linear ($R^2 = 0.996$) decrease in their CPT (0.81 °C per mol-% BuOX). The cloud point temperature was slightly higher at lower copolymer concentrations in a solution and this concentration dependence was somehow more pronounced in statistic IprOX-*co*-BuOX copolymers compared to pure IprOX homopolymer (see Supporting Information), probably due to statistical intermolecular heterogeneity (similar to that reported for other polyoxazoline copolymers).[20,21]

The triblock copolymers poly[MeOX-*b*-(IprOX-*co*-BuOX)-*b*-MeOX] were synthesized in high yields (> 90% after purification). Their molar weights were only slightly lower than theoretically expected (found $\overline{M}_{\mathrm{w}} = 8.58$ kDa in the range ± 0.34 kDa) with slightly higher polydispersities ($I = 1.39$ in the range ± 0.04) compared to the model copolymers poly(IprOX-*co*-BuOX); see Supporting Information for a typical size-exclusion chromatogram. The slightly higher polydispersities may be due to the use of ethylene glycol ditosylate as an initiator, which results in slower initiation compared to methyl tosylate which yields broader molar mass distributions. This is comparable to the recently reported difference using butyne tosylate and propargyl tosylate initiators.[22] Monomeric unit composition, as followed by ^{1}H NMR (see Experimental Part for details and Supporting Information for typical NMR) was identical within the experimental error with the monomer feed (correlation coefficient 0.996 within 15 relative-% of the theoretical value in all cases), consistent with the near

© 2010 WILEY-VCH Verlag GmbH & Co. KGaA, Weinheim

DOI: 10.1002/mabi.201000034

quantitative conversion, as was also the case for the model copolymers.

Temperature-responsive Aggregation Behavior

Static and dynamic light scattering methods are common tools to characterize temperature-dependent structural changes of thermoresponsive polymers with LCST. The intensity of the scattered light is sensitive to the molar mass and the size of the scatters and thus can be used to follow the phase separation. A detailed review of the properties of temperature-sensitive polymers, including light scattering studies, has been published.[23] Recently, light and neutron scattering methods were exploited extensively for the investigation of these polymers, e.g., of poly(*N*-isopropylacrylamide)[24,25] (PNIPAM), poly(*N*-vinyl caprolactam)[24,26] (PVCL), poly(methyl vinyl ether)[24] (PVME), hydrophobically modified poly(*N*-isopropylacrylamide) (HM-PNIPAM)[27–31] or of hydrophobically modified polyoxazolines.[32–34]

Several scenarios for the structural transition in a solution during phase separation could come to life, depending on the chemical composition and concentration of the thermoresponsive polymer. It was proven that PNIPAM with high molecular weight at low concentrations exists in a coil conformation below the LCST. On approaching the LCST, a homopolymer undergoes a coil-globule transition, wherein the loose macromolecules at first collapse into a compact globule with further aggregation of globules into a so-called mesoglobule. The PNIPAM mesoglobules are uniform and colloidally stable particles with some amount of water. Once created, they have a tendency to shrink with increasing temperature. At high concentrations, PNIPAM macromolecules form intermolecular aggregates below the CPT. The propensity to aggregate in cold water below the CPT was found for other thermosensitive homopolymers - PVCL and PVME, disregarding their molecular weight and concentration. Loose and polydisperse aggregates transform above the CPT into nearly monodisperse compact (although non-uniform) mesoglobules with a sponge-like structure. The density of such mesoglobules declines from the center to the periphery. The third scenario is realized when a macromolecule contains chemically different moieties: thermoresponsive/hydrophobic or thermoresponsive/hydrophilic. Inclusion of hydrophilic groups in a macromolecule shifts CPT to higher values; hydrophobic moieties have an opposite effect. Below CPT at low concentrations, hydrophobically modified macromolecules form multi-chain assemblies, presumably flower-like micelles, with low aggregation numbers.[25,27,30–33] At higher concentrations, flower-like micelles form inter-micelle aggregates with lower density. When approaching the CPT, flower-like micelles undergo a coil-to-globule transition and monodisperse aggregates or mesoglobules are formed.[23] It was noticed that the mesoglobules occurring above the CPT adopt a core-shell structure resembling a micelle.

In the majority of cases, the hysteresis in the temperature dependence of apparent R_h is manifested. One can see that the mesoglobules disintegrate at a lower temperature in comparison with the one of creation. The R_h value of the mesoglobules also shows non-monotonous behavior near the CPT. Occurrence of hysteresis was explained by the presence of intra- or interchain hydrogen bonds that are broken during cooling.[23,25]

Our light scattering experiments prove that the synthesized thermosensitive polyoxazolines have similar features to the thermosensitive polymers described above. We have completed a basic characterization in water to make the system as principally transparent as possible. In physiological solution (0.9 wt-% NaCl), the temperature-dependent behavior is exactly the same in shape, but everything is shifted 3 °C to lower temperatures. All samples visually become turbid when heated above CPT where dynamic light scattering reveals the formation of nanosize objects (see Supporting Information for chart). On cooling down the samples to below CPT, turbidity disappears, so a transparent solution is formed. Formation of nanoparticles is completely reversible in all cases. Because the perspective structure of nanoparticles built from the studied polymers will be a core-shell one, we will exploit hereafter the term micelle rather than mesoglobule.

The CPT value is a function of the polymer composition (see Supporting Information for chart and Table 1). One can see that through the whole polymer series the CPT increases as the content of hydrophilic MeOX groups increases. Conversely, increasing the content of hydrophobic BuOX moieties results in CPT reduction.

In all cases, the micelle-formation temperatures of the triblock copolymers are significantly higher than CPTs of the thermoresponsive copolymers of the same composition as the thermoresponsive block of the triblock copolymer. If we also compare triblock copolymers with different thermoresponsiveness to hydrophilic block ratios (but the same ratio of monomeric units in the thermoresponsive block), the increase in the hydrophilic block content considerably increases CPT. One can thus conclude that the overall hydrophilicity/hydrophobicity of the whole triblock copolymer is at least of the same importance as the ratio of monomeric units and subsequently the CPT of the thermoresponsive block itself. These triblock copolymers thus behave more like Pluronics [poly(ethylene oxide-*block*-propylene oxide-*block*-ethylene oxide) block copolymers] or poly(ethylene oxide-*block*-lactide) than like, for example, *N*-isopropyl acrylamide copolymers, where the CPT of the thermoresponsive block itself is dominant in determination of the thermal behavior of the block and graft copolymers. The effect also cannot be attributed to the

© 2010 WILEY-VCH Verlag GmbH & Co. KGaA, Weinheim

Table 1. Chemical composition and properties of ABA triblock copolymers poly[2-methyl-2-oxazoline-*block*-(2-isopropyl-2-oxazoline-*co*-2-butyl-2-oxazoline)-*block*-2-methyl-2-oxazoline]; n_{MeOX} - average number of 2-methyl-2-oxazoline monomeric units per polymer chain, n_{IprOX} - average number of 2-isopropyl-2-oxazoline monomeric units per polymer chain, n_{BuOX} - average number of 2-butyl-2-oxazoline monomeric units per polymer chain.

Triblock colymer	Thermoresponsive to hydrophilic block	BuOX in thermoresponsive block	T_{dem}	CMC at 37 °C	n_{MeOX}	n_{IprOX}	n_{BuOX}
	w/w	mol-%	°C	$g \cdot mL^{-1}$			
P2574-1:2	1:2	10	62	–	78	27	2.6
P2574-1:1	1:1	10	63	–	59	40	3.9
P2574-2:1	2:1	10	64	–	39	53	5.2
P2639-1:2	1:2	15	44	–	78	25	3.9
P2639-1:1	1:1	15	28	1.0×10^{-4}	59	38	5.9
P2639-2:1	2:1	15	27	2.5×10^{-5}	39	50	7.9
P2620-1:2	1:2	20	42	–	78	24	5.2
P2620-1:1	1:1	20	38	–	59	35	7.9
P2620-2:1	2:1	20	28	5×10^{-5}	39	47	10.5

effect of the molecular weight of the thermoresponsive blocks, because the molecular weights of the model thermoresponsive copolymers and of the thermoresponsive block in the triblock copolymers are comparable.

Below the CPT, the values of the hydrodynamic radius of the P2639-2:1 polymer correspond to the size of single macromolecules (1–2 nm average), implying that that they are fully dissolved (Figure 1(a)). The scattered light intensity increases approaching the CPT (Figure 1(b)). At the CPT it sharply increases and a simultaneously increasing apparent R_h indicates the formation of micelles (Figure 1).

Although all the triblock copolymers form micelles at certain temperatures, their properties above the CPT differ, depending on the ratio between hydrophobic, hydrophilic and thermosensitive moieties. Thus for P2620-1:1 polymer with the highest content of hydrophobic BuOX groups (20 mol-% in the thermosensitive block) and medium hydrophilicity, it was observed that the nanoparticle size continuously decreases with increasing temperature (Figure 2(a)). Meanwhile, the intensity of the scattered light grows (Figure 2(b)). Heating and cooling measurements shows minor hysteresis of about 2 °C (see Figure 2(a)). In contrast to that, for solutions of P2639-1:2, the intensity and size of the micelles above the CPT permanently grows (Figure 3). Heating and cooling measurements show almost complete absence of hysteresis. Hydrophobic/hydrophilic interactions among whole macromolecules (as a result of the overall hydrophilicity/hydrophobicity of the polymer chains) thus become dominant above CPT for the P2639-1:2 polymer compared to polymer P2620-1:1 due to the shorter length and lower hydrophobicity of the thermoresponsive block (a switch from block polymer-type behavior shown in Figure 2(a) and 2(b)).

The trend of changes during heating and cooling in apparent R_h for P2639-2:1 is quite different to those of P2639-1:2 and P2620-1:1 (see Supporting Information for chart). The apparent R_h dramatically increases above the cloud point and the sharp peak in the R_h vs. temperature dependence reveals the formation of large intermolecular aggregates. At higher temperatures, aggregates gradually shrink and micelles are formed above 40 °C. The shape factor (R_g/R_h) values at temperatures 15–20 °C above the CPT are approximately 0.8–1. Minor hysteresis is detectable for the polymer (see Supporting Information for chart). Such behavior is in agreement with previous observations for thermoresponsive polymers reported

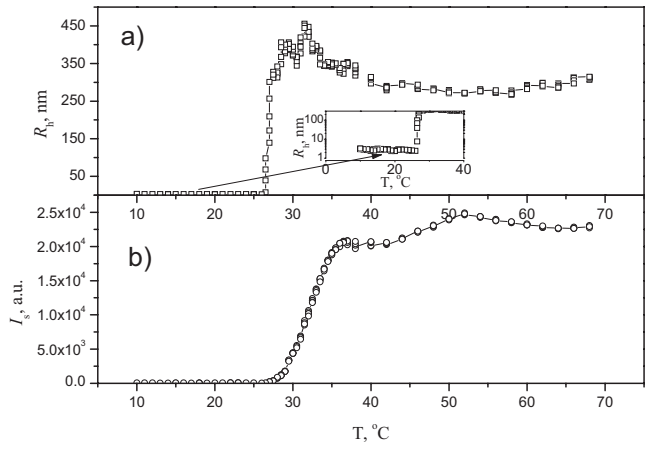

Figure 1. Temperature dependence of volume-weighted R_h (a) and the intensity of scattered light I_s (b) of P2639-2:1 polymer at $\theta = 173^{\circ}$, cooling ($c_P = 0.5\ g \cdot L^{-1}$).

© 2010 WILEY-VCH Verlag GmbH & Co. KGaA, Weinheim
Macromolecular Journals
DOI: 10.1002/mabi.201000034

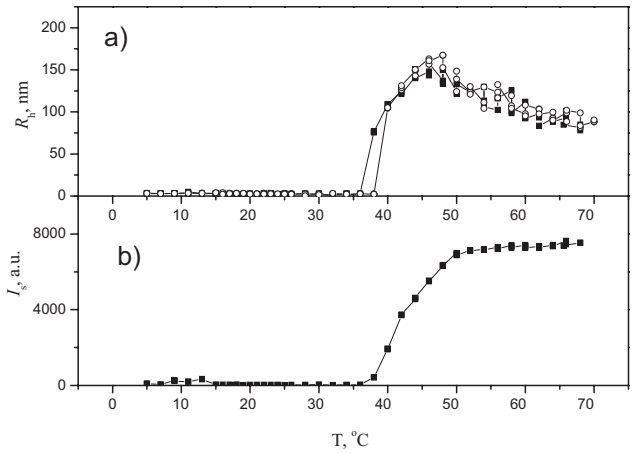

Figure 2. Temperature dependence of volume-weighted R_h (a) and the intensity of scattered light I_s (b) of P2620-1:1 polymer at $\theta = 173^\circ$, heating (○) and cooling (■) ($c_P = 0.5\ g \cdot L^{-1}$).

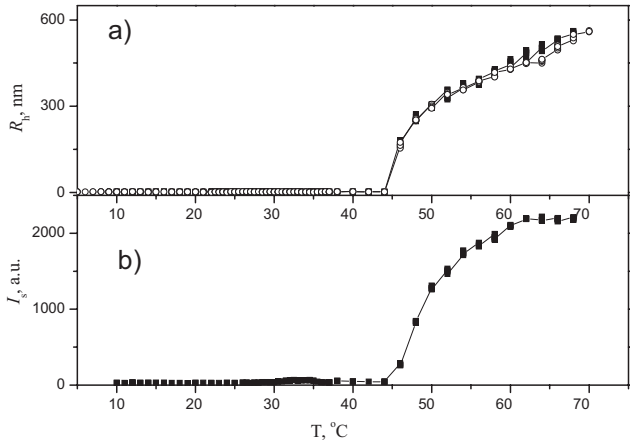

Figure 3. Temperature dependence of volume-weighted R_h (a) and the intensity of scattered light I_s (b) of P2639-1:2 polymer at $\theta = 173^\circ$, heating (○) and cooling (■) ($c_P = 0.5\ g \cdot L^{-1}$).

in the literature.[23] It is reasonable to assume that due to the smallest content of hydrophilic MeOX groups in the macromolecular structure, the thermosensitive IprOX block have control over behavior of the aggregates above the CPT.

A very important property of micelles designed for drug delivery purposes is their critical micellar concentration (CMC). The micelles must be sufficiently stable in dilution in the bloodstream (total blood volume in humans is ca. 5 L). They should not contain too much unimer in equilibrium with the micelles, since hydrophobic domains of unimers are not protected from unwanted interactions in the body by the hydrophilic corona and unimers may also be quickly eliminated through the kidneys due to their relatively low molecular weight. On the other hand, too stable micelles may have a problem with a too slow rate of elimination from the organism. The CMC values for the polymers (Table 1, since the measurements were carried out at 37 °C, only polymers forming micelles at this temperature were measured) are somehow higher but comparable with the CMC obtained with purely amphiphilic block and graft copolymers, in accordance with the literature. As mentioned above, this may lead to shorter blood circulation times, but, on the other hand, should facilitate polymer elimination from the organism after the system fulfills its task.

Radionuclide Labeling

Since copolymer micelles are intended as carriers for radiodiagnostics/radiotherapeutics and polyoxazolines without suitable functional moieties cannot be directly radiolabeled, we introduced radiolabelable phenolic moiety into the copolymers. Phenol is a highly activated aromatic moiety towards electrophilic radioiodination with iodine radioisotopes suitable for radiodiagnostics (^{123}I, ^{124}I) or radiotherapy (^{131}I). We have chosen the polymer P2639-1:1 containing 15 mol-% BuOX in the thermoresponsive block and a 1:1 thermoresponsive to hydrophilic block ratio as a starting copolymer for further modification due to its suitable properties (micelle-forming temperature and R_H, see Table 1 and Supporting Information). The radiolabelable moiety was introduced into the triblock copolymer by the introduction of pendant double bonds into the copolymer (part of BuOX in the polymerization mixture was substituted with EnOX to achieve on average one double bond per polymer molecule) and thiol-clock addition in analogy to ref.[18] of sulfanylethyl)-2-(4-hydroxyphenyl)acetamide onto the double bond (see Scheme 2). In analogy to ref.[35], AIBN was used as an initiator instead of UV-light. UV-light photocatalysis was originally described for another thiol-ene click reaction to polyoxazolines,[36] but the photoinitiated reaction offered unsatisfactory conversions only in our case. No polymer-bound initiator fragments can be detected by NMR since there is an excess of the thiol in the reaction mixture. The achieved phenolic moiety content ($36.2\ \mu mol \cdot g^{-1}$ polymer) and thus the theoretical labeling capacity (61 GBq ^{125}I/mg polymer) calculated from the phenol content assayed by ^1H NMR was more than sufficient for the possible application (the typical dose per human patient is 0.02–3 GBq depending on the particular radionuclide and application).

Radionuclide labeling was carried out using the chloramine method in good yield (66%). Most of the radioiodine was bound to polymer by a stable bond (see Supporting Information for a chart) and the remaining part was gradually released into low molecular weight fraction during incubation in PBS buffer at 37 °C. This means that part of the iodine is bound by a metastable bond; however, if GPC separation on a PD-10 desalting column is repeated after 2.5 h, a more stable product is obtained and should be sufficient for the intended radiodiagnostic purposes.

© 2010 WILEY-VCH Verlag GmbH & Co. KGaA, Weinheim

Haemolytic activity is a straightforward measure of eventual membrane toxicity due to the amphiphilic character of the copolymers. All the copolymers have shown no toxicity (haemolysis less than 3.5% even at the highest concentration used ($1\,mg \cdot mL^{-1}$) which corresponds to the hypothetical total dose of 5 g per human with a total blood volume of 5 L, (see Supporting Information for a chart).

Conclusion

We have synthesized ABA triblock copolymers poly[2-methyl-2-oxazoline-*block*-(2-isopropyl-2-oxazoline-*co*-2-butyl-2-oxazoline)-*block*-2-methyl-2-oxazoline] with two hydrophilic A blocks and one central thermoresponsive B block with different monomer unit ratios. These polymers are soluble in aqueous millieu, molecularly dissolved below the cloud point temperature of the thermoresponsive block and form micelles at higher temperature. Micelles are formed within a narrow temperature range. The CPT of the thermoresponsive block was adjusted with 2-butyl-2-oxazoline (hydrophobic monomer lowering the CPT) to 2-isopropyl-2-oxazoline (main monomer giving thermoresponsive properties to its copolymers) ratio and size of the micelles was also influenced by the A to B block weight ratio. A phenolic moiety was introduced into the above stated polymer to allow radionuclide labeling with iodine radioisotopes for both diagnostics and therapy of solid tumors. Such polymer was then radiolabeled with ^{125}I in good yield with sufficient in vitro stability under model conditions.

Acknowledgements: Financial support from the *Academy of Sciences of the Czech Republic* (grant # KAN 200200651), the *Grant Agency of the Czech Republic* (grant # P207/10/P054, # 202/09/2078) and the *Ministry of Education, Youth and Sports of the Czech Republic* (grant # IM 4635608802) is gratefully acknowledged.

Received: January 25, 2010; Revised: March 8, 2010; Published online: May 20, 2010; DOI: 10.1002/mabi.201000034

Keywords: drug delivery systems; micelles; radiation; synthesis; thermal properties

[1] N. Adams, U. S. Schubert, *Adv. Drug Delivery Rev.* **2007**, *59*, 1504.
[2] J. S. Park, Y. Akiyama, F. M. Winnik, K. Kataoka, *Macromolecules* **2004**, *37*, 6786.
[3] R. Hoogenboom, *Angew. Chem., Int. Ed.* **2009**, *48*, 7978.
[4] B. Pidhatika, J. Moller, V. Vogel, R. Konradi, *Chimia* **2008**, *62*, 264.
[5] C. Diab, Y. Akiyama, K. Kataoka, F. M. Winnik, *Macromolecules* **2004**, *37*, 2556.
[6] P. Persigehl, R. Jordan, O. Nuyken, *Macromolecules* **2000**, *33*, 6977.
[7] R. Hoogenboom, F. Wiesbrock, H. Huang, M. A. M. Leenen, H. M. L. Thijs, S. F. G. M. van Nispen, M. van der Loop, C.-A. Fustin, A. M. Jonas, J. F. Gohy, U. S. Schubert, *Macromolecules* **2006**, *39*, 4719.
[8] R. Hoogenboom, F. Wiesbrock, M. A. M. Leenen, H. M. L. Thijs, H. Huang, C.-A. Fustin, P. Guillet, J.-F. Gohy, U. S. Schubert, *Macromolecules* **2007**, *40*, 2837.
[9] M. Einzmann, W. H. Binder, *J. Polym. Sci. A, Polym. Chem.* **2001**, *39*, 2821.
[10] A. Mahmud, X. B. Xiong, H. M. Aliabadi, A. Lavasanifar, *J. Drug Targeting* **2007**, *15*, 553.
[11] V. P. Torchilin, *Pharm. Res.* **2007**, *24*, 1.
[12] M. Hruby, C. Konak, J. Kucka, M. Vetrik, S. K. Filippov, D. Vetvicka, H. Mackova, G. Karlsson, K. Edwards, B. Rihova, K. Ulbrich, *Macromol. Biosci.* **2009**, *9*, 1016.
[13] H. Uyama, S. Kobayashi, *Chem. Lett.* **1992**, *9*, 1643.
[14] D. Christova, R. Velichkova, W. Loos, E. J. Goethals, F. Du. Prez, *Polymer* **2003**, *44*, 2255.
[15] J. S. Park, K. Kataoka, *Macromolecules* **2006**, *39*, 6622.
[16] J. S. Park, K. Kataoka, *Macromolecules* **2007**, *40*, 3599.
[17] R. Hoogenboom, H. M. L. Thijs, M. J. H. C. Joachems, B. M. van Lankvelt, M. W. M. Fijten, U. S. Schubert, *Chem. Commun.* **2008**, *44*, 5758.
[18] A. Gress, A. Volkel, H. Schlaad, *Macromolecules* **2007**, *40*, 7928.
[19] M. Hruby, V. Subr, J. Kucka, J. Kozempel, O. Lebeda, A. Sikora, *Appl. Radiat. Isot.* **2005**, *63*, 423.
[20] S. Huber, R. Jordan, *Colloid Polym. Sci.* **2008**, *286*, 395.
[21] L. Del Villano, R. Kommedal, M. W. M. Fijten, U. S. Schubert, R. Hoogenboom, M. A. Kelland, *Energy Fuels* **2009**, *23*, 3665.
[22] M. W. M. Fijten, C. Haensch, B. M. van Lankvelt, R. Hoogenboom, U. S. Schubert, *Macromol. Chem. Phys.* **2008**, *209*, 1887.
[23] V. O. Aseyev, H. Tenhu, F. M. Winnik, "Temperature Dependence of the Colloidal Stability of Neutral Amphiphilic Polymers in Water", in: *Conformation-Dependent Design of Sequences in Copolymers II*, Advances in Polymer Science Series Volume 196, Springer, Berlin/Heidelberg 2006, p. 1.
[24] V. Aseyev, S. Hietala, A. Laukkanen, M. Nuopponen, O. Confortini, F. E. Du Prez, H. Tenhu, *Polymer* **2005**, *46*, 7118.
[25] P. Kujawa, V. Aseyev, H. Tenhu, F. M. Winnik, *Macromolecules* **2006**, *39*, 7686.
[26] A. Laukkanen, L. Valtola, F. M. Winnik, H. Tenhu, *Macromolecules* **2004**, *37*, 2268.
[27] P. Kujawa, H. Watanabe, F. Tanaka, F. M. Winnik, *Eur. Phys. J. E* **2005**, *17*, 129.
[28] K. Akiyoshi, E. C. Kang, S. Kurumada, J. Sunamoto, T. Principi, F. M. Winnik, *Macromolecules* **2000**, *33*, 3244.
[29] T. Koga, F. Tanaka, R. Motokawa, S. Koizumi, F. M. Winnik, *Macromolecules* **2008**, *41*, 9413.
[30] P. Kujawa, F. Tanaka, F. M. Winnik, *Macromolecules* **2006**, *39*, 3048.
[31] P. Kujawa, F. Segui, S. Shaban, C. Diab, Y. Okada, F. Tanaka, F. M. Winnik, *Macromolecules* **2006**, *39*, 341.
[32] R. Obeid, F. Tanaka, F. M. Winnik, *Macromolecules* **2009**, *42*, 5818.
[33] R. Obeid, E. Maltseva, A. F. Thunemann, F. Tanaka, F. M. Winnik, *Macromolecules* **2009**, *42*, 2204.
[34] N. Morimoto, R. Obeid, S. Yamane, F. M. Winnik, K. Akiyoshi, *Soft Matter* **2009**, *5*, 1597.
[35] M. Hruby, C. Konak, K. Ulbrich, *J. Controlled Release* **2005**, *103*, 137.
[36] C. Diehl, H. Schlaad, *Macromol. Biosci.* **2009**, *9*, 157.

© 2010 WILEY-VCH Verlag GmbH & Co. KGaA, Weinheim

DOI: 10.1002/mabi.201000034

Synthesis and studying properties of macroporous metal chelating polymer beads as potential therapeutics intended for radioembolization of liver malignancies and for the therapy of Wilson's disease

Publications:

D4. ***Lutetium-177 and iodine-131 loaded chelating polymer microparticles intended for radioembolization of liver malignancies***

Hrubý M, Škodová M, Macková H, Skopal J, Tomeš M, Kropáček M, Zimova J, Kučka J; Reactive and Functional Polymers, 71 (2011) 1155–1159; co-author

D7. ***Chelating polymeric particles intended for the therapy of Wilson's disease***

Škodová M, Jan Kučka, Miroslav Vetrík, Jan Skopal, Zuzana Walterová, Ondřej Sedláček, Petr Štěpánek, Pavla Poučková, Petr Urbánek, and Martin Hrubý; Reactive and Functional Polymers, *currently under second review* - first author

Reactive & Functional Polymers 71 (2011) 1155–1159

Contents lists available at SciVerse ScienceDirect

Reactive & Functional Polymers

journal homepage: www.elsevier.com/locate/react

Lutetium-177 and iodine-131 loaded chelating polymer microparticles intended for radioembolization of liver malignancies

Martin Hruby [a,*], Michaela Skodova [a], Hana Mackova [a], Jan Skopal [a], Marek Tomes [b], Martin Kropacek [b], Jana Zimova [b], Jan Kucka [a]

[a] Institute of Macromolecular Chemistry of the Academy of Sciences of the Czech Republic, Public Research Institution, Heyrovský Sq. 2, Praha 6, CZ-16206, Czech Republic
[b] Nuclear Physics Institute of the Academy of Sciences of the Czech Republic, Public Research Institution, Husinec-Řež 130, Řež, CZ-25068, Czech Republic

ARTICLE INFO

Article history:
Received 29 June 2011
Received in revised form 31 August 2011
Accepted 4 September 2011
Available online 10 September 2011

Keywords:
Macroporous chelating beads
Radioembolization
Quinoline-8-ol
8-Hydroxyquinoline-5-sulfonic acid
Liver cancer

ABSTRACT

We describe the synthesis, characterization and radiochemical studies on macroporous chelating polymer beads as carriers of beta-emitters lutetium-177 and iodine-131 intended for radioembolization of liver tumors. The starting poly(glycidyl methacrylate-*co*-ethylene dimethacrylate) (bead size 20–40 μ) was reacted with ammonia or methylamine to introduce primary and secondary amino groups, respectively. The primary amino groups containing polymer was used for the attachment of 1,4,7,10-tetraazacyclododecane-1,4,7,10-tetraacetic acid (DOTA) moieties, while quinoline-8-ol or 8-hydroxyquinoline-5-sulfonic acid moieties, respectively, were introduced onto the secondary amino groups containing polymer. All the polymers were labeled quantitatively by lutetium-177 in ammonium acetate buffer, DOTA containing beads however required heating to 80 °C while the quinoline-8-ol or 8-hydroxyquinoline-5-sulfonic acid moieties containing polymers were quantitatively radiolabeled within 1 h at room temperature. The quinoline-8-ol groups containing polymer was radioiodinated in 95% yield by a chloramine method. Both lutetium-177 and iodine-131 radiolabels were stable in an in vitro study in rat blood plasma. Quinoline-8-ol or 8-hydroxyquinoline-5-sulfonic acid moieties are thus more suitable for the radiolabeling of macroporous beads with lutetium-177 for radioembolization purposes than well-established DOTA moieties and in addition, quinoline-8-ol also allows radiolabeling with iodine-131.
© 2011 Elsevier Ltd. All rights reserved.

1. Introduction

Liver may be damaged and its function hampered by numerous malignant tumors, of primarily hepatic origin (mainly relatively common hepatocellular carcinoma, HCC) or by metastases of tumors originated elsewhere (colorectal carcinoma etc.), both with poor prognosis [1–3]. Normal liver tissue is supplied mainly from portal vein (which drains blood from digestive tract and contains nutrients uptaken from food), while typically strongly vascularized liver tumors take up nutrients and oxygen only from hepatic artery. If 20–50 μ microparticles are injected into hepatic artery which supplies blood to cancer lesion, these particles embolize vessels predominantly in tumor tissue [4–6]. The microparticles may carry an active therapeutical, a chemotherapeutic agent (chemoembolization [3]) or a radiotherapeutical (radioembolization [7]), the latter radiotherapeutical method gives especially promising results [4,7,8].

For such applications, therapeutic β^- emitters with half-life of several days (^{90}Y [4] and ^{131}I [7]) or 17.0 h in the case of ^{188}Re [9] are eligible [4], because β^- particles have typical range several milimeters in tissue depending on their energy. In some cases (^{131}I [7] and ^{188}Re [9]) the β^- emission is accompanied with γ-rays. Gamma photons have much lower biological effectivity than β^- particles and due to high tissue permeability they may be used for therapy monitoring by γ-cameras. For such use, due to typical doses several GBq per application [9], the optimal yield of gammas from such radionuclide should be several percent per decay, allowing imaging (and thus further customization of therapy for the particular patient – *theranostics*), but minimizing radiation burden of surrounding organs. The radionuclide which perfectly fits these requirements is ^{177}Lu, with half-life 6.734 days, 100% β^- decay mode and main accompanying γ-lines 113 keV (6.4%) and 208 keV (11%), which is in the range of optimal efficiency of the commercial medical γ-cameras [10,11]. The radionuclide ^{131}I is widely used in radiotherapy due to its very suitable nuclear properties (half-life 8.02 days, 100% β^- decay mode and main accompanying γ-line 364 keV (82%)), and also due its very low commercial price [10,11].

The material of the microbeads currently FDA-approved or in clinical trials for this use was designed in three main approaches [4]: Lipiodol® (iodinated oil-based contrast agent) labeled with

* Corresponding author. Tel.: +420 296 809 230; fax: +420 296 809 410.
E-mail address: mhruby@centrum.cz (M. Hruby).

1381-5148/$ - see front matter © 2011 Elsevier Ltd. All rights reserved.
doi:10.1016/j.reactfunctpolym.2011.09.003

^{131}I [7] (by isotope exchange, Lipiocis®) or with ^{188}Re (in the form of hydrophobic complex) [9], stable yttrium (^{89}Y)-containing glass beads (TheraSpheres®) [6,8,12] which are activated in reactor to contain ^{90}Y and strongly acidic ion exchanger beads containing sulfonic acid groups (SIRSpheres®) [13,14]. Unfortunately, every of the currently studied suffer from some disadvantage:

(i) Leak of radioactivity from the system and re-depostition of radionuclides within the body (SIRSpheres®, radiolabeled Lipiodol® and Lipiocis®).
(ii) Some systems (TheraSpheres®) cannot be radiolabeled with commercially available solution of radionuclides and must be irradiated in reactor after formation of microbeads.

On the basis of the above stated facts, we decided to study for this purpose macroporous chelating ion exchangers as ^{177}Lu and ^{131}I carriers. Our system should, unlikely the currently used and studied materials, fulfill all the above listed demands for the intended use in connection with modern, promising therapeutical radionuclides. We used methacrylate beads as support to achieve both rapid radiolabeling kinetics from radionuclide solution and high radionuclide loading due to maroporous structure and mechanically stable sphere-shaped particles of size 20–40 μ. We used quinoline-8-ol (8HQ) as metal-binding ligand, because it readily forms stable complexes with nearly all therapeutically or diagnostically used metal ion radionuclides (it forms complexes with yttrium, lanthanides, technetium, copper) [15,16], but also allows radioiodination into two positions (into one position after binding by Mannich condensation, respectively). Quinoline-8-ol containing resins are used for trace metal analysis [17,18], however use of this moiety for radiolabeling of a radiopharmaceutical in a kit-like manner is the new approach of this study. We also tested quinoline-8-ol-5-sulfonic acid (8HQ5S) as ligand since the sulfonic acid should, due to its permanent negative charge under physiological pH, facilitate metal cation binding into 8HQ chelate into otherwise rather cationic matrix. Hydrophilization of the matrix with the sulfonic acid group should also increase radiolabeling rate. In comparison, we tested ligand well-established from low-molecular-weight radiopharmaceuticals, 1,4,7,10-tetraazacyclododecane-1,4,7,10-tetraacetic acid (DOTA) [19] and strongly acidic ion exchanger containing sulfonic acid groups Dowex 50W X8 (DOW).

2. Experimental

2.1. Materials

Glycidyl methacrylate and ethylene dimethacrylate were purchased from Sigma–Aldrich Ltd. (Prague, Czech Republic) and distilled before use. 1,4,7,10-Tetraazacyclododecane-1,4,7,10-tetraacetic acid mono (*N*-hydroxysuccinimide ester) (DOTA-NHS-ester) was purchased from Macrocyclics Ltd. (Dallas, TX, U.S.A.). Sodium [^{131}I]-iodide solution (1 GBq/mL) was purchased from Lacomed Ltd. (Rez, Czech Republic). All other chemicals were purchased from Sigma–Aldrich Ltd. and used without additional purification.

2.2. Methods

Poly(glycidyl methacrylate-*co*-ethylene dimethacrylate) (G-gel, **1**) was synthesized according to [20] with glycidyl methacrylate to ethylene dimethacrylate ratio 60:40 w/w and average size 20–40 μ. Lutetium-177 stock solution (20 GBq/mL, 0.39 mg Lu/mL) was prepared from isotopically enriched ^{176}Lu target (1.0 mg Lu_2O_3, 60.6 atom.% ^{176}Lu enrichment, Isoflex Ltd., Moscow, Russia) by neutron activation at the neutron flux 5×10^{13} n cm^{-2} s^{-1} at the LWR-15 nuclear reactor in the Nuclear Research Institute, a.s., in Rez, with subsequent dissolution of the target in 0.01 mol L^{-1} aqueous hydrochloric acid (2.27 mL).

2.2.1. Aminolysis of G-gel with aqueous ammonia and methylamine (see Scheme 1)

G-gel (5.00 g, **1**) was immersed in 25% aqueous ammonia (synthesis of polymer **2**) or 41% aqueous methylamine (synthesis of polymer **3**), respectively (20 mL) and left stay 72 h at ambient temperature. The polymer was washed with water and methanol and dried on air. Yield 5.02 g for **2** and 5.05 g for **3**.

Amine content according to CHN elemental analysis: primary amino groups containing polymer **2** 2.36% N (1.69 mmol/g), secondary amino groups containing polymer **3** 3.51% N (2.51 mmol/g).

2.2.2. Attachment of 1,4,7,10-tetraazacyclododecane-1,4,7,10-tetraacetic acid (DOTA) moieties – synthesis of polymer **4** (see Scheme 1)

Primary amino groups containing polymer **2** (100 mg, 0.17 mmol) was reacted with DOTA-NHS-ester (259 mg, 0.34 mmol) and ethyldiisopropylamine (286 μL, 1.7 mmol) using 4-dimethylaminopyridine (10 mg) as catalyst and *N*,*N*-dimethylacetamide (600 μL) as solvent at 50 °C for 16 h. The suspension was then poured into water (20 mL) and the product was subsequently thoroughly washed with water, 10% aqueous acetic acid, 5% aqueous sodium carbonate and water and air-dried. Yield 105 mg.

The content of chelating group was assayed as chelating capacity for Cu^{2+}. The sorbent was treated with excess of 0.1 mol L^{-1} copper(II) sulfate in 1 mol L^{-1} acetate buffer pH 4.75, washed with water, air-dried and Cu content was assayed by atomic absorbtion spectrophotometry (AAS). The Cu content in Cu^{2+}-loaded polymer **4** was 0.56% (0.088 mmol/g).

2.2.3. Attachment of quinoline-8-ol and 8-hydroxyquinoline-5-sulfonic acid moieties to polymer **3** by Mannich reaction – synthesis of polymer **5** and **6** – modified procedure according to [16] (see Scheme 1)

Polymer **3** (2.00 g, 5.02 mmol secondary amino groups) was reacted with 8HQ (1.90 g, 13 mmol, synthesis of polymer **5**) or 8HQ5S (2.93 g, 13 mmol, synthesis of polymer **6**), respectively, in the presence of formaldehyde (40% aqueous solution, 6.00 mL, 65 mmol) and anhydrous sodium sulfate (13.4 g, 94.3 mmol) in methanol (30 mL) at room temperature for 7 days. The polymer was successively washed with methanol, 1 mol L^{-1} aqueous hydrochloric acid, water, 0.5 mol L^{-1} ammonium acetate and water and air-dried. Yield 2.23 g of polymer **5** and 1.85 g of polymer **6**, respectively.

Ligand content was assayed as Cu^{2+} sorption capacity at pH 4.75 as described for the characterization of polymer **4** (see above), the Cu content was 3.05% (0.480 mmol/g) for **5** and 2.42% (0.381 mmol/g) for **6**, respectively.

2.2.4. Labeling of polymer beads with ^{177}Lu and ^{131}I

Labeling was peformed in ammonium acetate buffer, which is a preferred environment for the complexation of lanthanides.[10] Polymer beads (6.0 mg) were immersed in aqueous ammonium acetate (125 μL, 4 mol L^{-1}, with pH adjusted to pH 4.4, 6.0 and 8.7 with 1 mol L^{-1} hydrochloric acid and 1 mol L^{-1} sodium hydroxide, respectively), aqueous sodium chloride (865 μL, 0.15 mol L^{-1}) and ^{177}Lu stock solution (10 μL, 200 MBq) were added and the mixture was shaken for the specified time (1, 2, 5 and 72 h, respectively) at room (23 °C) or elevated (80 °C) temperature, respectively. After that the beads were centrifuged and one-half of the supernatant (500 μL) and beads + rest of the supernatant

were measured for radioactivity using an ionization chamber Atoblab 100 (Biodex, USA.). After the experiment, pH was checked and did not differ drom the initial value more than 0.1 in any case. The yield of labeling was calculated according to the following equation:

$$Y = (A_{res} - A_{sup})/(A_{res} + A_{sup}) * 100 \quad (1)$$

where A_{sup} is radioactivity of 500 μL supernatant in Bq, A_{res} is radioactivity of the rest of supernatant + beads and Y is radiolabeling yield in %.

Radioiodination with ^{131}I was carried out by a standard chloramine method [21] adapted to polymer beads. Briefly: quinoline-8-ol groups containing polymer **5** (20 mg) was suspended in phosphate buffered saline (PBS, pH 7.4, 300 μL) and the stock solution of $Na^{131}I$ (40 μL, 22.3 MBq) and chloramine T solution (5 μL, 10 mg mL^{-1} in PBS) was shaken at room temperature for 45 min. The reaction was stopped with the solution of L-ascorbic acid (200 μL, 20 mg mL^{-1} in PBS) with shaking for additional 1 h. The beads were washed by immersion ito 1 mL PBS, shaking for 5 min and centrifugation thrice. Radioactivity was measured on a Bqmetr 4 ionization chamber (Empos Ltd., Prague, Czech Republic). Radiochemical yield was calculated according to the following equation:

$$Y = A_{beads}/A_{NaI} * 100 \quad (2)$$

where A_{beads} is radioactivity of beads, A_{NaI} is radioactivity of the starting $Na^{131}I$ solution and Y is radiochemical yield in %.

2.2.5. Stability studies in vitro

Beads for stability studies were purified by washing + centrigugation with 3 × 1 mL aqueous sodium chloride (0.15 mol L^{-1}). Radiolabeled beads (5 mg) were immersed into PBS or rat serum (1.00 mL) and incubated at 37 °C for 2 h, 6 h, 24 h, 48 h, 72 h, 7 days and 14 days (PBS) and for for 2 h, 6 h, 24 h and 48 h (rat serum), respectively. At each point suspension was shaken, centrifuged and one-half of the supernatant (500 μL) was measured for radioactivity (in the same way as for labeling with the particular radionuclide) as well as the rest of the supernatant + beads. After measurement, 500 μL supernatant was returned to the incubation vial, the suspension was agitated for a short time and incubation was continued. Stability was calculated in each time point according to the same equation as radiolabeling yield (Eq. (1)).

3. Results and discussion

The precursor for the synthesis of chelating microbeads was the epoxide groups containing macroporous poly(glycidyl methacrylate-*co*-ethylene dimethacrylate), synthesized according to [20] with glycidyl methacrylate to ethylene dimethacrylate ratio 60:40 w/w and average size 20–40 μ. This polymer allows to introduce both polyacid and quinoline-8-ol-type ligands and assures proper size, mechanical properties and chemical stability.

Primary amino groups were introduced by aminolysis of the oxirane moieties on the polymer with aqueous ammonia, secondary amino groups in analogy by aminolysis with aqueous methylamine. The aminolysis yielded 1.69 mmol/g primary amino groups and 2.51 mmol/g secondary amino groups, respectively, according to nitrogen content.

Primary amino groups were used to attach polyacid chelator DOTA by aminolysis of the respective commercially available bifunctional derivative monosucinimidyl ester of DOTA by a stable amide bond. Polyacid chelator DOTA was chosen because it is in routine use for conjugation of polyvalent metal ion radionuclides to homing moieties in nuclear medicine. The obtained ligand content (as capacity for Cu^{2+}) was 0.088 mmol/g. The amine to amide conversion was calculated from the following equation:

$$Y_a = c_{Cu}/(c_N - 4 \times c_{Cu}) \quad (3)$$

where c_{Cu} is the copper content in copper-saturated sorbent in mmol/g, c_N is the nitrogen content in copper-saturated sorbent in mmol/g and Y_a is the amine to amide conversion.

The relatively low primary amine to amide conversion (5%) may be attributed to sterical hindrance of the relatively sterically demanding DOTA succinimidyl ester when approaching polymer surface as well as electrostatic repulsion of the already attached negatively charged carboxylates with the carboxylates of the approaching molecule on the case of DOTA succinimidyl ester. However, the ligand content was still more than sufficient for the radiolabeling purposes.

The 8HQ and 8HQ5S moieties were introduced by Mannich condensation of the secondary amino groups with formaldehyde and the particular phenol (8HQ or 8HQ5S, respectively), in analogy to our previous preliminary experiments with polymer containing 8HQ for chromatographic purposes [16]. The 8HQ5S is in fact the same type of ligand as ligand as 8HQ, but contains an additional sulfonic acid group. This sulfonic acid group introduces a permanent negative charge, which is highly advantageous for the binding of Lu^{3+} due to elimination of electrostatic repulsion between lutetium cation bound to the matrix and lutetium cation coming from solution as well as repulsion of the lutetium cation coming from solution with the protonated amines in the polymer matrix. In addition, sulfonic acid group hydrophilizes the whole polymer which further enhances metal ion sorption rate. Similar approach (supplementation of permanent negative charge to ion selective cation exchanger to enhance metal chelation rate and acheivable chelation capacity) was used by, e.g., Alexandratos and coworkers [22] with the combination of ion-selective phosphonic and anionic sulfonic acid groups. The obtained ligand contents (expressed as capacity for Cu^{2+}) were 0.480 mmol/g for polymer **5** and 0.381 mmol/g for polymer **6**, respectively (see Scheme 1), which is a much higher content than obtained for DOTA (see above). The ligand content was expressed as capacity for Cu^{2+} for all three ligands (DOTA, 8HQ, 8HQ5S). The known stoichimetry for the Cu^{2+} complexation is 1:1 for DOTA. For 8HQ and 8HQ5S, the stoichiometry of complexation with Cu^{2+} in solution is 2:1, however, due to sterical reasons, on a resin this may be probably only 1:1. However, not all 8HQ5S is probably available for complexation; this was confirmed by elemental analysis of sulfur in the 8HQ5S-containing resin **6**, where the sulfur content was 4.52% (1.41 mmol/g).

Radiolabeling of the chelating beads with $^{177}Lu^{3+}$ was studied as a function of time, pH and temperature, the results are summarized in Table 1. The specific radioactivity was 33 MBq ^{177}Lu/mg beads for 100% labeling yield in all cases. Except of the beads containing DOTA, 8HQ and 8HQ5S acid chelating moieties, sulfonic acid containing resin DOW was used as control to both simulate SIRSpheres® and to serve as control to help interpret differencies between 8HQ and 8HQ5S-containing beads.

One can clearly see that at room temperature both polymers **5** and **6** quickly and quantitatively bind $^{177}Lu^{3+}$ at neutral and alcaline pH (i.e. at pH 6.0 and pH 8.7), while the complexation with 8HQ on polymer **5** is slower in mildly acidic pH 4.4. It is necessary to mention that quantitative radiolabeling is highly advantageous since it simplifies radiopharmaceutical kits to simple mixing, incubation and administration avoiding radioconjugate purification steps. Since polymer **6** binds $^{177}Lu^{3+}$ quickly even at pH 4.4, it is most plausible that the reason for slower complexation of $^{177}Lu^{3+}$ by polymer **5** in acidic milieu is purely electrostatic - $^{177}Lu^{3+}$ is cation and the matrix of polymer **5** is prevailingly cationic at pH [pK_a of 8HQ is 5.13 (tertiary amine) and 9.89 (phenol) and pK_a of the aliphatic tertiary amine spacer was estimated in analogy to trimeth-

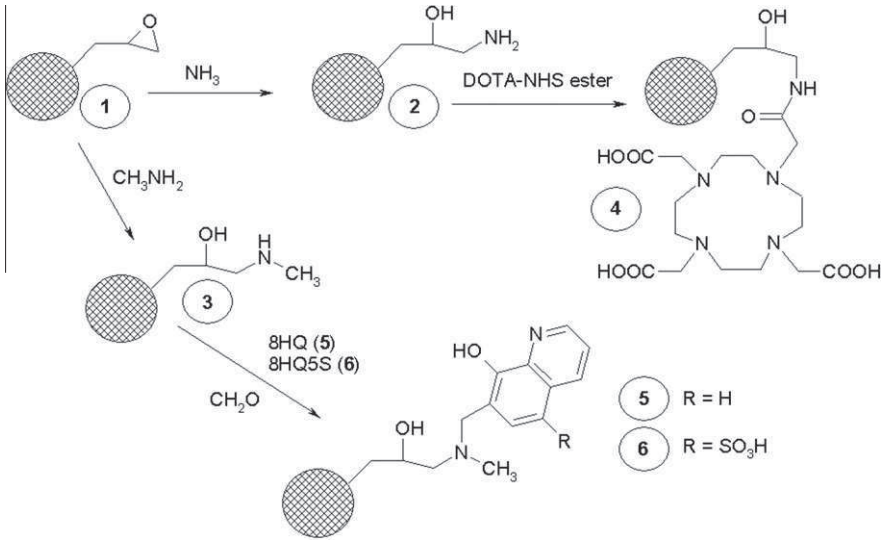

Scheme 1. Synthesis of chelating beads.

Table 1
Radiolabeling of the chelating beads with $^{177}Lu^{3+}$ as a function of pH at room temperature and at 80 °C; 8HQ is quinoline-8-ol, 8HQ5S is 8-hydroxyquinoline-5-sulfonic acid, DOW is Dowex 50W X8 and DOTA is 1,4,7,10-tetraazacyclododecane-1,4,7,10-tetraacetic acid.

		Radiolabeling yield (%)				
		23 °C			80 °C	
Ligand	pH	1 h	5 h	72 h	1 h	2 h
8HQ	4.4	68	94	96	98	97
8HQ	6.0	99	100	100	100	99
8HQ	8.7	98	100	99	100	100
8HQ5S	4.4	100	100	100	100	100
8HQ5S	6.0	100	100	100	99	100
5HQ5S	8.7	99	100	100	100	100
DOW	4.4	44	64	64	77	86
DOW	6.0	16	47	46	52	48
DOW	8.7	75	83	80	51	50
DOTA	4.4	15	50	77	99	99
DOTA	6.0	29	72	99	99	99
DOTA	8.7	83	94	99	99	91

ylamine to ca 10] while the matrix of the polymer **6** is partly anionized by the presence of permanently negatively charged sulfonates.

The $^{177}Lu^{3+}$ binding rate for the DOTA ligand containing polymer **4** is significantly slower than that for polymers **5** and **6**, especially in acidic milieu. This is probably caused by low conformational flexibility typical for complexation with DOTA especially in acidic milieu [10]. This hypothesis was confirmed by labeling experiments at 80 °C, where the conformational changes are significantly accelerated. At 80 °C it is possible to reach quantitative labeling yield for DOTA-modified beads within 1 h even at pH 4.4, while at 23 °C it takes 72 h at pH 6.0 and 8.7 and at pH 4.0 labeling is not quantitative even after 72 h. Heating also does not disturb labeling of polymers **5** and **6** with $^{177}Lu^{3+}$, but yields are quantitative already at room temperature within 1 h so further experiments with polymers **5** and **6** were conducted at room temperature.

Labeling of strongly acidic cation exchanger with $^{177}Lu^{3+}$ gave only moderate labeling yields with highest yield under acidic and basic conditions and low at neutral pH, revealing necessity of strong chelation for complete binding of $^{177}Lu^{3+}$.

Sufficient specific radioactivity is of key importance for all radiopharmaceuticals, so we decided to study maximal reasonably achievable lutetium loading. Capacity of the polymers **5** and **6** for Cu^{2+} is 0.480 mmol/g and 0.381 mmol/g, respectively, and since due to sterical reasons stoichiometry metal to ligand ratio 1:1 is retained also for lanthanides on polymer (in solution it is 1:3), theoretical capacity for Lu^{3+} should be the same. However, radiolabeling yield drops even before the maximal loading is reached, which leads to loss of an expensive radionuclide. It is reasonable to conclude that the maximal loading which is reasonably achievable is that which allows >85–90% radiochemical yield. We thus added increasing amounts of $^{177}Lu^{3+}$ to the polymer until radiochemical yield dropped below ca 85% and then calculated the bound amount of radionuclide (ammonium acetate was used as buffer). For both polymers **5** and **6** the optimal addition was 10% theoretical capacity, which offered yield 87% for polymer **5** and 95% for polymer **6**. This corresponds to the lutetium loading 0.74% (0.042 mmol/g) for polymer **5** and 0.64% (0.36 mmol/g) for polymer **6**, respectively. This is more than enough for the radiopharmaceutical use with ^{177}Lu. We produce ^{177}Lu by reactor irradiation of isotopically enriched lutetium target (60.6% ^{176}Lu) and the achievable radioactivity is typically 302 GBq ^{177}Lu/mg Lu. This means that the typical radioembolization dose 1–3 GBq/human being may be placed into 70–200 μg of beads.

The advantage of polymer-bound 8HQ (but not of polymer-bound 8HQ5S) is the possibility to be also radioiodinated to the position 5 of the quinoline moiety (by an electrophilic mechanism, i.e. by standard chloramine or iodigen methods) without loss of complexation ability. One can thus use the same carrier for iodine and metal radionuclides or even produce double-labeled beads. Iodine-131 was chosen as a theranostic radionuclide for this purpose. We obtained by the chloramine method specific radioactivity 0.96 MBq ^{131}I/mg beads while the theoretical value for 100% radiolabeling yield is 1.01 MBq ^{131}I/mg. The radiochemical yield was thus 95%. Theoretical labeling capacity for the ligand content 0.480 μmol/mg in polymer **5** and stoichiometry 1:1 would mean theoretical capacity 289 GBq ^{131}I/mg, which is fully sufficient for the intended use even if we consider lower radiolabeling yields at higher loadings (therapeutical dose 1–3 GBq would be introduceable into 3.4–10.4 μg beads).

The key factor for polymer complexes of radiometals is stability in blood plasma, because eventual leak of radionuclide leads to loss of effectivity of treatment and to unwanted side effects due to redistribution of the liberated radionuclide elsewhere. In the case of lanthanides such as lutetium, resdistribution of ^{177}Lu is mainly

into bones (leading to bone marrow damage and myelotoxicity) [23] and free ^{131}I accumulates in thyroid [21]. This is why we tested radiochemical stability of the ^{177}Lu-labeled polymers **5** and **6** and ^{131}I-labeled polymer **5**. We tested the stability of radiolabeling in rat blood plasma as a challenge solution, since it represents microenvironment in organism better than any artifical challenge solution. After 48 h, ^{177}Lu showed 100% stability and ^{131}I label 96% stability. Longer-term stability for ca. 2 half-lives of the radionuclides ^{177}Lu and ^{131}I (14 days) was tested in PBS since blood plasma undergoes irreversible enzymatic and microbial changes after several days. After 14 days incubation in PBS, there was no measurable leak of ^{177}Lu from the beads (100% stability) and 83% ^{131}I remained on beads (91% after 7 days). Since radioactivity measurements are relative to the sum of radioactivity at the particular time, decay correction is self-contained.

4. Conclusions

We synthesized, characterized and radiolabeled macroporous chelating polymer beads with ^{177}Lu and ^{131}I for radioembolization purposes. Quinoline-8-ol or 8-hydroxyquinoline-5-sulfonic acid moieties are suitable for the radiolabeling of macroporous beads with ^{177}Lu for radioembolization purposes and in addition, quinoline-8-ol also allows radiolabeling with ^{131}I. Quantitative radiolabeling with ^{177}Lu was reached allowing facile preparation of a kit while radiolabeling with ^{131}I gave 95% yield. The typical radioembolization dose 1–3 GBq ^{177}Lu/human being may be placed into 70–200 μg of beads and the radiolabel is stable in blood plasma.

Acknowledgements

Financial support of the Grant Agency of the Czech Republic (Grant # P207/10/P054) and of the Ministry of Education, Youth and Sports of the Czech Republic (Grant # IM4635608802) is gratefully acknowledged.

References

[1] F.X. Bosch, J. Ribes, M. Diaz, R. Cleries, Gastroenterology 127 (2004) S5–S16.
[2] J.M. Llovet, A. Burroughs, J. Bruix, Lancet 362 (2003) 1907–1917.
[3] J.M. Llovet, J. Bruix, Hepatology 37 (2003) 429–442.
[4] J.L. Raoul, E. Boucher, Y. Rolland, E. Garin, Nat. Rev. Gastroenterol. Hepatol. 7 (2010) 41–49.
[5] S.W. Zielhuis, Lanthanide bearing radioactive particles for cancer therapy and multimodality imaging. Dissertation thesis, University Medical Center Utrecht, Utrecht University, Utrecht, 2006.
[6] R. Salem, R.J. Lewandowski, B. Atassi, S.C. Gordon, V.L. Gates, O. Barakat, Z. Sergie, C.Y.O. Wong, K.G. Thurston, J. Vasc. Interv. Radiol. 16 (2005) 1627–1639.
[7] J.L. Raoul, E. Boucher, Y. Roland, E. Garin, Q. J. Nucl. Med. Mol. Imaging 53 (2009) 348–355.
[8] A. Riaz, R.J. Lewandowski, L.M. Kulik, M.F. Mulcahy, K.T. Sato, R.K. Ryu, R.A. Omary, R. Salem, J. Vasc. Interv. Radiol. 20 (2009) 1121–1130.
[9] E. Garin, B. Denizot, N. Noiret, N. Lepareur, J. Roux, M. Moreau, J.Y. Herry, P. Bourguet, J.P. Benoit, J.J. Lejeune, Nucl. Med. Commun. 25 (2004) 1007–1013.
[10] M.J.R. Welch, C.S. Redvanly, Handbook of Radiopharmaceuticals: Radiochemistry and Applications, John Wiley & Sons, Ltd., Chichester, United Kingdom, 2003.
[11] I.A. Abassi, Nucl. Med. Biol. 38 (2011) 417–425.
[12] L.M. Kulik, B.I. Carr, M.F. Mulcahy, R.J. Lewandowski, B. Atassi, R. Ryu, K.T. Sato, A. Benson, A.A. Nemcek, V.L. Gates, M. Abecassis, R.A. Omary, R. Salem, Hepatology 47 (2008) 71–81.
[13] G. Van Hazel, A. Blackwell, J. Anderson, D. Price, P. Moroz, G. Bower, G. Cardaci, B. Gray, J. Surg. Oncol. 88 (2004) 78–85.
[14] C. Van de Wiele, L. Defreyne, M. Peeters, B. Lambert, Q. J. Nucl. Med. Mol. Imaging 53 (2009) 317–324.
[15] M. Atanassova, Russ. J. Inorg. Chem. 52 (2007) 1304–1311.
[16] M. Hruby, J. Hradil, M.J. Benes, React. Funct. Polym. 59 (2004) 105–118.
[17] S. Dadfarnia, T. Assadollahi, A.M.H. Shabani, J. Hazard. Mater. 148 (2007) 446–452.
[18] C. Duran, S.H. Senturk, A. Gundogdu, V.N. Bulut, L. Elci, M. Soylak, M. Tufekci, Y. Uygur, Chin. J. Chem. 25 (2007) 196–202.
[19] M.R. Lewis, J.L. Zhang, F. Jia, N.K. Owen, C.S. Cutler, M.F. Embree, J. Schultz, L.J. Theodore, A.R. Ketring, S.S. Jurisson, D.B. Axworthy, Nucl. Med. Biol. 31 (2004) 213–223.
[20] F. Svec, J. Hradil, J. Coupek, J. Kalal, Angew. Makromol. Chem. 48 (1975) 135–143.
[21] J. Kucka, M. Hruby, O. Lebeda, Appl. Radiat. Isot. 68 (2010) 1073–1078.
[22] S.D. Alexandratos, C.A. Shelley, E.P. Horwitz, R. Chiarizia, Solvent Extr. Ion Exch. 16 (1998) 951–966.
[23] S. Hirano, K.T. Suzuki, Environ. Health Perspect. 104 S1 (1996) 85–95.

Elsevier Editorial System(tm) for Reactive and Functional Polymers
Manuscript Draft

Manuscript Number:

Title: Chelating polymeric particles intended for the therapy of Wilson's disease

Article Type: Research Paper

Corresponding Author: Dr. Martin Hruby, Ph.D.

Corresponding Author's Institution: Institute of Macromolecular Chemistry AS CR

First Author: Michaela Skodova, M.Sc.

Order of Authors: Michaela Skodova, M.Sc.; Jan Kucka, Ph.D.; Miroslav Vetrik, M.Sc.; Jan Skopal; Zuzana Walterova, Ing.; Ondrej Sedlacek, M.Sc.; Petr Stepanek, Ph.D.; Pavla Pouckova, Ph.D.; Petr Urbanek, M.D., Ph.D.; Martin Hruby, Ph.D.

Suggested Reviewers:

Opposed Reviewers:

Manuscript
Click here to view linked References

Chelating polymeric particles intended for the therapy of Wilson's disease

Michaela Škodová[1], Jan Kučka[1,2], Miroslav Vetrík[1] Jan Skopal[1], Zuzana Walterová[1], Ondřej Sedláček[1], Petr Štěpánek[1], Pavla Poučková[3], Petr Urbánek[3], and Martin Hrubý[1,*]

[1]*Institute of Macromolecular Chemistry of the Academy of Sciences of the Czech Republic, v.v.i. Heyrovského nám. 2, 162 06 Prague 6, Czech Republic*

[2]*Nuclear Physics Institute, Academy of Sciences of the Czech Republic, v.v.i. Řež 130, 250 68 Řež, Czech Republic*

[3]*Institute of Biophysics and Informatics, First Faculty of Medicine, Charles University in Prague, Salmovská 1, 120 00 Prague 2, Czech Republic*

corresponding author: *mhruby@centrum.cz

Key words: Wilson's disease, polymer beads, copper metabolism, selective sorbent, amines

Abstract

Wilson's disease is a genetic disorder that leads to a high accumulation of copper in multiple organs with subsequent toxic effects. In this paper, a gentle therapy to eliminate harmful copper concentrations in patients with Wilson's disease is proposed using an oral administration of insoluble polymeric sorbents containing selective chelating groups for copper(II). The sorbents contained triethylenetetramine, *N*,*N*-di(2-pyridylmethyl)amine, 8-hydroxyquinoline or 8-hydroxyquinoline-5-sulfonic acid chelating groups bound to a methacrylate-based macroporous support. Nearly quantitative copper(II) uptake within

minutes was achieved in buffers modeling the pH range present in the gastric environment (pH 2.0 and 4.0). The sorbents demonstrated chelating selectivity for copper(II) against zinc(II) with ratios of up to 940. The sorbents demonstrated sufficient stability of the copper complexes against rechelation using studies in a model environment for the small intestine (the presence of chelating amino acids, pH 6.8).

1. Introduction

Wilson's disease is a genetically conditioned disorder of copper metabolism, leading to toxic damage of mainly the liver and brain. [1, 2] The cause of the disease is a malfunction of ATPase 7B, [3] with more than 400 mutations of the respective gene that have been described to date. [4] The average prevalence in the general population is 1:30 000. [1] The malfunction of ATPase 7B significantly decreases the secretion of copper into the bile, the main pathway for the elimination of copper, leading to an accumulation of copper, mainly in the liver and the central nervous system. Increased concentrations of copper within tissues can lead to a number of symptoms, resulting in toxic oxidative stresses that can damage the liver, brain and parenchymal organs. [1,2,4,5] Untreated Wilson's disease is lethal, with the most serious complications arising from liver cirrhosis, portal hypertension and massive bleeding in the alimentary tract. [1,6]

Current first line therapy is based on a decrease in the amounts of copper by an administration of low-molecular-weight copper(II) chelators (penicillamine, triethylenetetramine or tetrathiomolybdate), [1,4] leading to a decreased absorption of copper from food with a subsequent increase in biological elimination. As an adjuvant therapy, high doses of zinc(II) salts are administered as these ions competitively block copper uptake from the gastrointestinal tract. [1]

Suitable forms of zinc are not always available worldwide. Current therapies also suffer from serious side effects, such as myelosuppression, lupus and penicillamine-associated myasthenia

[57] as a consequence of the re-formation of a complex of essential elements after the gastrointestinal absorption of the chelating agent. Zinc therapy is typically accompanied with strong gastrointestinal adverse effects, with typical doses of zinc of up to 1200 mg / day, [8] which is approximately one hundred-fold more than the daily intake of zinc (ca 8 – 15 mg). [9,10]

The average uptake of copper from food ranges from 0.6 – 1.6 mg per day. At the beginning of the therapy for Wilson's disease, a diet with low quantities of copper is often recommended (*i.e.,* avoiding food with high copper content, such as liver, nuts or mushrooms). [1] Considering the omnipresence of copper in food, a copper-less diet can be near impossible to fully obtain. [11] A significant amount of copper is eliminated through the alimentary tract followed by a subsequent re-uptake, representing higher amounts than the quantities obtained from food (ca 4.4 – 5.3 mg of copper is secreted daily, with 7 % from saliva, 20 % from gastric juices, 50 % from bile, 18 % from pancreatic juices and 5 % from duodenal secretion). [11]

The oral administration of cholestyramine is used for the treatment of hypercholesterolemia (high blood levels of cholesterol). Cholestyramine is a strongly basic anion exchange resin based on a styrene-divinylbenzene matrix [12-16] that selectively adsorbs anionic bile acids to form an insoluble polymeric carrier in the intestine. An impaired recycling process of the bile acids can result in an increased metabolization of cholesterol to bile acids.

Various polymeric matrices for the selective sorption of copper ions in the presence of other heavy metal ions have been developed for wastewater treatment and hydrometallurgical industrial applications. [17-25]

To the best of our knowledge, peroral administration of chelating polymers that are selective for copper ions has not been reported for Wilson's disease therapy. The aim of this study was to screen suitable sorbents [containing *N*,*N*-di(2-pyridylmethyl)amine (DPA), triethylenetetramine (TTA), 8-hydroxyquinoline (8HQ) or 8-hydroxyquinoline-5-sulfonic acid

(8HQ5S) chelating groups] for the rapid absorbance of copper in the gastric milieu without releasing these ions under rechelating challenge as experienced in the intestinal environment. Effective sorbents should be able to adsorb copper released from food prior to uptake by the gastrointestinal tract and also exhibit an ability to scavenge copper secreted into the gastrointestinal tract, with an eventual elimination in the feces.

2. Experimental

2.1. Materials

Poly(glycidyl methacrylate-*co*-ethylene dimethacrylate) (**1**, 60:40, particle size 20 – 40 micrometers) particles were synthesized by suspension copolymerization using a procedure described in the literature. [26] (CHN: 58.59 % C, 7.32 % H, 0.00 % N.) All other chemicals were purchased from Sigma-Aldrich (Prague, Czech Republic) and were used as received.

2.2. Methods

2.2.1. Synthesis of the sorbents (*see* Scheme 1)

2.2.1.1. Sorbent with DPA chelating groups (polymer **2***)*

Polymer **1** (16 mmol epoxide groups, 4.00 g) was reacted with *N*,*N*-di(2-pyridylmethyl)amine (24 mmol, 4.31 mL) in propan-2-ol (10 mL) at 75 °C for 16 h. Product **2** was subsequently washed in methanol and dried. Elemental analysis: 59.77 % C, 6.87 % H, 4.81 % N (3.45 mmol/g N; 1.15 mmol/g of ligand). Capacity for Cu^{2+} (in excess 0.1 mol L^{-1} $CuSO_4$ in 1 mol.L^{-1} acetate buffer, pH 4.75) was 0.666 mmol/g.

*2.2.1.2. Sorbent with TTA chelating groups (polymer **3**)*

Polymer **1** (16 mmol epoxide moieties, 4.00 g) was reacted with triethylenetetramine (48 mmol, 4.69 mL) in methanol (16 mL) at room temperature for 6 days. Product **3** was washed with methanol and dried with air. Elemental analysis CHN: 54.49 % C, 7.96 % H, 4.49 % N (3.20 mmol/g N; 0.80 mmol/g of ligand). Capacity for Cu^{2+} (in 0.1 mol.L^{-1} excess of $CuSO_4$ in 1 mol.L^{-1} acetate buffer, pH 4.75) was 0.544 mmol/g.

*2.2.1.3. Sorbents with 8HQ groups (**5**) and 8HQ5S groups (**6**)*

Sorbents **5** (containing 8HQ moieties) and **6** (containing 8HQ5S moieties) were synthesized via secondary amine intermediate **4** according to the literature. [27] Briefly, Polymer **1** (20 mmol epoxide moieties, 5.00 g) was immersed in 41 % aqueous methylamine (20 mL) and held for 72 h at ambient temperature. The polymer was washed with water and methanol and dried with air. The yield was 5.05 g of polymer **4**. CHN elemental analysis: 52.80 % C, 7.35 % H, 3.51 % N (2.51 mmol/g secondary amine).

Polymer **4** (2.00 g, 5.02 mmol secondary amino groups) was reacted with 8-hydroxyquinoline Q (1.90 g, 13 mmol, synthesis of polymer **5**) or 8HQ5S (2.93 g, 13 mmol, synthesis of polymer **6**) in the presence of formaldehyde (40 % aqueous solution, 6.00 mL, 65 mmol) and anhydrous sodium sulfate (13.4 g, 94.3 mmol) in methanol (30 mL) at room temperature for 7 days. The polymer was successively washed with methanol, 1 mol.L^{-1} aqueous hydrochloric acid, water, 0.5 mol.L^{-1} ammonium acetate and water and dried with air. The yields were 2.23 g of polymer **5** and 1.85 g of polymer **6**. CHN elemental analysis: polymer **5**: 57.70 % C, 7.35 % H, 4.02 % N; polymer **6**: 52.39 % C, 7.67 % H, 3.38 % N, 1.15 % S (0.359 mmol/g S or ligand).

The capacity for Cu^{2+} (in 0.1 mol L^{-1} excess of $CuSO_4$ in 1 mol.L^{-1} acetate buffer, pH 4.75) was measured to be 0.480 mmol/g (polymer **5**) and 0.287 mmol/g (polymer **6**).

2.2.2. Ultra-trace copper concentration absorption test

The suspension of each sorbent (20 mg; in acetate buffer (1 mL, 1 mol.L^{-1}, pH 4.0)) was mixed with aqueous radioactively labeled [^{64}Cu]-$CuCl_2$ (8 μL, activity A_0 = 525 kBq, corresponding to $5.75.10^{-14}$ mol of copper) and shaken for 1 h at room temperature. The activity of the samples was measured using a Bqmetr 4 ionization chamber (Empos Ltd., Prague, Czech Republic). Each suspension was then centrifuged with one-half of the supernatant volume (504 μL) removed and measured for radioactivity (A). The percentage of residual copper w_{CuR} in the solution was calculated according to **Equation 1**:

$$w_{CuR} = 2A/A_0 * 100\ \% \qquad \textbf{(Eq. 1)}$$

The experimental error was less than 5 % of the measured value for all samples (number of repetitions, n = 5).

2.2.3. The copper(II) adsorption study

Two buffers (pH 2.0 - 0.01 mol.L^{-1} hydrochloric acid or pH 4.0 - 1 mol.L^{-1} acetate buffer, 100 mL each) containing 5 mg copper as $CuSO_4$ were combined and shaken with 500 mg of each sorbent sample. The samples (aa 10 mL) were collected at specific time points (0, 2, 5, 10, 20 and 60 min), filtered and the copper content determined in the filtrate by atomic absorption spectrometry (AAS). The experimental error was less than 5 % of the measured value for all samples (n = 5).

2.2.4. The copper(II) desorption study (copper-chelating challenge)

Solutions with copper-chelating amino acids (93 mg of L-histidine, 133 mg of L-cysteine and 6.67 g of glycine, 200 mL, pH 6.8) were mixed with 500 mg of the test sorbents containing 5 mg of the absorbed copper (from acetate buffer), and the suspension was shaken at room

temperature. Samples (aa 10 mL) were collected at selected time points (10, 30, 90, 135, 300 and 1440 min), filtered and the copper content determined in the filtrate by AAS. The experimental error was less than 5 % of the measured value for all samples (n = 5).

2.2.5. Selectivity of sorption - competition with Zn^{2+}

Each sorbent (50 mg) was suspended in the buffers (pH 2 or 4, see above, 10 mL) containing copper sulfate (3.15 mmol.L^{-1}) and zinc sulfate (315 mmol.L^{-1}). After 2 h of shaking, the concentrations of copper and zinc in solution and in the water-washed and dried sorbent after mineralization were determined by AAS with the selectivity for copper in presence of zinc calculated using **Equation 2**,

$$\text{selectivity} = [\text{Cu(sorbent)}/\text{Cu(solution)}] * [\text{Zn(solution)}/\text{Zn(sorbent)}] \quad \textbf{(Eq. 2)}$$

where Cu(sorbent) is the concentration of copper in the sorbent (mmol/g), Cu(solution) is the concentration of copper in solution (mmol.L^{-1}), Zn(sorbent) is the concentration of zinc in the sorbent (mmol/g) and Zn(solution) is the concentration of zinc in solution(mmol.L^{-1}). The experimental error was less than 5 % of the measured value for all samples (n = 5).

3. Results and Discussion

The synthesis of sorbents using polymer **1** with relevant moieties was performed as described in Scheme 1. Epoxide groups of polymer **1** were reacted with the amines [*N*,*N*-di(2-pyridylmethyl)amine, triethylenetetramine or methylamine]. Both the polymer support and the amines contain carbon and hydrogen, making the calculation of the conversion using the carbon and hydrogen contents highly inaccurate, in addition to the possible experimental errors. As the starting polymer **1** does not contain nitrogen and the products contain

covalently bound amines, the progress of reaction can be easily and accurately followed by an analysis of the nitrogen content; the reaction was continued until the nitrogen content no longer increased.

The reaction with DPA was performed in propan-2-ol at 75°C. The reaction was completed after 16 h (2.25 % N after 2 h; 3.41 % N after 4 h, 4.20 % N after 6 h; 4.65 % N after 8 h; 4.78% N after 10 h; 4.81 % N after 16 h). The final content of 4.81 % N corresponds to 3.45 mmol/g N and 1.15 mmol/g of ligand.

The reaction with TTA was performed in methanol at room temperature. The reaction was completed after 6 days (3.10 % N after 2 days; 4.41 % N after 4 days; 4.49 % N after 6 days). The final content of 4.49 % N corresponds to 3.20 mmol/g N or 0.80 mmol/g of ligand.

The reaction with aqueous methylamine was performed at room temperature. The reaction was completed after 72 h (1.89 % N after 0.5 h; 2.47 % N after 1 h; 2.75 % N after 2 h; 3.11 % N after 5 h; 3.22 % N after 24 h; 3.51 % N after 72 h). The final content of 3.51 % N corresponds to 2.51 mmol/g N of secondary amine.

The progress of the reaction of the amines with the epoxides was followed by infrared spectroscopy (see Figure 4). For all samples, the epoxide absorption band at 908 cm^{-1} in the products after complete conversion of epoxides on polymer **1** was not observed. The amide C=O band was not observed in the products, suggesting that the side reactions were either hydrolysis or basically catalyzed alcoholysis with the solvent, but not aminolysis of the ester to the amide (and thus the nitrogen content shows the real content of the active ligands). Only the absorption band of the C=O bond of ester of the methacrylate matrix at 1718 cm^{-1} was observed in the infrared spectra (see Figure 4).

The Mannich condensation reactions with formaldehyde and 8-HQ or 8HQ5S were followed as an estimate of the copper adsorption capacity, as the analysis of C, H and N is unreliable with both starting polymer **4** and products containing similar amounts of these elements as well as the contributions from the possible experimental errors. For the synthesis of polymer

6, the progress of the reaction can be followed using a sulfur analysis, which correlates well with the copper adsorption capacity. The reaction was found to be completed after 7 days, as reported previously [27] (e.g., the Cu^{2+} adsorption capacity in the course of the synthesis of polymer **5** was 0.24 mmol/g after 4 h, 0.33 mmol/g after 24 h, 0.43 mmol/g after 96 h, 0.48 mmol/g after 168 h and 0.48 mmol/g after 336 h).

The capacity for Cu^{2+} adsorption was comparable for all sorbents. With the capacities of sorbents for Cu^{2+} adsorption at values that were slightly lower than the ligand contents calculated from the elemental analysis, the ligand accessibility for copper adsorption was assumed to be good, even at high ligand contents. All adsorption experiments were performed with sorbents using maximal ligand contents for each particular sorbent (to optimize for practical use). With the high degree of copper release in the stomach, the modeling of the copper entrapment in the gastric environment was performed in aqueous solutions buffered to pH 2.0 (gastric content fasting) and pH 4.0 (gastric content with food). In these experiments, 5 mg of sorbent was used (according to a presumed dose for human of 500 mg with the amount of copper), corresponding to the total amount of copper in nutrients and the amount of copper eliminated in the alimentation tract. The investigated sorption capacity of environment was found sufficient to prevent change in pH during the sorption (tested, ΔpH is less than 0.1). For the sorption capacity of the sorbents, the results as a function of the copper residues are expressed in proportion to the original concentration in the solution, as shown in **Figure 1** and **2**. For the sorbent with *N*,*N*-di(2-pyridylmethyl)amine (polymer **2**), copper ions in solution at pH 2.0 and pH 4.0 were almost quantitatively entrapped within several minutes (after 60 min, only 0.7% of the copper ions at pH 2.0 and 2.5% at pH 4.0 remained in solution).

For the sorbent with triethylenetetramine (polymer 3), the entrapment of copper from solution was also rapid (within the time scale of minutes) at both pH 2.0 and 4.0. At pH 4.0, the sorption was almost quantitative (after 60 min, only 0.9% of the copper ions remained in solution).

Sorbents with 8-hydroxyquinoline and 8-hydroxyquinoline-5-sulfonic acid (polymer **5** and **6**) entrapped copper rapidly (within the time scale of minutes) at both pH 2.0 and 4.0. At pH 4.0, the sorption was quantitative with the sorption at pH 2.0 satisfactory [5.4% of the copper ions (polymer **5**) or 22.6 % (polymer **6**) remained in solution after 60 min].

The sorbents were able to absorb copper, even in ultra-trace concentrations. For these experiments, *carrier-free* radioactive copper-64 was used. After the sorption experiments, the solutions contained less than 2 % of the original radioactivity for all sorbents, suggesting a high degree of sorption effectiveness even in picomolar concentrations of copper.

The small intestine environment represents a considerable competitive rechelating challenge (due to protease activity, there are high concentrations of free amino acids), which may lead to significant leakage of the absorbed copper from the sorbent. The intestinal environment was simulated by a solution of amino acids, with two of the most strongly copper chelating amino acids added at concentrations corresponding to their average daily uptake as determined from the average weight of ingested aliment with beverages totaling a volume of 1.5 L (1000 mg of L-cysteine and 700 mg of L-histidine per 1.5 L). The remaining amino acids were simulated with glycine at concentrations corresponding to amounts that are consistent with an average daily ingestion (50 g per 1.5 L). The amino acid concentrations were adjusted to 93 mg of L-histidine, 133 mg of L-cysteine and 6.67 g of glycine in 200 mL. The pH value was set at 6.8, representing an average pH of the intestinal conditions. For a 200 mL aliquot of this solution, 500 mg of sorbent containing 5 mg of copper (previously adsorbed from acetate buffer) was added, and the suspension was shaken for 24 hours at room temperature. The copper in solution was expressed proportionally with the amount that was released by a complete desorption, as shown in **Figure 3**.

The desorption experiments in a model of the small intestine environment demonstrated that only small quantities of copper were released in this rechelating environment. The released

amounts of copper(II) were determined to be 33% for polymer 2, 2.8% for polymer 3, 0.4% for polymer 5 and 10.8% for polymer 6.

Zinc ions are similar to copper ions with coordinating properties. This attribute is used in the current treatment of Wilson's disease by high doses of dissolved zinc salts competing with copper uptake from the gastrointestinal tract. For ordinary foods, the content of zinc can be significantly higher than that of copper (daily uptake of zinc in food averages 8 - 15 mg [9]). A key characteristic of a sorbent useful in the treatment of Wilson's disease is a sufficient selectivity for the sorption of copper ions in the presence of an excess of zinc salts. The sorbent selectivities of copper ion adsorption were tested in the presence of zinc ions (Cu:Zn molar ratio 1:100) in an environment imitating stomach conditions (pH 2.0 and 4.0). This zinc concentration (in the given model experiment) corresponds with a daily uptake of 1700 mg of zinc, which exceeds the ordinarily used doses for the therapy of Wilson's disease (1200 mg of zinc per day maximally).

The experimental results are shown in Table 1, suggesting that the sorbents possess a high degree of selectivity for copper ion sorption in the presence of zinc ions at both pH 2.0 and 4.0. The sorbent with the DPA groups (polymer 2) and the sorbent with the 8HQ groups (polymer 5) were the most selective among the tested sorbents.

Table 2: **Sorption selectivities for copper ions in the presence of zinc ions**

Sorbent	pH	Selectivity for Cu^{2+} compared to Zn^{2+}
Polymer 2	2.0	132
	4.0	940
Polymer 3	2.0	59
	4.0	424
Polymer 5	2.0	904
	4.0	798
Polymer 6	2.0	90
	4.0	93

4. Conclusions

Four sorbents with different Cu^{2+}-chelating moieties (*N*,*N*-di(2-pyridylmethyl)amine, triethylenetetramine, 8-hydroxyquinoline and 8-hydroxyquinoline-5-sulfonic acid) were prepared and characterized, with the results suggesting that under model conditions, these sorbents may be useful as therapeutics for the treatment of Wilson's disease. The sorbents effectively and quickly entrapped copper in an environment modeling the gastric conditions without significantly releasing copper in an environment modeling the intestinal conditions. Effective even at ultra-trace concentrations, the sorption was not disturbed by zinc salts, even at amounts of significant excess that correspond with therapeutic doses of zinc salts. These results suggest that the polymers have the potential as novel therapeutics for Wilson's disease, as these sorbents are also expected to be completely non-toxic (macroporous polymer beads are insoluble and thus cannot be taken up from the gastrointestinal tract) with an expected elimination from the body in the feces.

Acknowledgements:

The authors would like to express our appreciation for the financial support of the Grant Agency of the Czech Republic (grant # P304/12/0950 and 13-08336S). The authors would also like to thank the Charles University in Prague for the support of these PhD studies.

References

[1] A. Ala, A.P.Walker, K. Ashkan, J.S. Dooley, M.L. Schilsky, Wilson's disease, Lancet 369 (2007) 397-408.

[2] R. F.Butterworth, Metal Toxicity, Liver Disease and Neurodegeneration, *Neurotoxicity Research* 18 (2010) 100-105.

[3] R. Bruha, Z.Marecek, L. Pospisilova, S. Nevsimalova, L.Vitek, P. Martasek, J. Nevoral, J. Petrtyl, P. Urbanek, A. Jiraskova , P. Ferenci Long-term follow-up of Wilson Disease: natural history, treatment, mutations analysis and phenotypic correlation. *Liver International* 31 (2010) 83-91.

[4] U. Merle, M.Schaefer, P. Ferenci, W. Stremmel, Clinical presentation, diagnosis and long-term outcome of Wilson's disease: a cohort study, *Gut* 56 (2007) 115-120

[5] D. Huster, Wilson's disease, *Best Practice & Research in Clinical Gastroenterology* 24 (2010) 531-539

[6] A. Uno, H. Ishida, K. Konno, Y. Ohnami, H. Naganuma, M. Niizawa, Y. Hamashima, O. Masamune, Portal hypertension in children and young adults: Sonographic and color Doppler findings, *Abdominal Imaging* 22 (1997) 72-78

[7] S. K. Das, K. Ray Wilson's disease: an update, *Nature Clinical Practice Neurology* 2 (2006) 482-493

[8] G.J. Brewer, V. Yuzbasiyan-Gurkan, V. Johnson, R.D. Dick, Y. Wang, Therapy of Wilson's Disease with Zinc XII: Dose Regimen Requirements, The American Journal of the Medical Sciences 305 (1993) 199-202

[9] Dietary Reference Intakes (DRIs): Estimated Average Requirements, Dietary Reference Intakes for Vitamin A, Vitamin K, Arsenic, Boron, Chromium, Copper, Iodine, Iron, Manganese, Molybdenum, Nickel, Silicon, Vanadium, and Zinc (2001), www.nap.edu

[10] N. Shimizu, J. Fujiwara, S. Ohnishi, M. Sato, H. Kodama, T. Kohsaka, A. Inui, T. Fujisawa, H. Tamai, S. Ida, S. Itoh, M. Ito, N. Horiike, M. Harada, M. Yoshino, T. Aoki, Effects of long-term zinc treatment in Japanese patients with Wilson disease: efficacy, stability, and copper metabolism, *Translational Research* 156, (2010) 350-357

[11] P. V. E. van den Berghe, L. W. J Klomp, New developments in the regulation of intestinal copper absorption] *Nutrition Reviews*, 67 (2009) 658-672

[12] I. Ullah, G.J Wiley, Cholesterol-lowering tablets, (2000) US 6.066.336

[13] T. Goto, T. Meno, Tablets containing anion exchange resin, (2000) US 6.022.533

[14] M.S. Amer, J.C. Gray, Cholestyramine compositions and method for preparation thereof, (1990) US 4.895.723

[15] T.G. Wood, C.J. Xenides, Edible, baked compositions containing cholestyramine, US (1991) 5.015.477

[16] J.R. Andre, J.A. Colliopoulos, Anion exchange resin compositions containing almond paste for taste improvement, (1996) US 5.500.190

[17] L .Lehtinen, M. Lahtinen, M. Jyrala, M. Vuokko, Method for the removal of copper from a zinc sulphate solution. (2010) US 7.682.581

[18] K.R. Zinn, Process for separating a radionuclide from solution. (1995) US 5.409.677

[19] W. Chouyyok, , Y. Shin, J. Davidson, W.D.Samuels, N.H. LaFemina, R.D. Rutledge, G.E. Fryxell, Selective Removal of Copper(II) from Natural Waters by Nanoporous Sorbents Functionalized with Chelating Diamines, Environmental Science and Technology 44 (2010) 6390–6395

[20] M. Richter, O. Schumacher, Process for preparing chelating ion exchanger resins and the use thereof for the extraction of metals, (1994) U.S. 5.290.453

[21] A.Warshawsky, R. Kalir, A. Patchornik, Metal complexing polymers, (1982) US 4.317.887

[22] H.B. Scher, Microencapsulated chelating agents and their use in removing metal ions from aqueous solutions, (1985) US 4.500.494

[23] J.O. Porath, Ion adsorbent for metals having a coordination number greater than two, (1983) US 4.423.158

[24] D. Horak, M.J. Benes, K. Gumargalieva, G. Zaikov, A Novel Highly Copper(II)-Selective Ion Exchanger Based on Poly(Glycidyl Methacrylate-co-Ethylene Dimethacrylate) Beads Modified with Aspartic Acid Derivative, *Journal of Applied Polymer Science* 80 (2001) 913-916

[25] P.M. an Berkel, W.L. Driessen, G.J.A.A. Kodhass, J.Reedijk, D.C.Sherington, A Novel, Highly Copper(II)-selective Chelating Hydrophilic Ion Exchanger based on Imidazole modified Poly(glycidyl methacrylate), *Journal of the Chemical Society, Chemical Communications* 2, (1995) 147-148

[26] F. Svec, J. Hradil, J. Coupek, J. Kalal, Reactive Polymers.1. Macroporous Methacrylate Copolymers Containing Epoxy Groups, *Angewandte Makromolekulare Chemie* 48 (1975) 135-143

[27] M. Hruby, M. Skodova, H. Mackova, J. Skopal, M. Tomes, M. Kropacek, J. Zimova, J. Kucka: Lutetium-177 and iodine-131 loaded chelating polymer microparticles intended for radioembolization of liver malignancies, Reactive & Functional Polymers 71 (2011) 1155–1159

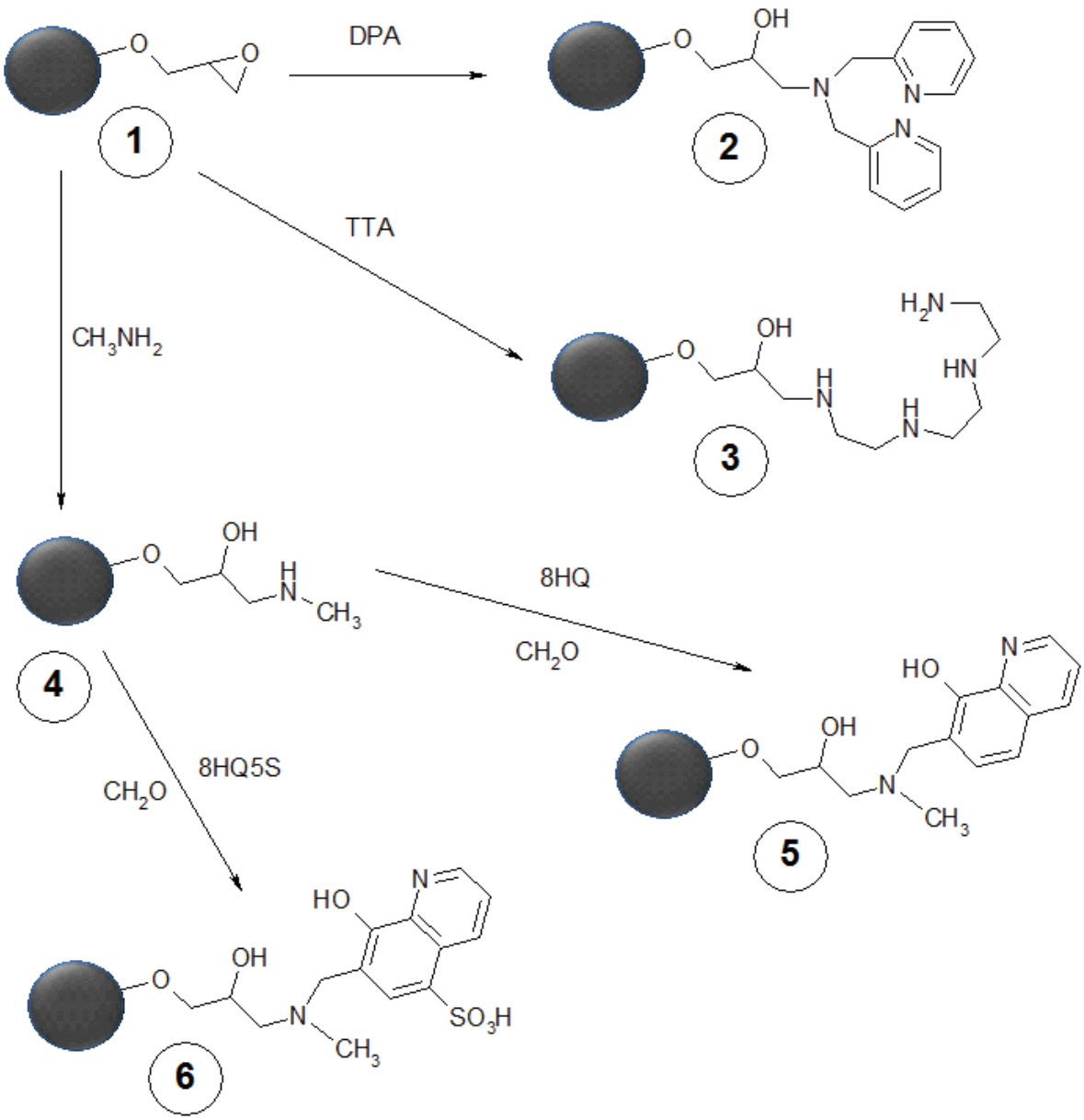

Scheme 1 – Synthesis of the sorbents from poly(glycidyl methacrylate-*co*-ethylene dimethacrylate (1); DPA= *N*,*N*-di(2-pyridylmethyl)amine, TTA= triethylenetetramine, 8HQ = 8-hydroxyquinoline, 8HQ5S =8-hydroxyquinoline-5-sulfonic acid

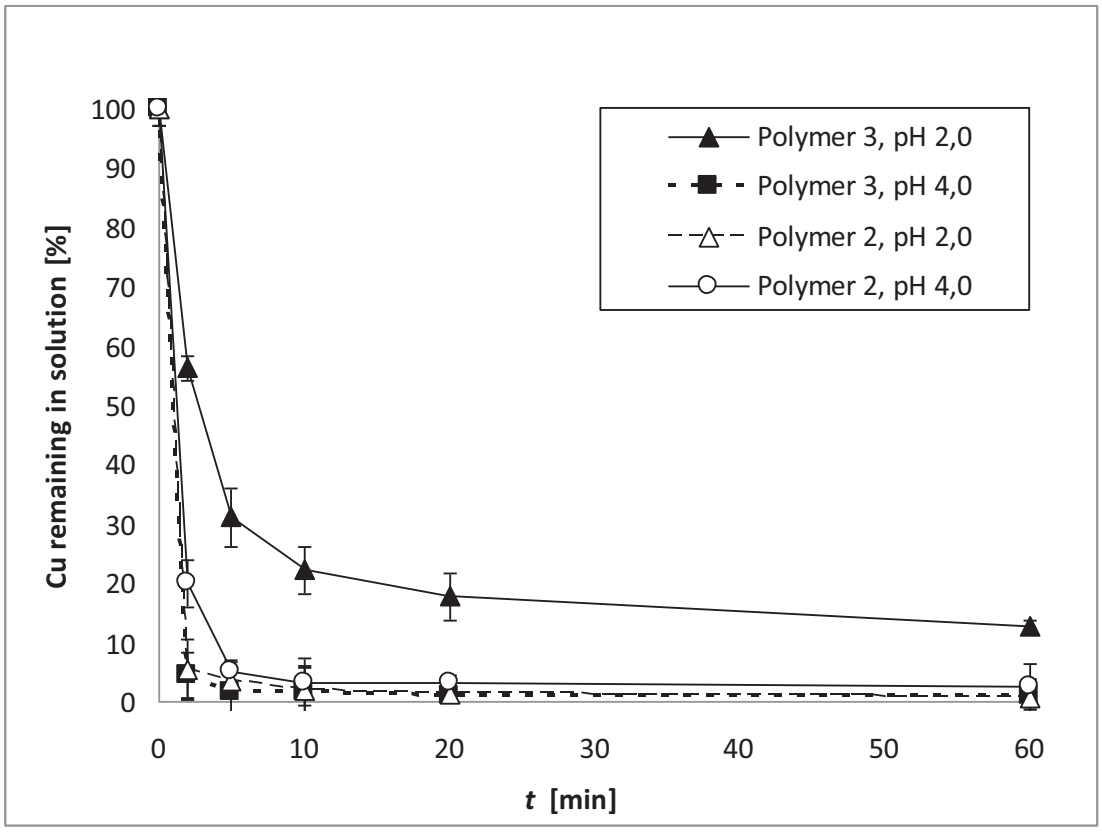

Figure 1 - Adsorption of Cu^{2+} on polymers **2** and **3** at pH 2.0 and 4.0.

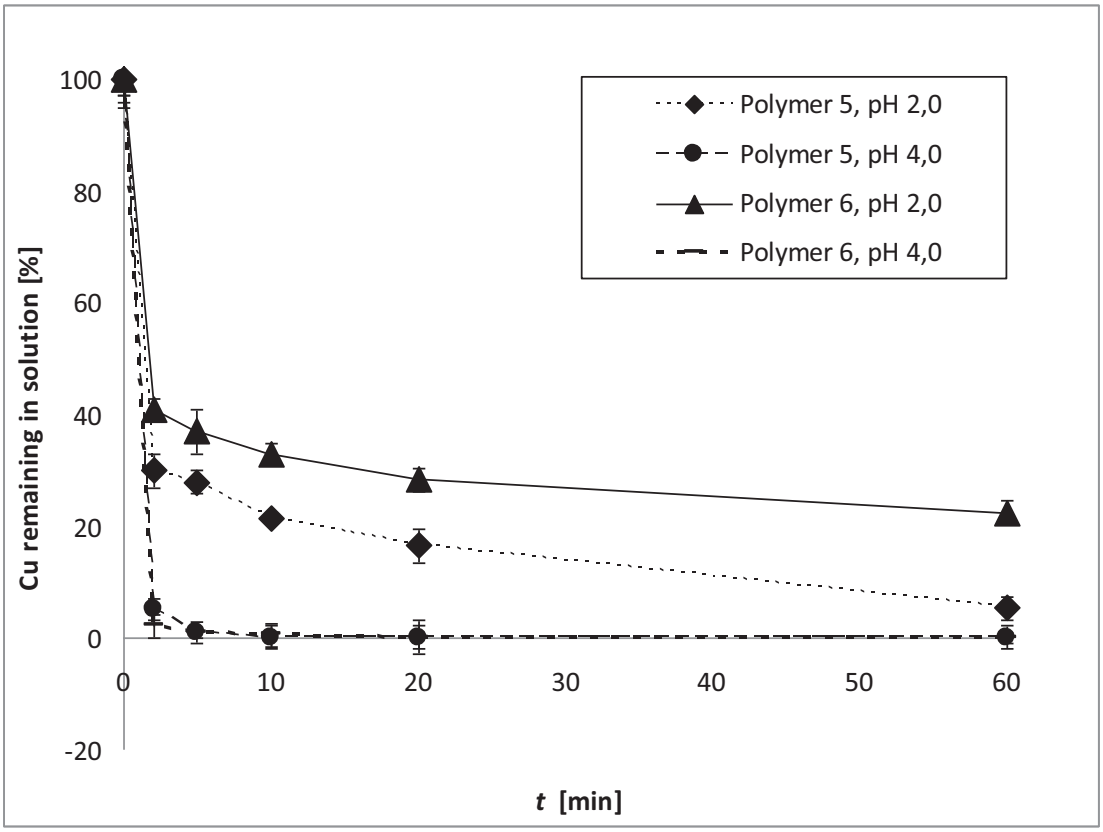

Figure 2 - Adsorption of Cu^{2+} on polymers 5 and 6 at pH 2.0 and 4.0

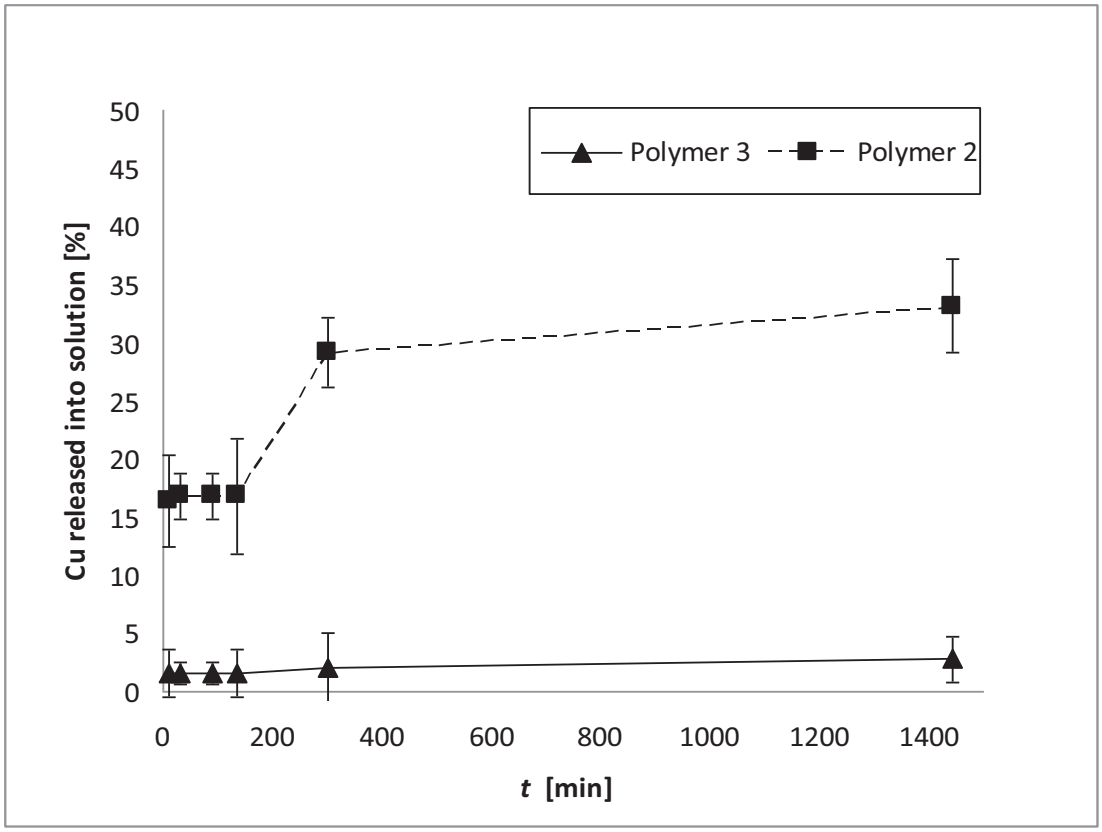

Figure 3 - Desorption of copper(II) from sorbents using an amino acids challenge solution.

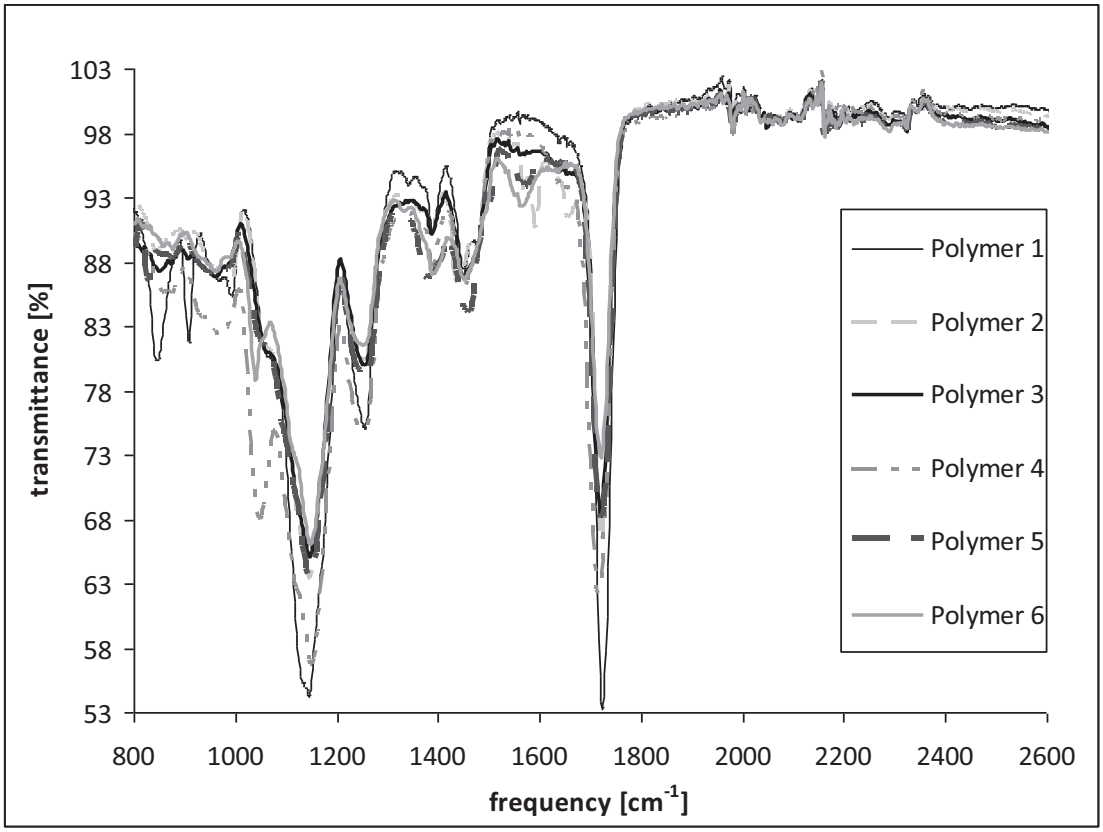

Figure 4 – IR spectra of polymers 1-6

Synthesis and studying properties of supramolecular metal cation-assembled core-shell nanoparticles as potential radionuclide theranostics for solid tumors

Publications:

D5. ***Novel polymeric nanoparticles assembled by metal ion addition***

Škodová M, Hrubý M, Filippov S K, Karlsson G, Macková H, Špírková M, Kaňková D, Steinhart M, Štěpánek P, Ulbrich K; Macromolecular Chemistry and Physics, 212, (2011), 2339-2348 - first author

D6. ***Self-Assembled Polymeric Chelate Nanoparticles as Potential Theranostic Agents***

Škodová M, Černoch P, Štěpánek P, Chánová E, Kučka J, Kálalová Z, Kaňková D, Hrubý M; ChemPhysChem, 13 (18), (2012), 4244-4250 - first author

Novel Polymeric Nanoparticles Assembled by Metal Ion Addition

Michaela Skodova, Martin Hruby,* Sergey K. Filippov, Goran Karlsson, Hana Mackova, Milena Spirkova, Dana Kankova, Milos Steinhart, Petr Stepanek, Karel Ulbrich

Potentially biodegradable graft polymer core-shell nanoparticles assembling by addition of metal ions intended to be used for radionuclide and drug delivery purposes are described. With Cu^{2+} ions, the self-assembly is slow (within minutes) with low efficiency. With Fe^{3+} ions the nanoparticles are formed immediately and are of convenient size for passive tumor accumulation by the enhanced permeation and retention effect. Full in vitro degradation of these particles is achieved with deferoxamine as a model of in vivo transchelation capacity.

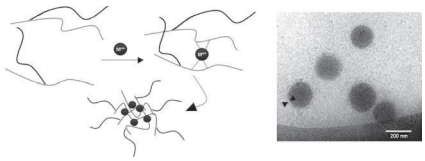

1. Introduction

Drug delivery systems based on various supramolecular structures were previously described in literature.[1,2] Block copolymers with amphiphilic character have the ability to self-assemble in aqueous milieu and to form nanoparticles. Drug delivery systems based on self-assembled systems (micelles, etc.) are used for carrying cytotoxic agents in their core; various systems were previously described in literature.[3–5] Investigation of their behavior in vivo showed that the drug inside the nanoparticle is well protected against unwanted reaction of the immune system. Polymeric structures with size convenient for these applications can be passively accumulated in solid tumors, due to the enhanced permeation and retention (EPR) effect[6,7] and due to leaking vasculature of the tumor tissue.

M. Skodova, Dr. M. Hruby, Dr. S. K. Filippov, Dr. H. Mackova, Dr. M. Spirkova, D. Kankova, Dr. M. Steinhart, Dr. P. Stepanek, Prof. K. Ulbrich
Institute of Macromolecular Chemistry, Academy of Sciences of the Czech Republic, Heyrovsky sq. 2, Prague 6, 162 06, Czech Republic
E-mail: mhruby@centrum.cz
G. Karlsson
Department of Physical and Analytical Chemistry, Uppsala University, Box 579, SE-751 23, Uppsala, Sweden

In this contribution, we describe the synthesis of potentially biodegradable nanoparticles assembled with essential metal cations that have a number of advantages. First, this system can be used for passive tumor targeting because it has suitable size (the nanoparticles are large enough for efficient EPR effect). The second advantage is the presence of iron or copper, which are essential micronutrients for all living organisms.[8–10] The excess of iron and copper cations in free form is toxic (it causes oxidative stress); therefore, these elements must be stored, handled, and transported in living organism as chelates. This is why low rechelation strength is present in bloodstream (to keep transport complexes with transferrin and coeruloplasmin stable),[11] whereas strong biochelation capacity for these ions (Fe^{3+} and Cu^{2+}) is expressed inside human organism cells to make these metals available for organelles in the cell. Transchelation is usually connected with intracellular bioreduction to Fe^{2+} and Cu^{+} after internalization of the transport complex into the cell. This should lead to biodegradability of the system once it reaches the target cell (but not in bloodstream where the rechelation competition is considerably lower) if these ions are used as chelating "micelle" core cross-linkers with the ligand–metal ion–ligand bond. On the other hand, if a high dose of Fe^{3+}-chelating low molecular weight or polymeric agent is applied into bloodstream, it may be used to treat diseases connected with pathologically high iron

© 2011 WILEY-VCH Verlag GmbH & Co. KGaA, Weinheim

DOI: 10.1002/macp.201100431

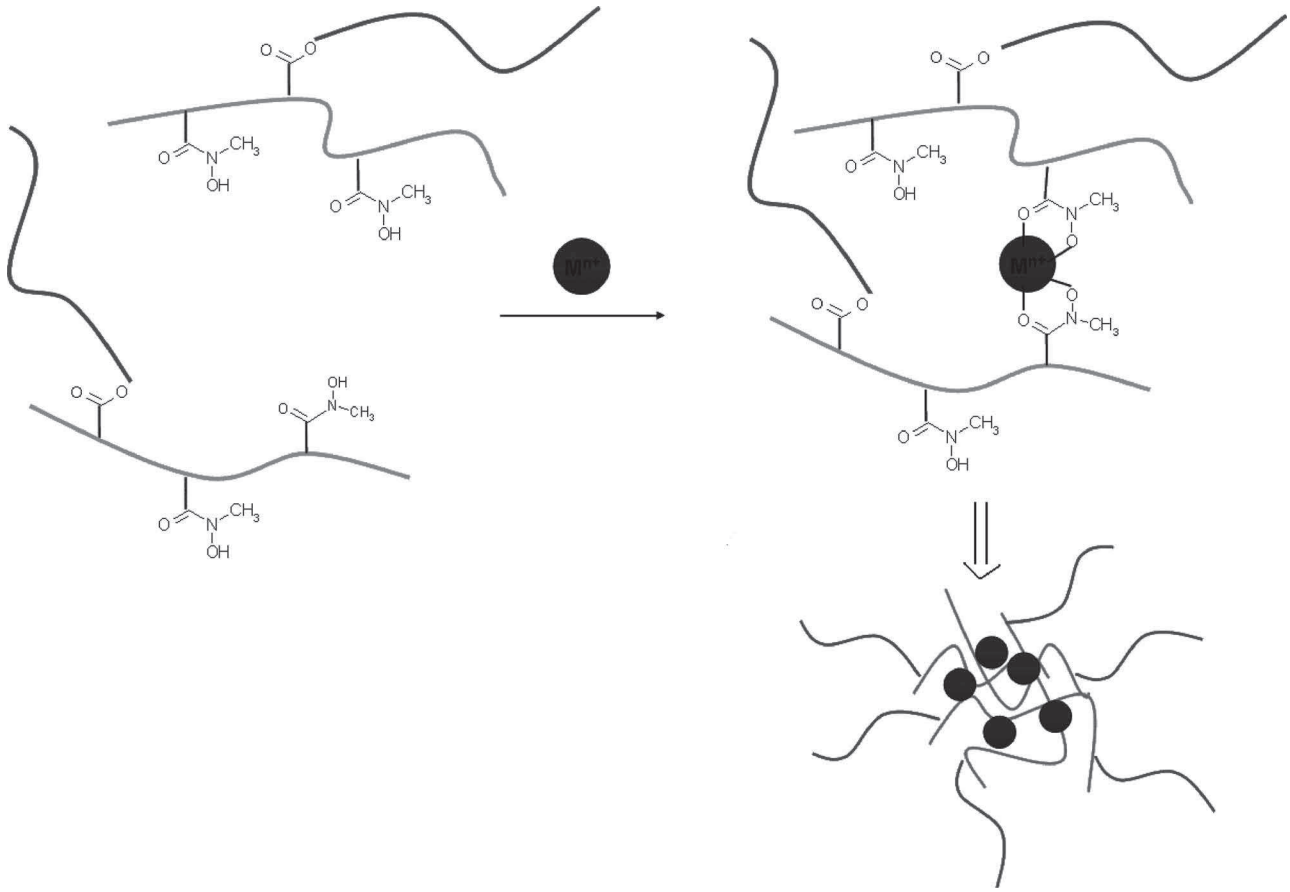

Figure 1. Scheme of reaction of the graft-polymer (PMMHA–PEO) with metal cation (Fe^{3+} or Cu^{2+}) and formation of the "micelle-like" structure.

uptake and accumulation (hemochromatosis, iron poisoning, etc.).[9,12,13]

Our system is based on the use of these ions as core cross-linkers of polymeric micelle-like structures for which we elucidate details of the chelation-driven metal ion-based self-assembly process. These ions may also serve as an active payload because some radionuclides of these metals (^{64}Cu, ^{67}Cu, ^{59}Fe) are promising radiodiagnostic and radiotherapeutical agents.[14] In this paper, we describe the incorporation of natural copper and iron as a model of their suitable radionuclides. The coordination bond may also be used to entrap cytostatic drugs into the micelle core (formation of the chelate of polymer–metal ion–drug; suitable chelating properties possess, e.g., bleomycin or doxorubicin).

Polymeric structures consisting of a backbone polymeric chain of poly(*N*-methyl methacryloyl hydroxamic acid) (PMMHA) with poly(ethylene oxide) (PEO) grafts have the advantage of biocompatibility and good solubility in bioacceptable solutions (DMSO, water). The chelate properties of the PMMHA–PEO structure enable the implementation of a metal ion inside the structure, but keep the possibility of eventual biodegradation of the nanoparticle in the cell by metal-ion transchelation from these complexes (see Figure 1). To the best of our knowledge, no system with such properties has been described so far.

The first goal of this paper is the synthesis of principally new polymeric nanostructures potentially applicable as drug delivery systems for cancerostatics.

The synthesis or preparation of nanoparticles is only the first step on the way to a potential drug delivery system. Many rather strict conditions have to be fulfilled for the successful application of newly synthesized nanocarriers.[15] Besides the above-mentioned biocompatibility and good solubility in bioacceptable solutions, the nanoparticles must have an appropriate size, be biodegradable, and should be stable at various values of pH because pH of their environment is significantly changed during the drug delivery process. Also, the presence of a shell that protects the drug against unwanted reaction of the immune system will be a benefit. Thus, the second goal of our paper is the optimization of nanoparticle properties to make them eligible for prospective medical applications.

© 2011 WILEY-VCH Verlag GmbH & Co. KGaA, Weinheim

For this purpose, we search through several factors that might influence the behavior of nanoparticles in solution and make them ready made for biological tests on laboratory animals.

2. Experimental Section

2.1. General

All reagents were purchased from commercial sources and used as received. For evaluation of the synthesized polymers, high-performance liquid chromatography (HPLC), CHN analyses, and ^{1}H NMR were used. The formation kinetics of nanostructures was evaluated using VIS spectroscopy, dynamic light scattering (DLS), small-angle X-ray scattering (SAXS), and the existence and conformation of the nanostructures was documented with atomic force microscopy (AFM) and cryo-transmission electron microscopy (cryo-TEM).

NMR spectra were measured on Bruker Advance MSL 200 MHz NMR spectrometer (Bruker Daltonik, Germany). Molecular weights of polymers were determined by size-exclusion chromatography (SEC) in a mixture of acetate buffer and methanol (20:80, v/v) as a mobile phase (pH 6.5; 0.3 mol L^{-1}) on a TSK 4000 column (Polymer Laboratories Ltd., UK) and TSK 3000 column (TSK 4000 for $\overline{M}_w$ > 20 000 Da), respectively, using a Shimadzu HPLC System (Shimadzu GmbH, Czech Republic) equipped with UV and multiangle light-scattering DAWN DSP-F detectors (Wyatt, USA).

2.2. Synthesis of Polymeric Carriers

Preparation of *N*-hydroxysuccinimide methacrylate (MAOSu) – modified procedure according to ref. [13]:

Triethylamine (14.23 mL; 0.102 mol) and methacryloyl chloride (9.96 mL; 0.102 mol), each in 30 mL of dichloromethane, were added dropwise with stirring and ice cooling to *N*-hydroxysuccinimide (11.51 g; 0.100 mol) in anhydrous methylene dichloride (40 mL). After 6 h stirring at room temperature, the precipitated triethylammonium chloride was removed and the filtrate was shaken with, successively, water, saturated sodium hydrogen carbonate solution, and again water, dried with $MgSO_4$ and evaporated. The residue was recrystallized from ethyl acetate–light petroleum mixture, yield: 9.8 g (53%).

δ_H (300 MHz, $CDCl_3$, Me_4Si) 2.05 (3 H, s, =C(CH_3) –), 2.85 (4 H, s, –CH_2 –), 5.88 (1 H, s, *E* –H–CH=), 6.40 (1 H, s, *Z*– H–CH=); δ_C (300 MHz, $CDCl_3$, Me_4Si) 18.3 (1 C, –CH_3), 25.7 (2 C, –CH_2 –), 130.6 (1 C, =CH_2), 131.9 (1 C, =C(CH_3) –), 162.2 (1 C, –COO–), 169.3 (2 C, –CO– hydroxysuccinimidyl); $C_8H_9NO_4$ (183.17): Calcd. C 52.46, H 4.95, N 7.65; Found: C 52.32, H 4.76, N 7.42.

2.3. Synthesis of Poly(ethylene oxide) Methyl Ether Methacrylate (MA-PEO)

PEO methyl ether ($\overline{M}_w$ = 5000, 10.0 g, 2.0 mmol) was dissolved in benzene (60 mL), benzene was removed in vacuo and the azeotropic drying was repeated once more. The dried polymer was dissolved in dichloromethane (60 mL), the solution was cooled to +5 °C and triethylamine (1.40 mL, 10 mmol) and methacryloyl chloride (0.48 mL, 5 mmol) were added. The mixture was left overnight at room temperature and then washed three times with 5% aqueous sodium chloride (ca. 50 mL). The dichloromethane layer was dried with $MgSO_4$ and concentrated to ca. 40 mL. Diethyl ether (300 mL) was added and the precipitated polymer was filtered off after staying 2 h at –18 °C. The product was purified by precipitation from dichloromethane (40 mL) into diethyl ether (300 mL) and dried in vacuo, yield 7.5 g, with a degree of esterification (D_e) = 97%.

The D_e was calculated from ^{1}H NMR spectra according to Equation (1)

$$D_e = 100 \times S_{6.12}/(S_{3.37}/3)\ [\%] \quad (1)$$

where $S_{6.12}$ is the integral signal of the E –H–C=C nuclei in the methacrylate moiety [δ_H (300 MHz, $CDCl_3$, Me_4Si) 6.12 (1 H, s)] and $S_{3.37}$ is the integral signal of the methyl end group hydrogen nuclei of the PEO chain [δ_H (300 MHz, $CDCl_3$, Me_4Si) 3.37 (3 H, s)].

2.4. Synthesis of Poly(*N*-methyl methacryloyl hydroxamic acid)-*graft* -PEO (Figure 2)

PEO methyl ether methacrylate ($\overline{M}_w$ = 5000; 250 mg) was dissolved in benzene and the solvent was evaporated in vacuo. *N*-hydroxysuccinimide methacrylate (250 mg) was dissolved, together with the dried PEO methyl ether methacrylate, in anhydrous tetrahydrofuran (6 mL). Azobis(isobutyronitrile) (10 mg) was added to the reaction mixture, and the reaction was stirred overnight under nitrogen at 60 °C.

Next day, methyl hydroxyl amine hydrochloride (1.14 g), triethylamine (1.9 mL), and methanol (7.5 mL) were added to the reaction mixture and stirred until the dissolution of all the reagents. After that, 4 mL of dimethyl sulfoxide (DMSO) was added and the solution was dialyzed against water for 48 h using dialysis tubing with cut-off 3500 Da (water was exchanged in the outer bath three times). The polymer was lyophilized yielding 481 mg (96%) of the product.

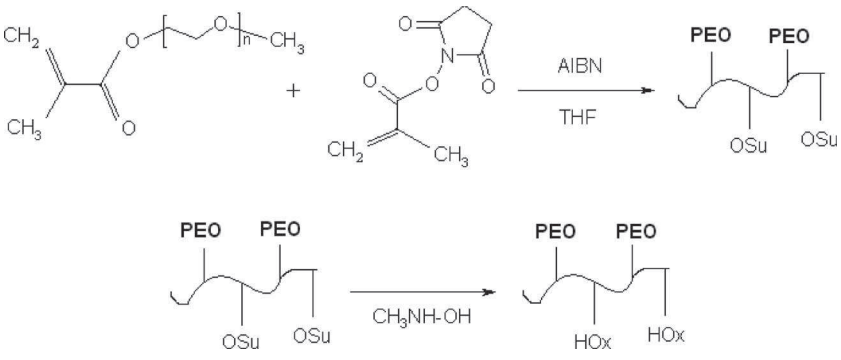

Figure 2. Scheme of synthesis of poly(*N*-methyl methacryloyl hydroxamic acid)-*graft*-PEO (PEO = polyethylene oxide; OSu = *N*-hydroxysuccinimidyl; HOx = *N*-methyl methacryloyl hydroxamic acid).

© 2011 WILEY-VCH Verlag GmbH & Co. KGaA, Weinheim

2.5. UV-Vis Spectroscopy

Creation of chelates of polymers with Cu^{2+} (green) and Fe^{3+} (red) can be observed because of their absorption of light in the visible part of spectrum measured by UV-Vis spectroscopy. The polymers were dissolved in advance in a small amount of DMSO and water was added to reach the desired concentration of polymer and of DMSO (10%, v/v) in solution. Absorbancies of the polymer complexes gradually formed by addition of a solution containing Fe^{3+}/Cu^{2+} ions into the polymer solution upon stirring at 200 rpm at 23 °C were measured on a UV-Vis spectrometer in the range 250–800 nm. The solution added to form Fe complexes was $FeCl_3 \cdot 6H_2O$ in 0.05 M HCl and the solution containing Cu^{2+} ions was $[Cu(NH_3)_4]^{2+}$ in ammoniacal environment.

Aliquots (10 μL) of $FeCl_3$ and $[Cu(NH_3)_4]^{2+}$ solution were regularly added to the polymer solution (2 mL) during the measurement of the spectra; the addition of a total of 100 μL of solution in both cases was pre-established to be the saturating amount of each metal for the polymeric complex.

For $FeCl_3 \cdot 6H_2O$ alone in 0.05 M HCl, there is no absorbance in the measured range of wavelengths but for $[Cu(NH_3)_4]^{2+}$, absorbance around 600 nm can be observed, so the contribution of the $[Cu(NH_3)_4]^{2+}$ complex was measured separately and subsequently subtracted to obtain real absorbance of the polymeric complex.

2.6. Dynamic Light Scattering

All measurements were carried out on ALV instrument equipped with a 22 mW He–Ne laser. An ALV 6000, multibit, multi-tau autocorrelator covering ≈12 decades in the delay time t was used for measurements of time autocorrelation functions. The experiments were conducted at the scattering angle $\theta = 90°$ and dust-free glass 2 mL ampoules with the prefiltered solution were used. The inverse Laplace transformation using the REPES method of constrained regularization,[16] which is similar in many aspects to the inversion routine CONTIN,[17] was performed in analysis of time autocorrelation functions. REPES directly minimizes the sum of the squared differences between the experimental and calculated intensity time correlation functions using nonlinear programming. This method uses an equidistant logarithmic grid with fixed components (here a grid of 20 components per decade) and determines their amplitudes. As a result a distribution function $A(\tau)$ of decay times is obtained which can be easily transformed into a distribution function of diffusion coefficients or hydrodynamic sizes.

The hydrodynamic radius, R_h, was calculated[18] from the diffusion coefficient, D, using the Stokes–Einstein equation [Equation (2)]

$$R_h = kT/6\pi\eta D \quad (2)$$

where k is the Boltzmann constant, T is the absolute temperature, and η is the viscosity of the solvent.

Polymers were dissolved in 10% DMSO–water solution; the refractive index and viscosity values were taken from literature.[19,20] Accumulation time per one measurement was 30 s with a 45 s delay between measurements. Such accumulation time is a reasonable compromise between requirements to accumulate a good enough correlation function $g_2(t)$ and to monitor fast kinetics of the system.[21] The statistics of correlation functions accumulated over 30 s was sufficient to obtain a good distribution function without artifacts, although the uncertainty in R_h values was definitely higher then in usual DLS experiments leading to some scatter in the R_h values.

2.7. Atomic Force Microscopy

The Fe–PMMHA–PEO complex (c = 10 mg L^{-1}; 10% DMSO–water solution) was deposited on fresh mica substrate and characterized by atomic force microscopy. The surface morphology (height image) and the sum of tip-sample interactions (phase image) were characterized by AFM. All measurements were performed under ambient conditions using a commercial atomic force microscope (NanoScope Dimension IIIa, MultiMode Digital Instruments, Santa Barbara, CA, USA) equipped with the NCLR POINTPROBE - Silicon SPM-Sensor - probe covered by reflex aluminum coating (NanoWorld AG, Switzerland; spring constant 45 Nm^{-1}, resonant frequency 154 kHz). Tapping Mode AFM technique was used for collecting all images.

2.8. Cryo-Transmission Electron Microscopy

To carry out a cryo-TEM experiment, a drop of the solution under study was placed on a pretreated copper grid which was coated with a perforated polymer film. Excess solution was removed by blotting with a filter paper. The preparation of the sample film was done under controlled environment conditions, i.e., in a chamber at a constant temperature of 25 °C and with a relative humidity of 98–99% to avoid evaporation of the liquid. Rapid vitrification of the thin film was achieved by plunging the grid into liquid ethane held just above its freezing point. The sample was then transferred to the electron microscope, a Zeiss 902A instrument (Carl Zeiss NTS, Oberkochen, Germany), operating at an accelerating voltage of 80 kV and in zero-loss bright-field mode. The temperature was kept below –165 °C and the specimen was protected against atmospheric conditions during the entire procedure to prevent sample perturbation and formation of ice crystals. The resolution in this method was 3–5 nm. Digital images were acquired with a BioVision Pro-SM Slow Scan CCD camera (Proscan electronische systeme GmbH, Germany). iTEM software (Olympus Soft Imaging Solutions, GmbH, Germany) was used for image processing. The polymer concentration used was 10 mg L^{-1}.

3. Results and Discussion

The synthesis of MAOSu and preparation of PMMHA–PEO was carried out as described in the Experimental Section. Radical polymerization of MAOSu monomer and PEO methacrylate (PEOMA) ($\overline{M}_w$ = 5000 Da) and the subsequent amidation were done in one pot without isolation of the polymeric *N*-hydroxysuccinimidyl ester intermediate to avoid hydrolysis of the *N*-hydroxysuccinimidyl ester

© 2011 WILEY-VCH Verlag GmbH & Co. KGaA, Weinheim

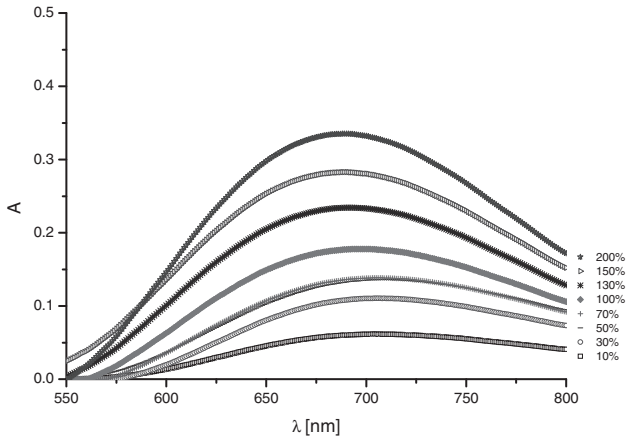

Figure 3. The absorbance *A* of Cu^{2+} –polymer complexes (after subtraction of the contribution of $[Cu(NH_3)_4]^{2+}$ complex), polymer concentration c_p = 5 mg mL^{-1}; 100% is theoretical equivalent amount of Cu^{2+} for 2:1 ratio with hydroxamic acid groups.

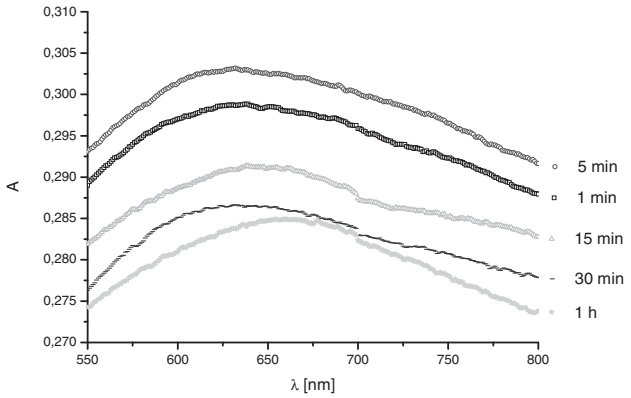

Figure 4. The absorbance *A* of Cu^{2+} –polymer complex, polymer concentration c_p = 5 mg mL^{-1} and 100% stoichiometric equivalent of Cu^{2+}.

groups. We did not use direct polymerization of *N*-methyl-*N*-methacryloyl hydroxamic acid due to its transfer properties during radical polymerization. The conversion of *N* -hydroxysuccinimide ester to hydroxamic acid may be accompanied with unwanted hydrolysis during the synthetic process; in such a case, nitrogen content in the purified product would drop. The elemental analysis (CHN) gave very good agreement of the measured *N* content (5.91%) with the theoretical value (6.09%) confirming negligible degree of hydrolysis. The obtained weight-averaged molecular weight $\overline{M}_w$ = 30.9 kDa (polydispersity $I = \overline{M}_w/\overline{M}_n$ = 1.54) should both provide sufficient length of the chelating block (in average 134 *N*-methyl methacryloyl hydroxamic acid units per molecule) to form stable nanoparticles (stabilized by 3.1 PEO grafts per polymer molecule in average) and keep the possibility to eliminate the polymer from organism by kidneys (threshold for renal filtration is ca. 40–45 kDa for methacrylamide-type polymers).[15]

The UV-Vis spectrum of the Cu^{2+} –polymer complex (Figure 3) shows that with gradual addition of Cu^{2+} ions, the absorbance grows as the chelate is formed. The interesting point is that the wavelength λ_{max} of maximum absorbance A_{max} is slightly shifted from 710 nm at the beginning (10 μL) to 690 nm at the end at 200% of stoichiometric equivalent of Cu^{2+} ions (2:1 ratio in case of Cu^{2+} ions to hydroxamic acid). This behavior is probably caused by partial reformation of the chelates and different space coordination of Cu^{2+} inside the polymer coil.

The maximum absorbance, A_{max} increases in the first 5 min (see Figure 4), due to slow formation of the complex and then drops in time most likely due to partial decomposition of the Cu^{2+} complex; this was later confirmed by time-resolved light-scattering experiments.

In case of Fe complexes, the wavelength shift of maximum of absorbance has a reverse trend. With addition of Fe^{3+} ions (3:1 ratio in case of Fe^{3+} ions to hydroxamic acid) the maximum of absorbance λ_{max} moves from ≈430 to ≈470 nm as shown in Figure 5,6. This trend can be explained as a reformation and also probable change in stoichiometry of Fe^{3+} ions within the polymer coil when changing available metal-ligand ratio, similarly to the copper complexes (the spectral shift may be both to shorter and longer wavelengths depending on the nature of the metal and of the ligand).[22,23] At the beginning, there is high excess of ligand and the stoichiometry metal:ligand is 1:3. As the amount of Fe^{3+} increases during complex formation, the stoichiometry shifts toward higher content of complexes with metal:ligand stoichiometry 1:2 and finally 1:1. This aspect has been discussed in literature for other Fe^{3+} –hydroxamic acid complexes[22,23] and the same conclusions have been reached.

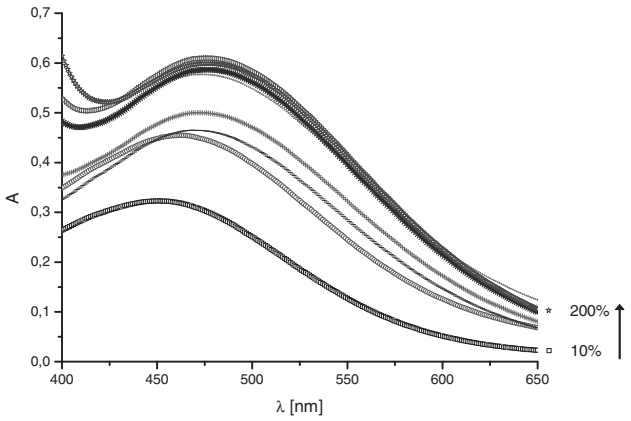

Figure 5. The absorbance *A* of Fe^{3+} –polymer complexes; polymer concentration c_p = 1 mg mL^{-1}; 100% is theoretical equivalent amount of Fe^{3+} for 3:1 ratio with hydroxamic acid groups.

© 2011 WILEY-VCH Verlag GmbH & Co. KGaA, Weinheim

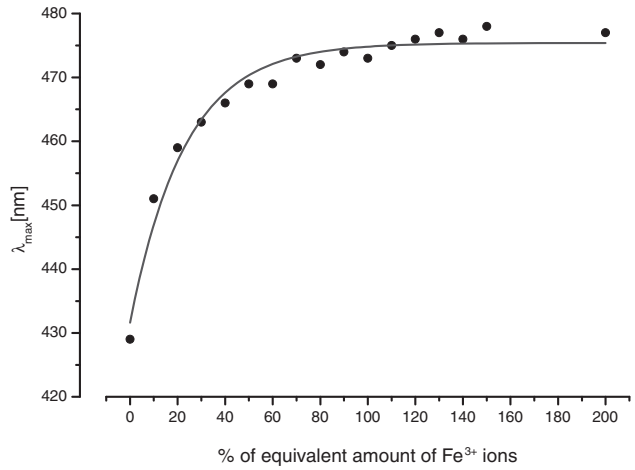

Figure 6. Dependence of λ_{max} value on added volume of Fe^{3+} ions for Fe^{3+} –polymer complex; polymer concentration $c_p = 1$ mg mL^{-1}.

In contrast to Cu complexes, A_{max} (for a fixed concentration) shows no time dependence in case of the Fe complexes. For a better analysis of the kinetics of complex formation, time-resolved light-scattering method was used.

We measured the apparent hydrodynamic radius R_h of particles in the solution of PMMHA–PEO polymer with subsequent addition of Cu^{2+} and Fe^{3+} using time-resolved dynamic light scattering (TR-DLS) to evaluate the kinetics of the formation of the Fe – and Cu –polymer complexes.

For complexes with Cu, the solutions contain two types of particles: small ones with R_h of several nanometers and big ones with R_h of about 30–100 nm (Figure 7). The estimated volume fraction of the big particles for Cu complexes is (in approximation of hard spheres) below 0.1%.

The size of small particles is almost constant with time in contrast to the size of the big ones that grow as a function of time. Keeping in mind that the size of a single polymer chain is several nanometers also, we can associate it with the smaller size observable in the distribution function (Figure 7). The bigger size was attributed to nanoparticles formed through chelate formation with Cu.

Time-resolved dynamic light scattering shows that the formation of complexes with Cu follows kinetics on a time scale of a few hours (Figure 7). The characteristic time τ of the complex formation obtained from the fitting of the time dependence of R_h by a modified exponential function [Equation (3)] is 266 min (Figure 7).

$$y = A\,(1 - \exp\,(-t/\tau)) \tag{3}$$

For the Fe complexes only one peak with R_h about 30 nm appears in the distribution of sizes (inset in Figure 8). The small entities with R_h of several nanometers were not observed even after conversion to volume weighted distribution. This implies that nanoparticles are dominant in the solution. The size of particles for complexes with Fe does not change on a time scale of hours (Figure 8) and, therefore, we can conclude that the formation of the Fe complexes in comparison to that of Cu complexes, is much faster (on a time scale of milliseconds or less according to time-resolved small-angle X-ray scattering (TR-SAXS), where the first time point already shows the nanoparticles, see Supporting Information). This is also in accordance with known high stability of the hydroxamic acid–Fe^{3+} complexes, which is significantly higher than stability of the hydroxamic acid–Cu^{2+}complexes (ref. [24], also see below).

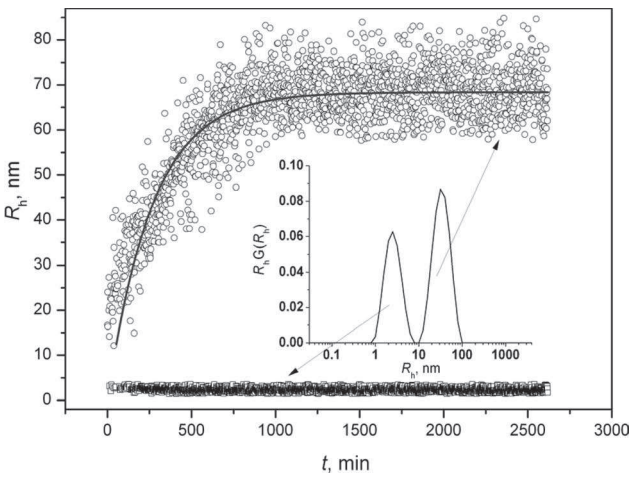

Figure 7. Time dependence of the size of Cu–polymeric complexes. Inset: intensity weighted distribution function of Cu complexes from TR-DLS data; c_p = 5 mg mL^{-1}. ○: Cu complexes; □: single polymer chain; full curve: the fit.

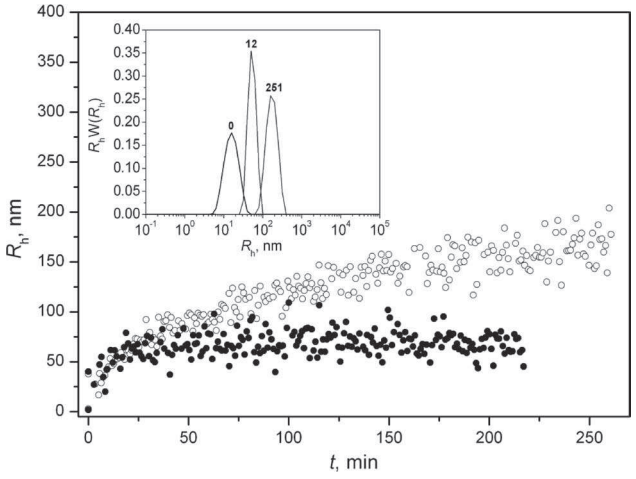

Figure 8. Time dependence of hydrodynamic radius R_h of Fe–polymer complexes; Inset: intensity-weighted distribution function hydrodynamic radii obtained from TR-DLS for a solution of Fe complexes; $c_p = 1$ mg mL^{-1}.

© 2011 WILEY-VCH Verlag GmbH & Co. KGaA, Weinheim

The Fe complexes stay stable for at least 7 d (180 h). Stability is the same in media containing bovine serum albumin in PBS (5 mg mL^{-1} in PBS, data not shown).

We conclude that the most crucial factor for nanoparticle formation is the nature of a metal cation. Indeed, in solution with Cu^{2+} ions, small fraction of nanoparticles coexists with single polymers. The kinetics of complex formation is slow. On the other hand, with Fe^{3+} ions the nanoparticles were formed immediately and they have a constant hydrodynamic diameter around 60 nm, convenient for passive tumor targeting.

In addition to the water dispersions of the Fe–polymer nanoparticles examined above we also studied the stability of the nanoparticle structures and their possible decomposition and aggregation in phosphate buffered saline (PBS) and upon interaction with deferoxamine. Deferoxamine is a bacterial siderophore (high-affinity iron chelating compound) produced by the actinobacter *Streptomyces pilosus*. It has medical applications as a chelating agent used to remove excess from the body[25] because it is a very strong iron chelating agent with stability constant for Fe^{3+} 30.6,[26] which is several orders of magnitude higher stability constant than reported for polymeric hydroxamic acids.[27] In this experiment, we used deferoxamine to investigate in vitro whether the system may be (bio)degraded by metal transchelation. To evaluate the stability of the Fe complexes, the equivalent amount of Fe^{3+} ions (3:1 ligand to Fe ratio) was added to a PMMHA–PEO solution (c_p = 1 mg mL^{-1}) dissolved in 10% DMSO–water mixture and an excess (3 equivalents of Fe) of deferoxamine mesylate (0.9 mmol) was added to the solution. TR-DLS experiments were conducted under similar conditions (see Experimental Section).

Figure 9 shows that deferoxamine influences the size of Fe complexes. The original radius of the nanoparticles is about 30 nm (Figure 8). After an initial growth during about 30 min for both systems (both with deferoxamine), the nanoparticles keep a constant radius of about 60 nm in PBS solutions while they continue growing in the non-buffered deferoxamine solution. As the kinetics of formation of Fe complexes takes place on time scale of milliseconds as discussed above, we conclude that the observed temporal variation at longer times is related to interaction of the Fe–polymer nanoparticles with deferoxamine that leads to elimination of iron from the already formed Fe complexes. As a result, the complexes grow in size (Figure 9) because of the hydrogen bonding between demetalized PMMHA blocks and PEO grafts.

The initial growth of the nanoparticles during the first 30 min can be caused by breaking cross-links in the nanoparticle core due to removal of Fe^{3+} ions and subsequent nanoparticle swelling, or a reassembly/aggregation of the particles due to existence of free hydroxamic acid, which may possibly interact with the PEO grafts.

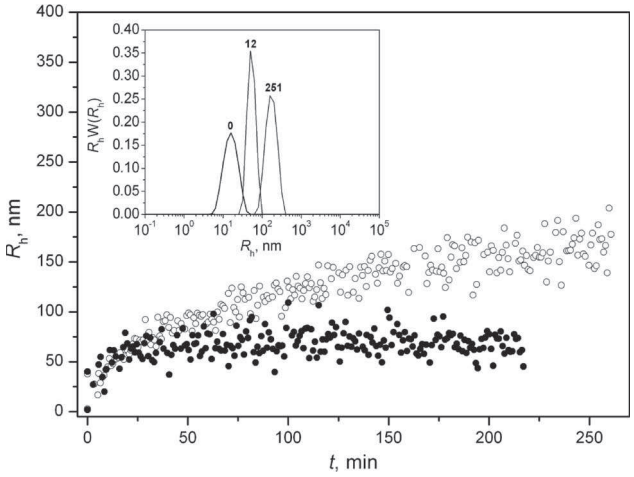

Figure 9. Time dependence of the hydrodynamic radius R_h of the Fe complexes in PBS (•) and in H_2O (◦); both with added deferoxamine. Inset: intensity weighted distribution function of Fe complexes from TR-DLS data at the indicated times (min); c_p = 1 mg mL^{-1} + 100% stoichiometric equivalent of Fe^{3+} ions.

As the deferoxamine-caused growth of the particles is strongly pH dependent, as shown below, we assume the latter case is valid. This is also supported by the pH-dependent behavior of the metal-free poly(*N*-methyl methacryloyl hydroxamic acid)-*graft*-poly(ethylene oxide) in aqueous milieu. Hydroxamic acids are weakly acidic with pK_A = 7.9 to 8.8 depending on substitution,[28] so we expected that the poly(*N*-methyl methacryloyl hydroxamic acid) backbone will behave as weakly acidic anionic polyelectrolyte with degree of ionization dependent on pH. When decreasing pH from basic to acidic milieu, one can see a gradual increase in light-scattering intensity (see Figure 10) pointing on probable

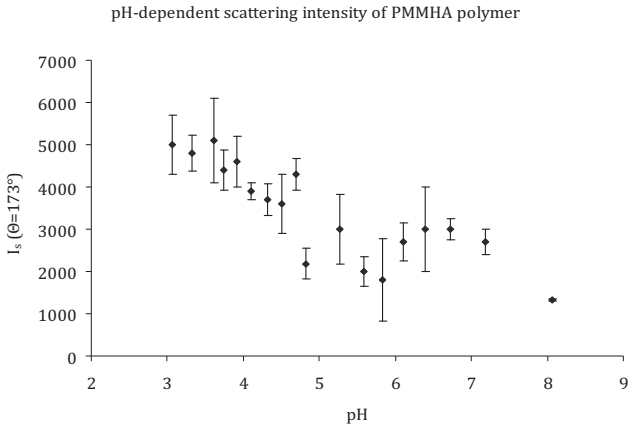

Figure 10. Dependence on pH of scattered intensity of PMMHA–PEO polymer; c_p = 1 mg mL^{-1} scattering angle = 173°.

© 2011 WILEY-VCH Verlag GmbH & Co. KGaA, Weinheim

intermolecular self-assembly. This behavior is similar to the formation of poly(meth)acrylic acid –poly(ethylene oxide) complex by multiple hydrogen bonds when decreasing pH. When poly(meth)acrylic acid is deprotonated in alkaline milieu, there is no acidic –COO**H** hydrogen that would bind PEO oxygen atom so no self-association occurs and also negative charges on the polymer backbone prevent assembly.[29] During the decrease of pH, the carboxyls become protonated and the number of negative charges also decreases with decreasing degree of ionization, which enables self-assembly by hydrogen bonds. Here, the poly(*N*-methyl methacryloylhydroxamic acid) behaves in a similar way as polymethacrylic acid. Although this is not the primary scope of our study, it has to be considered because during the complex formation with Fe^{3+} the system gets acidic. However, at pH 7.4 (i.e., pH of blood plasma), the polymer does not precipitate, so this effect should not adversely affect our studies.

We confirmed the degradation of Fe^{3+}-assembled nanoparticles by demetalation with deferoxamine using SEC. Not only the same conditions as used for the determination of molecular weight of the polymer were applied, but also the absorbance at 470 nm (approximate absorbance maximum for the hydroxamic acid–Fe^{3+} ion complex) was followed. Since both the polymer and deferoxamine are hydroxamic acid ligands, the ratio (polymer peak area/low-molecular-weight peak area) in absorbance at 470 nm was attributed to the ratio of the iron content in the respective species. Before addition of deferoxamine, the Fe^{3+}-assembled particles contained all polymer and all iron in the high-molecular-weight nanoparticle peak at exclusion limit of the column (with apparent $\overline{M}_w$ according to light scattering 60.2 MDa).

In water, addition of deferoxamine caused complete demetalation with no iron left in high-molecular-weight fractions (neither nanoparticles at exclusion limit nor polymer within the separation range of the column), so all iron was in the low-molecular-weight fraction of the deferoxamine complex with Fe. Also, the molecular weight of the polymer after demetalation was identical with the original molecular weight of the polymer before formation of the nanoparticles (as determined using the refractive index and light-scattering detection).

In phosphate-buffered saline after addition of deferoxamine, overwhelming majority of iron (99.02%) was recomplexed with deferoxamine into a low molecular weight fraction as shown by the SEC analysis, however, there was a small residual amount of Fe^{3+}-assembled nanoparticles left (0.98% total iron).

SEC results thus well correspond with the DLS data, where we have demonstrated reaggregation of nanoparticles in water after addition of deferoxamine that is most likely caused by hydrogen bonding between demetalized polyhydroxamic acid blocks and PEO grafts. As a conclusion, we have shown that, using deferoxamine, the nanoparticles may be completely degraded by removal of the cross-linker (Fe^{3+} ions) by rechelation, which is the new principle of nanoparticle degradation. That makes Fe^{3+}-assembled nanoparticles an ideal choice for further biological tests on laboratory animals.

In order to get more information on the formation of Fe complexes on a time scale of seconds, we performed TR-SAXS measurements that are commonly used to extract information on size and shape of nano-objects in solution. Detailed description of the TR-SAXS experiments may be found in Supporting Information to this manuscript.

Both AFM experiments and electron microscopy investigations confirm the average size of the Fe–polymer complex nanoparticles with diameter in the vicinity of 100 nm. AFM (Figure 11) shows that the Fe-assembled nanoparticles have spherical shape and their average size

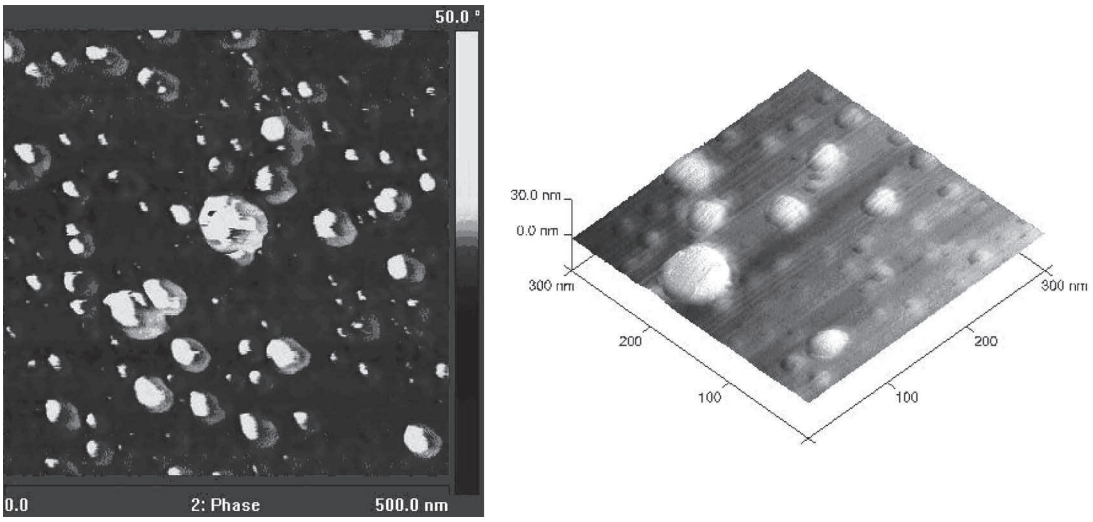

Figure 11. Fe^{3+}-assembled nanoparticles (2D and 3D image).

© 2011 WILEY-VCH Verlag GmbH & Co. KGaA, Weinheim

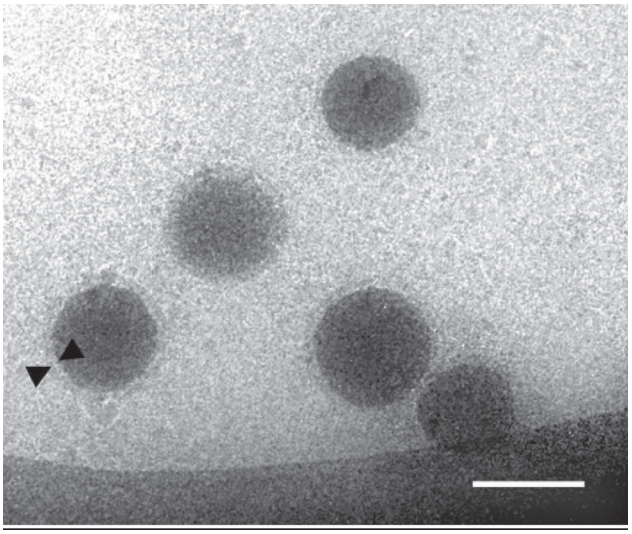

Figure 12. Cryo-TEM image of the nanoparticles with Fe^{3+}. Bar indicates 200 nm. The arrows indicate the shell.

(volume-weighted diameter $D = 63 \pm 27$ nm) corresponds well with DLS (volume-weighted hydrodynamic diameter $D_H = 60$ nm). The nanoparticles have a small polydispersity, which may be caused by the fact, that Fe^{3+}-mediated formation of the nanoparticles is very fast, as shown by the TR-SAXS experiments (see Supporting Information). Because homogenization of the solution upon mixing is not immediate, there exist places with higher and lower Fe^{3+} concentration, which probably leads to the observed small polydispersity. However, the size of the nanoparticles is within the range which is suitable for EPR effect ($D < 200$ nm).[30]

In the cryo-TEM pictures (Figure 12), it is visible that some nanoparticles consist of a shell surrounding and protecting a core inside. Core-shell structure is very well known from micelles, in which the self-assembly is caused by hydrophilic and hydrophobic interactions. In case of the micelles, the shell is made of hydrophilic part of the molecule (in case of hydrophilic environment), whereas the hydrophobic part is hidden inside. In our case the hydrophilic shell consists of the PEO grafts and the hydrophobic polyhydroxamic acid together with the chelation-trapped Fe^{3+} ion creates the core of the particle. The presence of a PEO shell is a benefit because the nanocarrier is well protected against unwanted reaction of the immune system. PEO was used previously to protect the surface of other nanocarrier systems.[31]

4. Conclusion

The polymeric nanoparticles consisting of PMMHA–PEO grafts are formed by self-assembly after addition of metal ion cations (Cu^{2+} or Fe^{3+}), which serve as potentially biodegradable cross-linkers. This phenomenon, to best of our knowledge, has not been yet described in literature. DLS time-resolved experiments have shown that Cu^{2+} complexes did not form satisfactorily; therefore, we further focused our study only on Fe^{3+} complexes. This difference can be caused by different number of bonds in Fe^{3+} (3) and Cu^{2+} (2) complex with PMMHA–PEO. With AFM and cryo-TEM methods, we were able to observe the 3D shape of the nanoparticles, and by SAXS, we have shown that the Fe complexes are formed on a time scale of milliseconds and that their internal structure is not compact. We have also proven that the already formed nanoparticles are robust to the change in pH, which is important for their perspective applications. Our results allow us to synthesize unique polymeric nanoparticles that can be used as a very good and ready-to-use drug delivery carrier for cancerostatics.

Supporting Information

Supporting Information is available from the Wiley Online Library or from the author.

Acknowledgements: The authors gratefully acknowledge the European Synchrotron Radiation Facility (Grenoble, France) for the provision of synchrotron beam time (SC2883). Financial support of the Grant Agency of the Czech Republic (grant # P207/10/P054 and 202/09/2078) and of the Ministry of Education, Youth and Sports of the Czech Republic (grant #1M 4635608802) are gratefully acknowledged. The authors acknowledge the Charles University in Prague, department of Natural Sciences for the opportunity of the PhD studies. They would also like to thank Prof. Katarina Edwards, Uppsala University, Department of Physical and Analytical Chemistry for help with cryo-TEM experiments.

Received: July 27, 2011; Published online: September 20, 2011; DOI: 10.1002/macp.201100431

Keywords: drug delivery systems; hydroxamic acid; nanoparticles; self-assembly

[1] J. Kozempel, M. Hruby, M. Novakova, J. Kucka, L. Leseticky, O. Lebeda, *Radiochim. Acta* **2009**, *97*, 747.
[2] M. Hruby, T. Etrych, J. Kucka, M. Forsterova, K. Ulbrich, *J. Appl. Polym. Sci.* **2006**, *101*, 3192.
[3] K. Kataoka, A. Harada, Y. Nagasaki, *Adv. Drug Delivery Rev.* **2001**, *47*, 113.
[4] A. Lavasanifar, J. Samuel, G. S. Kwon, *Adv. Drug Delivery Rev.* **2002**, *54*, 169.
[5] N. Nishiyama, K. Kataoka, *Pharm. Ther.* **2006**, *112*, 630.
[6] H. Maeda, J. Wu, T. Sawa, Y. Matsumura, K. Hori, *J. Controlled Release* **2000**, *65*, 271.
[7] J. Fang, T. Sawa, *Adv. Exp. Med. Biol.* **2003**, *519*, 29.

© 2011 WILEY-VCH Verlag GmbH & Co. KGaA, Weinheim

[8] L. Gambling, H. S. Andersen, H. J. McArdle, *Biochem. Soc. Trans.* **2008**, *36*, 1258.
[9] A. C. G. Chua, R. M. Graham, D. Trinder, J. K. Olynyk, *Crit. Rev. Clin. Lab. Sci.* **2007**, *44,* 413.
[10] V. Vassiliev, Z. L. Harris, P. Zatta, *Brain Res. Rev.* **2005**, *49*, 633.
[11] X. S. Sun, Q. Y. He, *Prog. Chem.* **2007**, *19*, 1986.
[12] D. V. P. R. Varaprasad, P. Desaraju, A. Winston, *Bioorg. Chem.* **1986**, *14*, 8.
[13] A. Winston, D. V. P. R. Varaprasad, J. J. Metterville, H. Rosenkrantz, *J. Pharmacol. Exp. Ther.* **1985**, *232*, 644.
[14] C. J. Anderson, M. A. Green, Y. Fujibayashi, in *Handbook of Radiopharmaceuticals: Radiochemistry and Applications*, (Eds: M. J. R. Welch, C. S. Redvanly), John Wiley & Sons, Ltd., Chichester, UK **2003** 401–422.
[15] M. Kissel, P. Peschke, V. Subr, K. Ulbrich, J. Schuhmacher, J. Debus, E. Friedrich, *J. Pharm. Sci. Technol.* **2001**, *55*, 191.
[16] D. V. P. R. Varaprasad, P. Desaraju, A. Winston, *Bioorg. Chem.* **1986**, *14*, 8.
[17] D. V. P. R. Varaprasad, J. Rosthauser, A. Winston, *J. Polym. Sci., Part A: Polym. Chem.* **1984**, *22*, 2131.
[18] M. J. Miller, *Chem. Rev.* **1989**, *89*, 1563.
[19] A. Winston, D. V. P. R. Varaprasad, J. J. Metterville, H. Rosenkratz, *J. Pharm. Exp. Ther.* **1984**, *232*, 644.
[20] A. Shrivastava, K. K. Ghosh, *Indian J. Chem.* **2007,** *46A*, 1630.
[21] C. Konak, M. Sedlak, *Macromol. Chem. Phys.* **2007**, *208*, 1893.
[22] J. Panek, S. K. Filippov, C. Konak, F. Nallet, L. Noirez, G. Karlsson, P. Stepanek, *J. Dispersion Sci. Tech.* **2011**, **32**, 888
[23] R. Duncan, Y. N. Sat, *Ann. Oncol.* **1998**, *9*, 39.
[24] F. S. Rehmani, Z. T. Maqsood, S. A. Kazmi, *J. Chem. Soc. Pak.* **1997**, *19*, 38.
[25] K. Lee, C. Cheong, E. K. Koh, H. S. Shim, M. Kim, Y. M. Kim, S. H. Lee, K. S. Hong, *J. Kor. Phys. Soc.* **2008**, *53*, 2535.
[26] J. B. Neilands, *Annu. Rev. Biochem.* **1981**, *50*, 715
[27] A. Winston, D. Kirschner, *Macromolecules* **1978**, *11*, 597.
[28] P. Stepanek, in *Dynamic Light Scattering, The Method and Some Applications*, (Ed: W. Brown), Clarendon Press, Oxford, UK **1993**, p. 177 –241
[29] S. W. Provencher, *Comput. Phys. Commun.* **1982**, *27*, 229.
[30] S. A. Schichman, R. A. Amey, *J. Phys. Chem.* **1971**, *75*, 99.
[31] R. G. LeBel, D. A. I. Goring, *J. Chem. Eng. Data* **1962**, *7*, 100.

© 2011 WILEY-VCH Verlag GmbH & Co. KGaA, Weinheim

CHEMPHYSCHEM

ChemPubSoc Europe

DOI: 10.1002/cphc.201200681

Self-Assembled Polymeric Chelate Nanoparticles as Potential Theranostic Agents

M. Škodová,*[a] P. Černoch,[a] P. Štěpánek,[a] E. Chánová,[a] J. Kučka,[a, b] Z. Kálalová,[a] D. Kaňková,[a] and M. Hrubý[a]

Improvements in cancer diagnostics and therapy have recently attracted the interest of many different branches of science. This study presents one of the new possible approaches in the diagnostics and therapy of cancer by using polymeric chelates as carriers. Graft copolymers with a backbone containing 8-hydroxyquinoline-5-sulfonic acid chelating groups and poly(ethylene oxide) hydrophilic grafts are synthesized and characterized. The polymers assemble and form particles after the addition of a biometal cation, such as iron or copper. The obtained nanoparticles exhibit a hydrodynamic diameter of around 25 nm and a stability of at least several hours, which are counted as essential parameters for biomedical purposes. To prove their biodegradability, a model degradation with deferoxamine is performed and, together with high radiolabeling efficiency with copper-64, their possible use for nuclear medicine purposes is demonstrated.

1. Introduction

Nanoparticles have become popular nowadays as drug and radionuclide delivery systems for imaging and therapy of solid tumors.[1–4] Targeting of the polymeric structures into tumor tissue is in most cases based on the enhanced permeation and retention (EPR) effect.[5] The EPR effect causes passive accumulation of macromolecular drug-delivery systems in solid tumors[6–8] due to leaking vasculature and missing lymphatic drainage in tumor tissue.

The aim of this study is to synthesize and examine the properties of novel biodegradable nanostructures consisting of graft copolymers self-assembled by the addition of metal ions with size suitable for the EPR effect, that is, less than approximately 200 nm.[5] The polymer structures are composed of a graft copolymer consisting of a polymer backbone with chelating 8-hydroxyquinoline-5-sulfonic acid moieties and biocompatible poly(ethylene oxide) (PEO) grafts.[9,10] The PEO grafts stabilize the system against aggregation. Moreover, they can provide immunological "stealth" for the whole polymer system, thus avoiding its entrapment[11] into the reticuloendothelial system (especially liver and spleen) before it reaches tumor tissue. The backbone polymer chain is able to bind essential metal ions (Fe^{3+} or Cu^{2+}) that serve as bioreversible crosslinkers on the same principle as polymers with a polyhydroxamic acid chelating group that we reported previously.[12] The bound metal cations may be transchelated directly or after reduction to lower oxidation states (Fe^{2+} and Cu^{1+}) inside cells (see Scheme 2, bottom), while the chelate bond is sufficiently stable during transport in blood. This means that after fulfilling their task as carriers, the structures should decompose inside the cells and the individual polymeric chains with molecular weights under the renal threshold (which is ca. 45–50 kDa for (meth)acrylamide-type polymers)[13,14] can be eliminated from the body by the kidneys. This principle allows us[15] to radiolabel the metal ions with a suitable radionuclide, for example, ^{64}Cu, thereby providing a potential application of such polymeric nanoparticles as theranostic[16] radiopharmaceuticals.

Experimental Section

Materials: *N*-BOC-*N*′-acroyl piperazine (BOC = *tert*-butoxycarbonyl) was synthesized according to ref. [17]. All other chemicals were purchased from Sigma–Aldrich (Prague, Czech Republic) and were used as received. Dialysis tubing (with cutoff 3500 Da) was purchased from GE Healthcare (Uppsala, Sweden).

Methods: The synthesis of polymer **III** was performed in three steps as depicted in Scheme 1.

Synthesis of Polymer **I**: Methacryloyl poly(ethylene oxide) monomethyl ether ($M_w = 5000$; 2.00 g), *N*-BOC-*N*′-acroyl piperazine (1.63 g; $M = 198.22$; 8.2 mmol), and azobis(isobutyronitrile) (AIBN, 20 mg) as an initiator were stirred at 60 °C for 12 h in tetrahydrofuran (12 mL). Polymer **I** was precipitated into excess diethyl ether, isolated by filtration, dissolved in tetrahydrofuran (10 mL), precipitated into excess diethyl ether, isolated by filtration, and dried in vacuo. Yield 2.25 g (62%); CNH found (%): C 56.15, H 9.21, N 3.54. Number-average molecular weight M_n, weight-average molecular weight M_w, and polydispersity $I = M_w/M_n$ were determined by gel permeation chromatography according to ref. [12]; $M_n = 11.5$ kDa, $M_w = 16.0$ kDa, $I = 1.39$.

[a] M. Škodová, Dr. P. Černoch, Dr. P. Štěpánek, Dr. E. Chánová, Dr. J. Kučka, Z. Kálalová, D. Kaňková, Dr. M. Hrubý
Institute of Macromolecular Chemistry
Academy of Sciences of the Czech Republic
v.v.i. (Czech Republic)
E-mail: skodova@imc.cas.cz

[b] Dr. J. Kučka
Nuclear Physics Institute
Academy of Sciences of the Czech Republic
v.v.i. (Czech Republic)

WILEY ONLINE LIBRARY

© 2012 Wiley-VCH Verlag GmbH & Co. KGaA, Weinheim

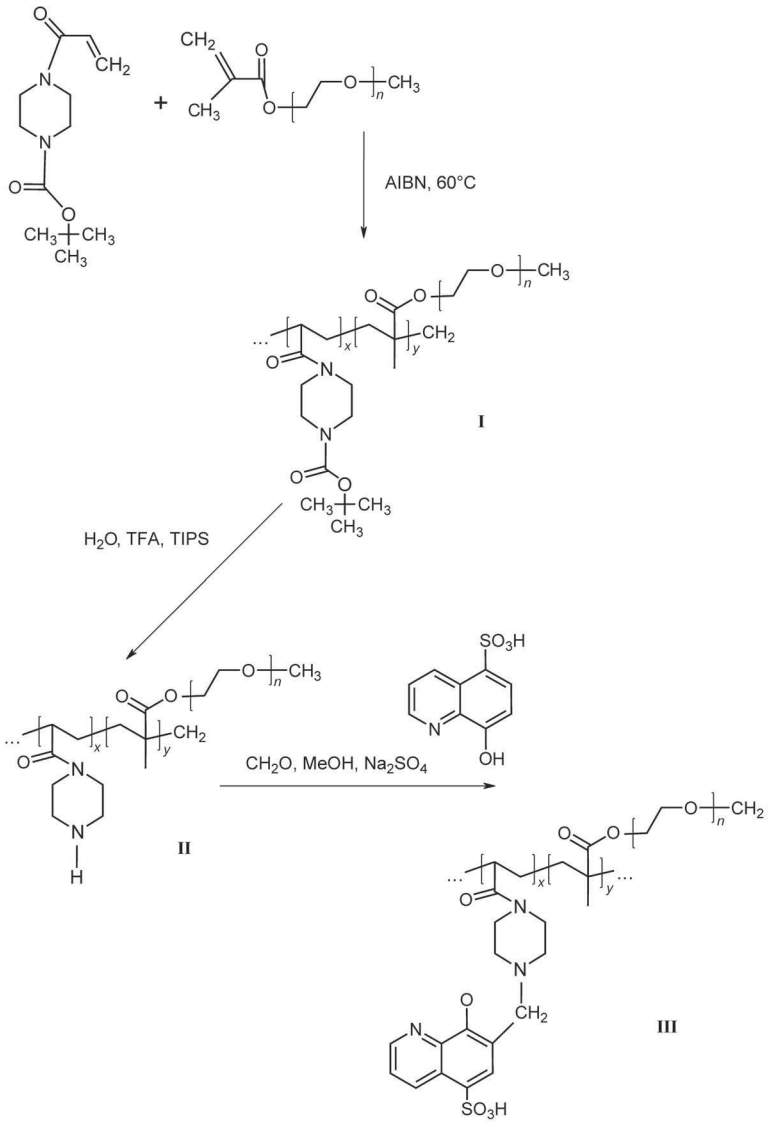

Scheme 1. Synthesis of polymer **III**. AIBN = azobis(isobutyronitrile), TFA = trifluoroacetic acid, TIPS = triisopropylsilane, MeOH = methanol.

Synthesis of Polymer **II**: The deprotection of BOC groups on polymer **I** (1000 mg) was carried out with a mixture of trifluoroacetic acid (TFA, 19 mL), triisopropyl silane (TIPS, 1000 μL), and H_2O (1000 μL) for 1.5 h at room temperature. The reaction mixture was evaporated, the residue was dissolved in water (20 mL) with an admixture of sodium carbonate (2.00 g), and the solution was dialyzed against water for 48 h. The resulting solution of deprotected product was freeze-dried to yield polymer **II** (620 mg). ^{1}H NMR (D_2O): no signal at $\delta = 1.40$ ppm; CNH found (%): C 56.66, H 9.34, N 3.96.

Synthesis of Polymer **III**: Polymer **III** was prepared by Mannich condensation of polymer **II** (500 mg, 0.707 mmol NH groups) with 8-hydroxyquinoline-5-sulfonic acid (0.796 g, 3.53 mmol) and formaldehyde (1.62 mL) in methanol (8 mL) with anhydrous sodium sulfate (3.62 g) for 7 days at room temperature, in analogy to our synthesis of chelating ion exchanger.[12] The reaction mixture was diluted with water (25 mL) and dialyzed against 0.9 wt% aqueous NaCl for 24 h and then against water for 48 h. The resulting solution of polymer **III** was freeze-dried. Yield 356 mg; S 2.90%. M_n = 15.5 kDa, M_w = 24.7 kDa, I = 1.59.

UV/Vis Spectrometry: UV/Vis spectrometry was used to determine the growth of the polymeric complex. A solution of polymer **III** ($c_{polymer} = 1$ mg mL^{-1} in 0.05 M HCl, 1 mL) was mixed with increasing amounts of $FeCl_3$ solution (2.93 mM of Fe^{3+} in 0.05 M HCl) from 20 to 150 μL (100 μL represents 100% of the stoichiometric amount of Fe^{3+} ions).

The kinetic aspect of particle formation was obtained from another measurement in which a solution of polymer **III** ($c_{polymer} = 1$ mg mL^{-1} in 0.05 M HCl, 1 mL) was mixed with a stoichiometric amount of Fe^{3+} ions (2.93×10^{-7} mol Fe^{3+} in 100 μL 0.05 M HCl) and spectra were measured at time intervals: immediately after mixing ($t = 0$), and after 5 min, 15 min, 60 min, 120 min, and 24 h. Spectra were measured in the wavelength range 250–800 nm. The presumed principle of nanoparticle formation from polymeric chelates is illustrated in Scheme 2 (top).

Dynamic Light Scattering (DLS): A solution of nanoparticles was investigated by DLS with an ALV-6010 correlator equipped with an ALV/CGS-8F goniometer, a 22 mW He–Ne laser (wavelength λ = 632.8 nm), and pair of avalanche photodiodes operated in a pseudo-cross-correlation mode. All measurements were made at a 90° angle. The measured intensity correlation function $g^2(t)$ was analyzed by using the algorithm REPES[18] performing the inverse Laplace transformation according to [Eq. (1)]:

$$g^2(t) = 1 + \beta\left[\int A(t)\exp(-t/\tau)\mathrm{d}\tau\right]^2 = 1 + \beta\left[\sum_{i=1}^{n} A_i \exp(-t/\tau_i)\right]^2 \quad (1)$$

where t is the delay time of the correlation function and β an instrumental parameter, thereby yielding the distribution $A(\tau)$ of relaxation times τ. The relaxation time τ is related to the diffusion coefficient D and relaxation (decay) rate Γ by the relation [Eq. (2)]:

$$\Gamma = \frac{1}{\tau} = D\mathbf{q}^2 \quad (2)$$

where $\mathbf{q}$ is the scattering vector defined as $\mathbf{q} = (4\pi n/\lambda)\sin(\theta/2)$, in which n is the refractive index of the solvent, θ is the scattering angle, and λ is the wavelength of incident light. The hydrodynamic

 © 2012 Wiley-VCH Verlag GmbH & Co. KGaA, Weinheim

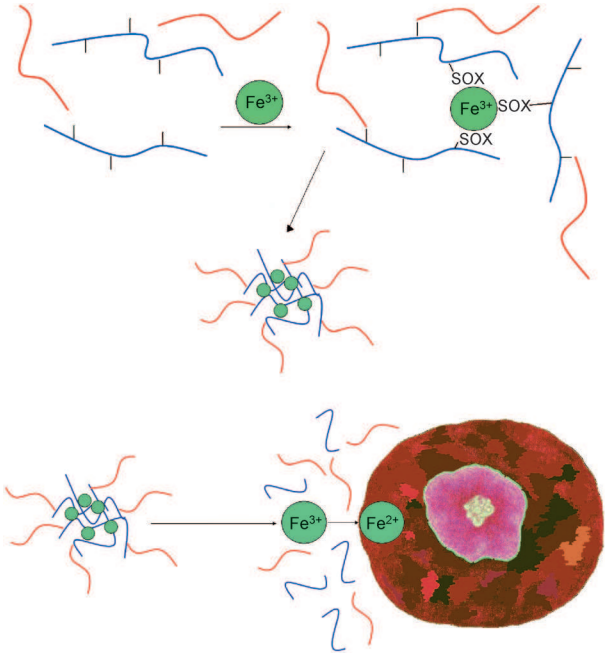

Scheme 2. Top: Formation of metal-ion-assembled nanoparticles; SOX = 8-hydroxyquinoline-5-sulfonic acid. Bottom: Presumed disintegration of the nanoparticle system and intracellular transchelation of Fe^{3+} ions after reduction into Fe^{2+} ions.

radius R_h of the particles can be calculated[19,20] from the diffusion coefficient by using the Stokes–Einstein equation [Eq. (3)]:

$$D = k_B T / 6\pi\eta R_h \quad (3)$$

where T is the absolute temperature, η the viscosity of the solvent, and k_B Boltzmann's constant. The solution was filtered directly before the measurement using a 0.2 μm PVDF syringe filter into a dust-free glass ampoule and sealed.

Small-Angle X-ray Scattering (SAXS): SAXS was used to investigate the nanoparticle kinetic behavior and to help identify the particle shape and internal structure. The measurements were carried out at the SAXS beamline of Elettra Sincrotrone Trieste, on the beamline D11A-SAXS, the wavelength of the X-rays being 0.1 nm. A collimated X-ray beam was passed horizontally through a capillary. The q-range covered by the detector was 0.05–2 nm^{-1}. The measurements were performed at 25 °C with an exposure time of 10 s. Calibration of the q-scale was obtained by means of silver behenate. Data obtained from the detector were corrected by taking into account the flat field and the dark current. Finally, the data were corrected for sample transmission and background scattering by using an empty cell as reference.

Atomic Force Microscopy (AFM): Selected complex systems were characterized by AFM after deposition on solid supports. Samples of Fe^{3+} complex with polymer **III** were prepared by a dip-coating process[21] on freshly cleaved mica from 0.05 M HCl (5 mg L^{-1}). The character of the nanoparticles was determined before and after rinsing the surface with water.

All images were acquired with a multimode atomic force microscope NanoScope IIIa (Digital Instruments, USA) as topographical scans in tapping mode under ambient conditions, by using tapping-mode etched silicon probes OTESPA (Veeco Instruments, USA) with a cantilever resonance frequency of about 310 kHz and typical spring constant 42 N m^{-1}. The 256×256 pixel images were scanned at a rate of 1.0–1.3 Hz.

Model In Vitro Degradation: Solutions of the Fe^{3+} complex of polymer **III** ($c_{polymer}$ = 1 mg mL^{-1}, 1 mL) and deferoxamine (2.72 mM) were heated to 37 °C, mixed, and then the mixture was incubated at 37 °C. The absorbance at 680 nm was recorded at selected time points (0 h—immediately after mixing, 18, 42, 144, 240, 504, and 864 h).

Radiolabeling: Radiolabeling of Fe^{3+}-assembled nanoparticles with ^{64}Cu was performed according to a procedure described in our previous study.[12] Three pH values were chosen for radiolabeling: pH 1.5 (set by aqueous HCl), 6.6, and 7.4 (set by 0.05 mol L^{-1} phosphate buffer). A solution of Fe^{3+} complex of polymer **III** ($c_{polymer}$ = 1 mg mL^{-1} in distilled water, 250 μL) was mixed with a particular buffer (250 μL) in an Eppendorf tube, and carrier-free [^{64}Cu]$CuCl_2$ solution (≈5 MBq, 5 μL) was added. The reaction mixtures were incubated at laboratory temperature (25 °C) for 2 h on a tube shaker. After that, labeled polymers were purified from unreacted [^{64}Cu]$CuCl_2$ by gel permeation chromatography on PD-10 desalting columns (GE Healthcare, USA) with phosphate-buffered saline (PBS) as eluent, and 1.5 mL fractions were collected. Radiochemical yields were determined as the ratio of the activity in macromolecular fractions (3 and 4) to the total activity applied on the column. Separated yields were corrected for the losses of activity on tips and tubes.

The stability of the complex in the presence of competing ions was determined as follows. The solution of ^{64}Cu-labeled polymer in PBS (merged fractions 3 + 4 from radiolabeling, 250 μL) was mixed with a twice concentrated stock solution of competing ions (containing $CaCl_2$ 2 mmol L^{-1}, $MgSO_4$ 20 mmol L^{-1}, KH_2PO_4 2 mmol L^{-1}, NaCl 300 mmol L^{-1}) and incubated for 24 h at 37 °C. The polymer fraction was then separated on a PD-10 column as described above for radiolabeling and the stability was calculated as the ratio of the activity in macromolecular fractions (3 and 4) to the total activity applied on the column.

2. Results and Discussion

The synthesis of graft copolymer composed of a backbone containing 8-hydroxyquinoline-5-sulfonic acid moieties and PEO grafts (polymer **III**) was carried out in three steps with polymers **I** and **II** as intermediates. Polymer **I** was synthesized by radical copolymerization of poly(ethylene oxide) monomethyl ether methacrylate (M_w = 5000 Da) with *N-tert*-butoxycarbonyl-*N'*-acroyl piperazine. The resulting polymer **I** had M_w = 16.0 kDa with polydispersity I = 1.39. The weight ratio of polymer blocks was calculated from elemental analysis of nitrogen (found 3.54%), and corresponded to 30.4 wt% poly(*N*-BOC-*N'*-acroyl piperazine) block content in the copolymer, considering the molecular weight M_w = 16.0 kDa. This means an average of 2.23 PEO blocks of M_w = 5 kDa per polymer chain.

Deprotection of BOC groups of polymer **I** was proven to be quantitative by ^1H NMR spectroscopy in D_2O. No signal corresponding to the shift of $-O-C(CH_3)_3$, that is, δ = 1.40 ppm, was detected in ^1H NMR spectra of polymer **II**.

The stoichiometry for the subsequent Mannich condensation was calculated based on the assumption that half of the nitrogen atoms in the polymer are in NH groups, that is, in the content $N/2$ = 1.98%, with $N \approx 1.41$ mmol g^{-1} NH.

 © 2012 Wiley-VCH Verlag GmbH & Co. KGaA, Weinheim

The Mannich condensation of the secondary amine groups of polymer **II** with formaldehyde and 8-hydroxyquinoline-5-sulfonic acid resulted in polymer **III** (Scheme 1). The content of 8-hydroxyquinoline-5-sulfonic acid moieties in polymer **III**, c_{SOX}, was determined from the elemental analysis of sulfur according to the equation $c_{SOX} = c_S/3.206\ \text{mmol g}^{-1}$, where c_S is the sulfur content in wt%. Found: $c_S = 2.90$ wt%, $c_{SOX} = 0.905\ \text{mmol g}^{-1}$. ^{1}H NMR spectroscopy in D_2O proved the presence of the ^{1}H of aromatic nuclei ($\delta = 6.5$–9.5 ppm). There was a slight increase in M_w and polydispersity when comparing polymer **III** with polymer **I** ($M_w = 24.7$ kDa for polymer **III** compared to $M_w = 16.0$ kDa for polymer **I**; $I = 1.59$ for polymer **III** compared to $I = 1.39$ for polymer **I**), probably due to a small extent of formation of interchain N-CH_2-N bridges by the reaction of formaldehyde with secondary amines; however, the molecular weight still remains well below the renal threshold.

We first determined the rate of formation of the nanoparticles upon addition of Fe^{3+} ions. The complex formation of polymer **III** containing 8-hydroxyquinoline-5-sulfonic acid groups with Fe^{3+} is relatively slow (tens of minutes) in comparison with our previously studied system[12] of similar architecture with hydroxamic acid (milliseconds). The calculated half-time (from Figure 1—by interleaved tangent of dependence of maximum absorbance values for $\lambda = 590$ nm on time) of nanoparticle formation is in this case 32 min.

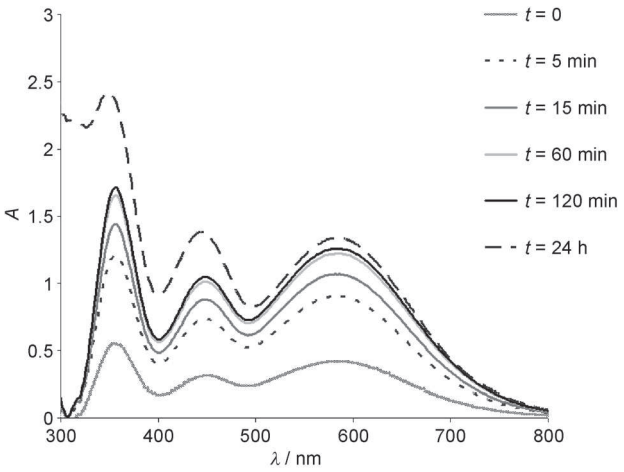

Figure 1. Growth of Fe^{3+}–polymer **III** complex in time determined from the dependence of absorbance on wavelength.

We also studied the complexation capacity of Fe^{3+} for our polymeric system. From the elemental analysis of sulfur we can calculate the theoretical stoichiometry of polymer **III**–Fe^{3+} (for low-molecular-weight 8-hydroxyquinoline-5-sulfonic acid–Fe^{3+} complex it is 3:1). However, there are steric considerations that may decrease the real capacity of polymer for complexation of Fe^{3+}. Figure 2 shows the growth of absorbance of the complex for each addition of Fe^{3+} equivalents from 30 to 150%; the real capacity is close to 100% of the theoretical capacity (110%). This is another difference from our previous system of similar architecture, but with hydroxamic acid[12] instead of 8-hydroxyquinoline-5-sulfonic acid groups, for which the real capacity was considerably lower than the theoretical capacity. Such a difference in complex capacity can be attributed to the kinetics of nanoparticle formation. In our previous system, the nanoparticles are formed within milliseconds; thus, there is not enough time for steric rearrangement and exploitation of the chelating capacity of the polymer. The chelate formation of polymer **III** described herein proceeds within minutes, which provides an idle period for steric rearrangement and hence higher chelating capacity.

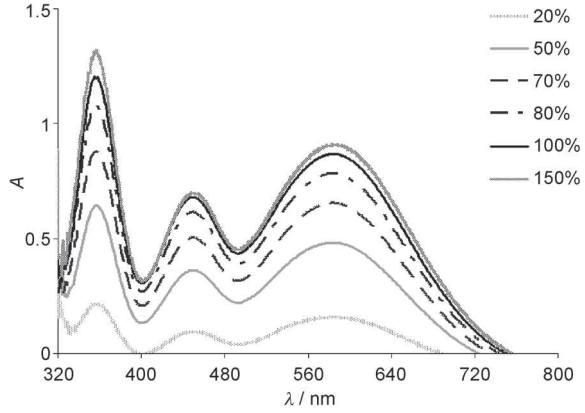

Figure 2. Growth of Fe^{3+}–polymer **III** complex after addition of Fe^{3+} equivalents determined from the dependence of absorbance on wavelength.

The stability of the complex was investigated by using DLS experiments. The time dependence of the hydrodynamic radii R_h of the nanoparticles in 0.05 M HCl (pH 1.3), PBS (pH 7.4), and water (pH 7.0) was measured. The R_h of the nanoparticles, that is, complexes of polymer **III** with Fe^{3+}, both in water and in buffered milieu, did not significantly change for at least 15 h (Figures 3 and 4, data shown for 0.05 M HCl). The same holds for their number given by the amplitude of the peaks in Figures 3b and 4b. Therefore, we can conclude that the particles are sufficiently stable for possible in vivo use as carriers of ^{64}Cu (half-life $T_{1/2} = 12.7$ h, electron capture 43.6%, β^+ 17.4%, β^- 39%). In both water and buffered environments two types of nanoparticles were detected: one with a diameter around 25 nm and aggregates with a diameter in hundreds of nanometers. After conversion from intensity-weighted distribution (as shown in Figure 3b) to volume-weighted distribution, the amount of the aggregates is extremely small (amplitude < 0.1%), so that their contribution can be neglected. The size of the nanoparticles is thus within the range that is suitable for the EPR effect (< 200 nm).[22]

A typical SAXS profile of an Fe^{3+} complex with polymer **III** in 0.05 M HCl ($c_{polymer} = 5\ \text{mg mL}^{-1}$) is shown in Figure 5. The data have been fitted with a model of polydisperse hard spheres providing an average nanoparticle radius of gyration $R_g = 13.7$ nm and a distribution width $\sigma = 0.45$. From this result and the value of $R_h = 11.7$ nm obtained by DLS we can calculate the structural ratio $\rho = R_g/R_h = 1.17$. The result substantially exceeds the theoretical value of $\rho = 0.77$ for hard spheres;[23] therefore, we can conclude that the nanoparticles are not compact spheres but exhibit internal porosity.

 © 2012 Wiley-VCH Verlag GmbH & Co. KGaA, Weinheim

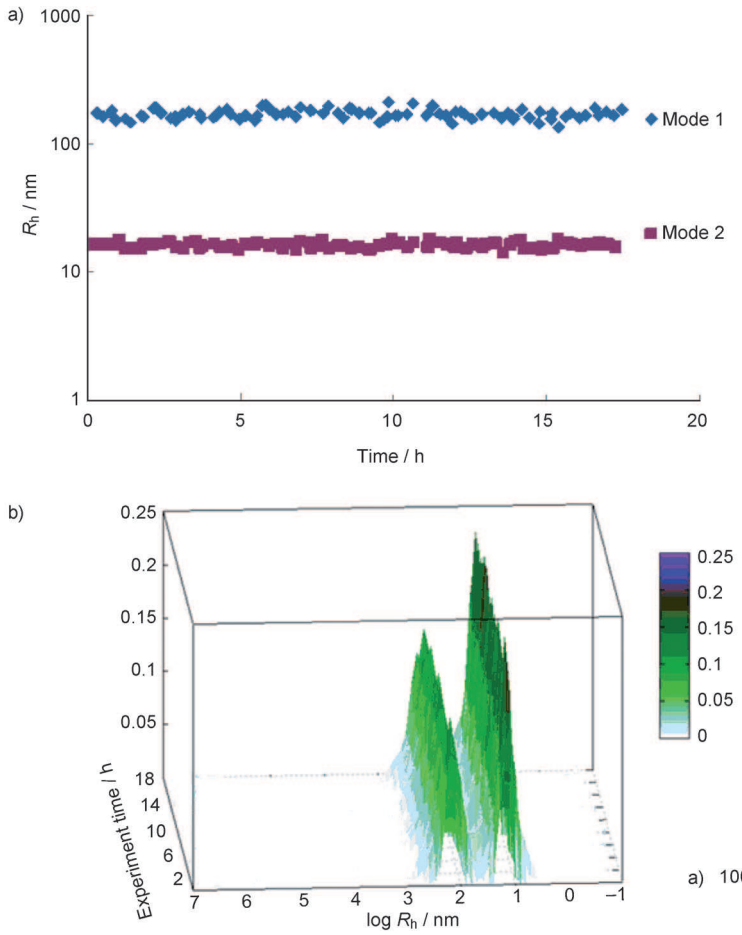

Figure 3. a) Dependence of R_h of the Fe^{3+} complex with polymer **III** (mode 2) and its aggregates (mode 1) on time in PBS. b) 3D particle size on a logarithmic scale in PBS.

The character of complex nanoparticles deposited on a solid support was studied using AFM under ambient conditions. As is clearly seen from Figure 6, the Fe complex nanoparticles deposited from 0.05 M HCl form a flowerlike structure (Figure 6a) on the mica surface with aggregate size in the range from hundreds of nanometers to micrometers (see detail in Figure 6b and the corresponding profile in Figure 6c). This structure was attributed to the presence of salt in the original nanoparticle solution and on the surface. Rinsing the surface with water after the deposition can affect the dissolution of the salt; thus, the aggregates disappeared from the mica surface and individual nanoparticles with diameter around 20–25 nm, corresponding well with the light scattering experiments, were observed (see Figure 7). The diameter of nanoparticles shown in Figure 7 corresponds to the result obtained by DLS and SAXS.

Moreover, the stability of the Fe^{3+}-assembled nanoparticles and their possible decomposition and aggregation upon interaction with deferoxamine was investigated as an in vitro model study of intracellular transchelation of Fe^{3+} and thus (bio)degradation of the polymeric system. Deferoxamine is a bacterial siderophore produced by the actinobacter *Streptomyces pilosus*.[24,25] It has medical applications to remove excess iron from the body in cases of iron overdose[26,27] because it is a very strong iron chelating agent with stability constant 30.6 for Fe^{3+},[19] that is, several orders of magnitude higher than reported for hydroxamic acids[28] and for 8-hydroxyquinoline-based ligands.[29] Deferoxamine was thus added in three times molar excess to the solution of nanoparticles and degradation was followed as the drop of absorbance at 680 nm, where the Fe^{3+} complex of polymer **III** absorbs but the complex of Fe^{3+} and deferoxamine is fully transparent.

The degradation follows first-order kinetics (confidence value: $R^2 = 0.989$) with half-life of 39.2 h. With respect to this result, we can assume that the system is suitable for potential application as a theranostic agent with ^{64}Cu, which possesses a half-life of 12.7 h, and the relative kinetic stability of the complex is likely to improve the in vivo stability of the nanoparticles during transport in the bloodstream.

Finally, the radiolabeling efficiency of Fe^{3+}–polymer particles with ^{64}Cu under different pH values was investigated. Our previous study indicated that the pH must be optimized,[12] as the polymer complex formation with Fe^{3+} ions proceeds in an acidic

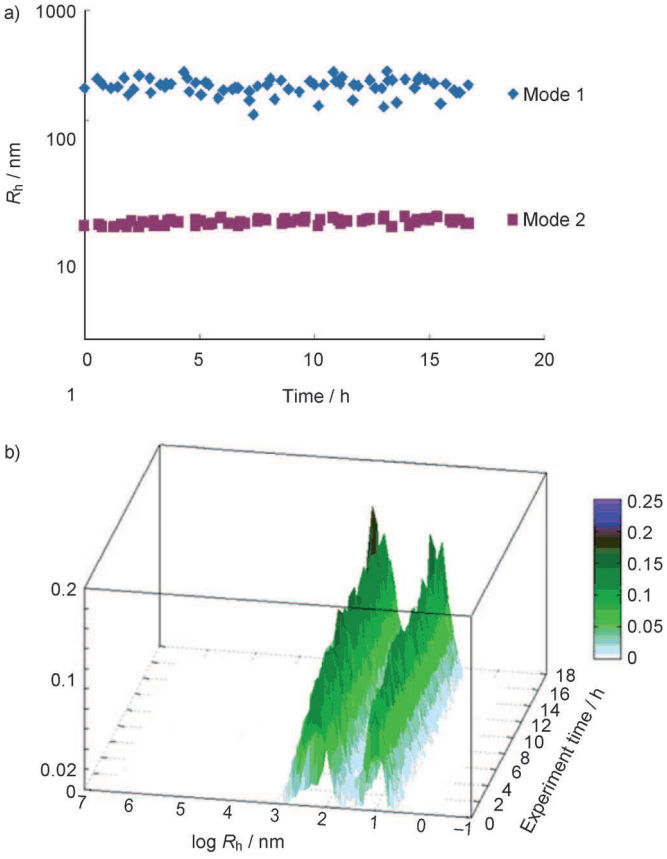

Figure 4. a) Dependence of R_h of the Fe^{3+} complex with polymer **III** (mode 2) and its aggregates (mode 1) on time in H_2O. b) 3D particle size on a logarithmic scale in H_2O.

 © 2012 Wiley-VCH Verlag GmbH & Co. KGaA, Weinheim

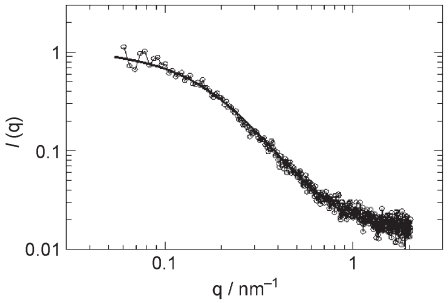

Figure 5. Dependence of SAXS intensity *I* on scattering vector **q** for an Fe^{3+} complex with polymer **III** in 0.05 M HCl ($c_{polymer} = 5$ mg mL^{-1}) and the fitted curve (model for polydisperse hard spheres).

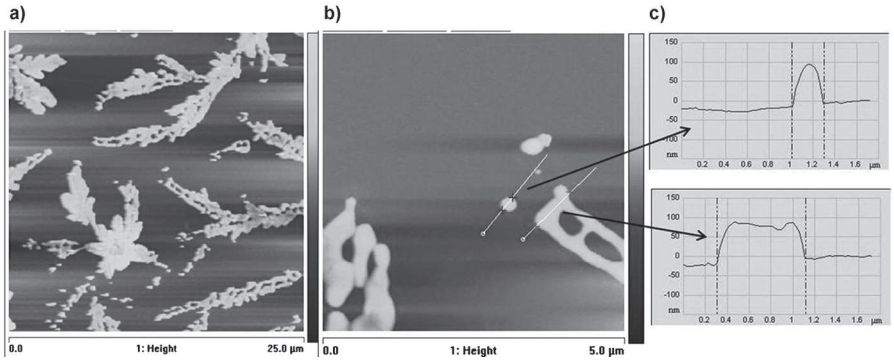

Figure 6. AFM images (topography) of complex nanoparticles deposited from 0.05 M HCl before rinsing the surface with water. a) Scan size 25×25 µm, b) scan size 5×5 µm (for both, Z-scale 250 nm), c) corresponding surface profiles highlighted in image (b).

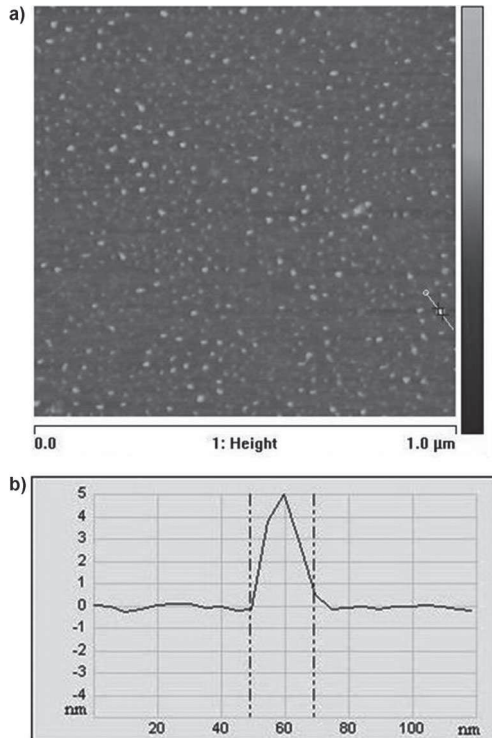

Figure 7. AFM image (topography) of complex nanoparticles deposited from 0.05 M HCl after rinsing the surface with water. a) Scan size 1×1 µm, Z-scale 10 nm; b) corresponding surface profile highlighted in image (a).

environment whereas the copper forms complexes preferably under higher pH values. Three solutions with different pH values were tested for the radiolabeling procedure. In an acidic environment (pH 1.5), the radiolabeling yield was low (39.2%) and inappropriate for biomedical application. In less acidic solution at pH 6.6 we obtained almost quantitative radiolabeling yield (98%), which was suitable for the intended application. In neutral environment at pH 7.4 the labeling efficiency decreased again to a lower yield (73.8%), which could be explained by continuing hydrolysis of Cu^{2+} ions to insoluble copper(II) hydroxide before labeling.

In the human organism, however, numerous ions are present that may compete with the complexation of ^{64}Cu with the polymer **III**–Fe^{3+} complex. This is why we tested the stability of the radiolabeled nanoparticles in an environment containing these ions, in concentrations similar to those in blood plasma, by a modified method according to ref. [30]. There was no significant in vitro leakage of ^{64}Cu from the labeled polymer (stability more than 97%) after 24 h of incubation at 37 °C.

3. Conclusions

We have synthesized and characterized a graft copolymer containing chelating 8-hydroxyquinoline-5-sulfonic acid moieties on the polymer backbone and hydrophilic biocompatibilizing PEO grafts. The graft copolymer forms spherical nanoparticles with internal porosity by Fe^{3+}-mediated self-assembly, as confirmed by DLS, SAXS, and AFM. The nanoparticles have a diameter around 25 nm, which is a size suitable for EPR effect-based targeting. The nanoparticles are stable in a buffered environment modeling physiological conditions; with deferoxamine we proved that they can be biodegraded by metal transchelation. We have found the conditions under which the nanoparticles can be radiolabeled with ^{64}Cu in almost quantitative yield and therefore could possibly be used for medicinal purposes.

Acknowledgements

We would like to thank Charles University in Prague for the opportunity of PhD studies. Financial support by the Grant Agency of the Czech Republic (grants P207/10/P054, 202/09/2078, and P304/12/0950) is gratefully acknowledged. We also acknowledge SAXS facility allocation No. 20115409 at Elettra Sincrotrone Trieste for the provision of beamtime.

Keywords: chelates · nanoparticles · polymers · radiopharmaceuticals · self-assembly

 © 2012 Wiley-VCH Verlag GmbH & Co. KGaA, Weinheim

[1] W. H. De Jong, P. J. A. Borm, *Int. J. Nanomed.* **2008**, *3*, 133 – 149.
[2] D. Wesselinova, *Curr. Cancer Drug Targets* **2011**, *11*, 164 – 183.
[3] M. Youns, J. D. Hoheisel, T. Efferth, *Curr. Cancer Drug Targets* **2011**, *12*, 357 – 365.
[4] T. Lammers, F. Kiessling, W. E. Hennink, G. Storm, *Mol. Pharm.* **2010**, *7*, 1899 – 1912.
[5] H. Maeda, *Adv. Enzyme Regul.* **2001**, *41*, 189 – 207.
[6] Y. Matsmura, H. Maeda, *Cancer Res.* **1986**, *46*, 6387 – 6392.
[7] J. Fang, H. Nakamura, H. Maeda, *Adv. Drug Delivery Rev.* **2011**, *63*, 136 – 151.
[8] H. Maeda, *J. Controlled Release* **2001**, *74*, 47.
[9] D. K. Han, K. Park, K. D. Park, K. D. Ahn, Y. H. Kim, *Artif. Organs* **2006**, *30*, 955 – 959.
[10] J. H. Park, Y. H. Bae, *J. Biomater. Sci. Polym. Ed.* **2002**, *13*, 527 – 542.
[11] K. S. Soppimath, T. M. Aminabhavi, A. R. Kulkarni, W. W. Rudezinski, *J. Controlled Release* **2001**, *70*, 1.
[12] M. Škodová, M. Hrubý, S. K. Filippov, G. Karlsson, H. Macková, M. Špírková, D. Kaňková, M. Steinhardt, P. Štěpánek, K. Ulbrich, *Macromol. Chem. Phys.* **2011**, *212*, 2339 – 2348.
[13] G. Gaucher, M. H. Dufresne, V. P. Sant, N. Kang, D. Maysinger, J. C. Leroux, *J. Controlled Release* **2005**, *109*, 169 – 188.
[14] M. Kissel, P. Peschke, V. Subr, K. Ulbrich, J. Schuhmacher, J. Debus, E. Friedrich, *PDA J. Pharm. Sci. Technol.* **2001**, *55*, 191 – 201.
[15] D. Ma, F. Lu, T. Overstreet, D. E. Miknic, M. W. Brechbiel, *Nucl. Med. Biol.* **2002**, *29*, 91 – 105.
[16] C. J. Anderson, M. A. Green, Y. Fujibayashi in *Handbook of Radiopharmaceuticals: Radiochemistry and Applications, 1st ed.* (Eds.: M. J. R. Welch, C. S. Redvanly), Wiley, Chichester, **2003**, pp. 401 – 422.
[17] Y. S. Jo, A. J. van der Vlies, J. Gantz, T. N. Thacher, S. Antonijevic, S. Cavadini, D. Demurtas, N. Stergiopulos, J. A. Hubbell, *J. Am. Chem. Soc.* **2009**, *131*, 14413 – 14418.
[18] J. Jakeš, *Collect. Czech Chem. Commun.* **1995**, *60*, 1781 – 1797.
[19] P. Stepanek in *Dynamic Light Scattering, The Method and Some Applications, 1st ed.* (Ed.: W. Brown), Clarendon, Oxford, **1993**, pp. 177 – 241.
[20] P. Štěpánek, C. Konak, *Adv. Colloid Interface Sci.* **1984**, *21*, 195 – 274.
[21] R. H. Barzegar, F. Nitze, T. Sharifi, M. Ramstedt, C. W. Tai, A. Malolepszy, L. Stobinski, T. Wågberg, *J. Phys. Chem. C* **2012**, *116*, 12232 – 12234.
[22] R. Duncan, Y. N. Sat, *Ann. Oncol.* **1998**, *9*, 39.
[23] W. Burchard in *Laser Light Scattering in Biochemistry* (Eds.: S. E. Harding, D. B. Sattelle, V. A. Bloomfield), Royal Society of Chemistry, Cambridge, **1992**, pp. 3 – 22.
[24] G. Müller, B. F. Matzanke, K. N. Raymond, *J. Bacteriol.* **1984**, *160*, 313 – 318.
[25] M. Chiani, A. Akbarzadeh, A. Farhangi, M. R. Mehrabi, *Pak. J. Biol. Sci.* **2010**, *13*, 1151.
[26] H. G. Batz, G. Franzmann, H. Ringsdorf, *Angew. Chem.* **1972**, *84*, 1189; *Angew. Chem. Int. Ed. Engl.* **1972**, *11*, 1103.
[27] H. Boukhalfa, A. L. Crumbliss, *Biometals* **2002**, *15*, 325 – 339.
[28] S. W. Provencher, *Comput. Phys. Commun.* **1982**, *27*, 229.
[29] C. S. Hassler, M. R. Twiss, *Environ. Sci. Technol.* **2006**, *40*, 2544.
[30] M. Hrubý, V. Subr, J. Kucka, J. Kozempel, O. Lebeda, A. Sikora, *Appl. Radiat. Isot.* **2005**, *63*, 423.

Received: August 20, 2012
Revised: September 25, 2012
Published online on November 6, 2012

 © 2012 Wiley-VCH Verlag GmbH & Co. KGaA, Weinheim